TWIST, JAMES ROBERT

LOW ENERGY IMPACT EXCITATION, ENERGY TRANSFER AND LIFETIME STUDIES OF THE TRIPLET B(LOWER-CAPE) SIGMA-PLUS (V'=0) STATE OF CARBON-MONOXIDE

The University of Oklahoma PH.D. 1979

PLEASE NOTE:

In all cases this material has been filmed in the best possible way from the available copy. Problems encountered with this document have been identified here with a check mark ✓.

1. Glossy photographs _____
2. Colored illustrations _____
3. Photographs with dark background _____
4. Illustrations are poor copy _____
5. Print shows through as there is text on both sides of page _____
6. Indistinct, broken or small print on several pages ✓ throughout _____
7. Tightly bound copy with print lost in spine _____
8. Computer printout pages with indistinct print _____
9. Page(s) _____ lacking when material received, and not available from school or author _____
10. Page(s) _____ seem to be missing in numbering only as text follows _____
11. Poor carbon copy _____
12. Not original copy, several pages with blurred type _____
13. Appendix pages are poor copy _____
14. Original copy with light type _____
15. Curling and wrinkled pages _____
16. Other _____

University Microfilms International

300 N. ZEEB RD., ANN ARBOR, MI 48106 (313) 761-4700

THE UNIVERSITY OF OKLAHOMA

GRADUATE COLLEGE

LOW ENERGY IMPACT EXCITATION, ENERGY TRANSFER AND LIFETIME STUDIES OF THE $b^3\Sigma^+(v'=o)$ STATE OF CARBON MONOXIDE

A DISSERTATION

SUBMITTED TO THE GRADUATE FACULTY

in partial fulfillment of the requirements for the

degree of

DOCTOR OF PHILOSOPHY

By

JAMES ROBERT TWIST

Norman, Oklahoma

1979

LOW ENERGY IMPACT EXCITATION, ENERGY TRANSFER AND LIFETIME STUDIES OF THE $b^3\Sigma^+(v=o)$ STATE OF CO

A DISSERTATION

APPROVED FOR THE DEPARTMENT OF PHYSICS AND ASTRONOMY

APPROVED BY

David E. Golde

Michael A. Lampton

Edward T. Byram

S. E. Babb, Jr.

W. J. Kinkaid

Roger Finch

LOW ENERGY ELECTRON IMPACT EXCITATION, ENERGY TRANSFER AND LIFETIME STUDIES OF THE $b^3\Sigma^+(v=0)$ STATE OF CARBON MONOXIDE

J. R. TWIST

Department of Physics and Astronomy

University of Oklahoma

Norman, Oklahoma

1979

MAJOR PROFESSOR: DAVID E. GOLDEN, PH.D.

Abstract

The lifetime of the $b^3\Sigma^+(v'=0)$ level of CO has been measured using a delayed coincidence technique. Lifetime components of 51.86±0.24, 358±20 and 1500±900 ns at the 95% confidence level have been unfolded by computer fitting and extrapolating to zero pressure. In addition, the collisional quenching cross sections for the prompt decay and the first cascade component were determined to be $(7.7\pm3.8)\times10^{-15}cm^2$ and $(7.1\pm3.5)\times10^{-15}cm^2$ at the 95% confidence level. These results agree with spectroscopic evidence that the $a'^3\Sigma^+(v''=32\text{-}41)$ levels strongly perturb the $b^3\Sigma^+(v'=0,1)$ levels. Discrepancies with previous lifetime results are explained.

An estimate of the $a'^3\Sigma^+$ to $b^3\Sigma^+$ collisional transfer of excitation coefficient and dipole transition probability is presented along with a comparison with other recent quenching experiments.

DEDICATED

TO

BETTY AND INGRID

ACKNOWLEDGEMENTS

I would like to express my appreciation to Dr. D. E. Golden for his support and assistance throughout this work. To my comrades at arms, I offer humble thanks. Dr. Bill Paske contributed hours in the data handling and analysis. Nick Steph shared much valuable information concerning coincidence techniques and the statistics of counting experiments. Dr. Tom Rhymes had the original idea for the present pulsed RPD element and always lent a helping hand on electronics problems. Special mention goes to Dr. Gerry Haddad and Dr. Vic Sutcliffe for helping me to get started with the atomic and molecular group at O.U.

Without the excellent technical assistance of Woody Porter, Wayne Ramsey and Gene Scott in the Instrument Shop the present apparatus could not have been built.

Throughout this whole period my family has accepted my absence and strange hours with patience and understanding; I am eager to get to know them once more.

Finally I must mention the almost heroic efforts of my typist, Jacquine Littell, who has worked night and day to finish the final work on this dissertation.

TABLE OF CONTENTS

LIST OF TABLES

LIST OF FIGURES

ELECTRON IMPACT EXCITATION OF CO

CHAPTER I

INTRODUCTION

The lifetime of the $b^3\Sigma^+$ (v'=0) state of CO has been studied by a number of authors [1-8] with widely varying results. While some have reported pressure dependent lifetime components [4,5,8,9] others have not. [1-3,6,7]

The most recent measurement of $b^3\Sigma^+$ (v'=0) lifetime was made by Carlson et al.[9] They used an electron gun employing the high frequency deflection technique.[10,11] An intense beam of electrons is used to excite the gas molecules to reduce the blow-up of the beam by space charge. The energy of the electrons produced from the electron gun is about 7 keV. The beam had dimensions of about 0.2 cm^2 in the target gas and a net current of 15 milliamps. They used a 2 meter Jarrell-Ash vacuum scanning monochromator to record emission functions at high optical resolution. The lifetime measurements were made utilizing short excitation pulses. The intensities with the electron beam not pulsed and the lifetimes using a pulsed electron beam were studied as a function of

pressure of the target gas and also as a function of added foreign gas. The pressure functions were examined for each excited state and for the different initial vibrational levels.

Another lifetime measurement of the v'=0 level of the $b^3\Sigma^+$ state was made by Van Sprang et al.[1] by studying the $b^3\Sigma^+(v')\rightarrow a^3\Pi(v")$ transition using a delayed coincidence technique with a pulsed electron gun and a monochromator of 5-20 Å resolution. The decay constants were determined by fitting the data to either one or two exponentials for the lifetimes studied as a function of pressure in a scattering cell which was differentially pumped. In this work, the excitation pulse was varied between 100 ns and 10 μs and a short pulse was used in the case of the b state decay. The maximum for the b-a emission function was found to be at 13 eV and the lifetime data were obtained at that energy.

The lifetimes of the v'=0,1 levels of the $b^3\Sigma^+$ state have been measured by Smith et al.[2] These authors reported coincidence measurements between energy analyzed (50 meV resolution) inelastically scattered electrons and emitted photons which were filtered by a 2400-4200 Å bandpass filter. The lifetimes were studied as a function of the pressure in their molecular beam target using a time window of 400 ns. They expected multiple exponentials

in the decay of the v'=1 level since spectroscopic measurements have shown this state to be strongly perturbed.[12,33] However, their experimental sensitivity to multiple exponentials was low. They only observed one exponential decay, although a 3% background slope correction was made to the higher pressure data before analysis.

The lifetime of the b state was measured by Rogers and Anderson,[3] by studying the $b^3\Sigma^+$ (v'=0)→$a^3\Pi$ (v"=1,2,3,4) transition for a pressure range from 10 to 125 mtorr. These measurements used a hot cathode invertron[13] and a delayed coincidence detection scheme. Their lifetime data were fitted to a single exponential by graphical techniques using a record length of 0.5 μs.[14] A discussion of the older work, [4-8] has been given by Van Sprang et al.[1] and will not be given here.

The subject of resonances in CO has been reviewed by Schulz.[15] More recently resonances in CO have been observed in the $b^3\Sigma^+$ state optical emission function by Fukui et al.[16] and Bose.[17] Both observations were made by viewing photons from gas cells perpendicular to the electron beam direction. The work of Bose [17] used an energy resolution of 60 meV while that of Fukui et al.[16] used 0.3 eV. While the general shape of both of their emission functions is the same, there are small differences which are mostly due to the different energy resolutions. The pronounced threshold peak in the

differential cross section results of Mazeau et al.[18] and Swanson et al.[19] was observed as a shoulder at 10.44 eV on the dominant peak at 10.66 eV in the results of Bose.[17] In addition, a broad low intensity peak appeared at 11.14 eV in the work of Bose.

Some of the higher energy structure reported by Swanson et al.[19] was seen in the previous transmission experiment of Sanche and Schulz.[20] The structure at 11.25 eV in the differential cross section results of Mazeau et al.[18] and Swanson et al.[19] was identified by Swanson et al. as being due to the presence of an additional unidentified state of CO. The inelastic scattering of electrons from CO was previously studied by Comer and Read[21] in the energy range of 9.5 to 11.5 eV using the v"=0,1 vibrational levels of the $X^1\Sigma^+$ ground state as exit channels. They observed a Feshbach resonance at 10.02 eV with an energy resolution of 0.045 eV FWHM. The probable parent of this resonance has been identified by Schulz[15] as the lowest energy Rydberg state in CO i.e., the $b^3\Sigma^+$ state.

The 10.04 eV resonance was studied by Mazeau et al.[18] in the differential cross section in various exit channels. The resonant contribution to the $a'^3\Sigma^+$ (v"=26) exit channel was of particular interest since the direct scattering component was found to be low in this channel. This allowed the symmetry of the 10.04 eV resonance to be determined as $^2\Sigma^+$.[15,19]

The recent differential cross section measurement of Swanson et al.[19] has shown that the 10.04 eV resonance decays into the $a^3\Pi$(v"=0 to 6), $A^3\Pi$(v"=0 to 9) and $a'^3\Sigma^+$ (v"=12 to 27). They found the $a'^3\Sigma$(v"=26) exit channel to give a small direct scattering contribution in agreement with the results of Mazeau et al.[18]

The production of metastables in CO has been studied by several groups with some disagreement in the results. A peak near 8.3 eV was observed by Newton and Thomas,[23] in their UV photon production curve, which was not observed by Wells and Zipf.[24] Both Borst and Zipf,[25] and Wells et al.[26] observed a metastable state in CO near 10 eV with a lifetime of 0.1 msec and found evidence for at least one other metastable state. The photon and metastable production has also been studied by Brunt et al.[27] by electron impact in the energy region of 6-16 eV with an energy resolution of 25 meV. At excitation energies above 10 eV, they observed a smooth increase in the rate of production of metastables. This implies that there are higher lying metastables than the lowest triplet ($a^3\Pi$) at 6.0 eV. These results agree with those of Borst and Zipf,[25] and Wells et al.[26] In addition, Brunt et al.[27] have also observed a resonance at 10.044 eV in their metastable production curves, but they did not observe the broad peak at 8.3 eV which was seen by Newton and Thomas.[23]

In an effort to understand the rather large differences between some of the previous results we have remeasured the lifetimes and the quenching cross sections of the $b^3\Sigma^+$ state and the cascade components in a delayed coincidence experiment between a rapid electron gun shut-off and photons from the $b^3\Sigma^+$ $(v'=0)\rightarrow a^3\Pi(v''=0,1,2)$ transitions. In addition, we have also determined the optical excitation function using the time resolved technique of Golden et al.[28]

CHAPTER II

VACUUM SYSTEM APPARATUS

A. Vacuum System and Pumping System

The ultra high vacuum system consists of a 304 SS cylinder 6" O.D. and approximately 15" long and contains the experiment. Various flanges, tubes and electrical connectors are mounted on this vacuum envelope. All welds are TIG (tungsten inert gas) welded and thoroughly leak checked using a mass spectrometer. The top and bottom flanges are 9" O.D. and about 1/4" thick 300 series stainless steel (SS). The top flange of the system contains all of the gas inlet and pressure measuring tubes and a capacitance manometer head. Most of the electrical connections to the electron gun, scattering cell and Faraday cup are mounted on the top flange. Two types of electrical connectors are utilized: a multipin connector which is welded onto the flange and weldable MHV type high vacuum fittings made by Cerama-seal. The MHV fittings are used where necessary for their shielding characteristics. The electron gun and associated mechanical mounting hardware and the magnetic shield are also attached to the top flange. Four side arms mounted midway on the main vacuum envelope allow mounting of a

scattered electron detector at 90 degrees to the electron beam. One other side arm has an ultraviolet grade quartz window mounted in a graded glass seal and non-magnetic mounting welded to the 5" flange. The third side arm in use at the present time has a high vacuum triode ionization gauge connected to it. The ion gauge allows pressure measurement of the background gas while the experiment is running. The ionization gauge is on a 90 degree 1" O.D. elbow with light baffles to keep stray light out of the optical detection channel. The last side arm is not currently in use.

Several different types of seals are in use on the vacuum system. All seals are metal to metal, but vary in detail described below. Varian Conflat flanges use knife edge seals which seal on soft copper gaskets. Cajon compression fittings are used on some of the small tubing. These use a ring of semicircular cross section to bite into soft aluminum gaskets. The most widely used gasket is a soft aluminum wire held between flat SS flanges. The aluminum wire is dead soft 0.030" O.D. and is supplied on 100' rolls. An amount sufficient to reach around the flange with about 8" extra is cut off the roll. The ends are twisted together and the wire is carefully laid onto the sealing surface. The seal formed is metal to metal and very reliable as long as the flange bolts are torqued evenly. All flange seals, welds and fittings are leak

checked after they are installed and are leak checked at any time that the background pressure in the vacuum system shows an increase above the normal base pressure.

Connected on the bottom flange is an optically opaque trap of approximately 3 liters volume. The trap is filled to approximately half of its volume with Linde molecular sieve type 13X. This sieve is contained in baskets around the inside wall of the trap and in a basket in the middle of the trap. This molecular sieve has an alumina-silica base with a pore size of 10Å. The purpose of the sieve is to stop the pump oil in the diffusion pump from migrating into the high vacuum region and thereby contaminating the surface of the electron gun and scattering cell. The trap is so configured that a molecule must make multiple bounces to go thru the trap. In addition, oil is prevented from creeping up the sides. In this way the trap efficiency for the absorption of the contaminants is increased. One disadvantage of this type trap as compared to a liquid nitrogen trap is the amount of water absorbed into the alumina in the trap when the system is exposed to air. For this reason it is important to keep the trap evacuated after the electron gun has been removed from the vacuum system. This precaution will decrease initial pump down time of the system, as will back filling the system with N_2. The cost of operating with this type trap however, is a significant advantage over a liquid nitrogen trap. A

Varian VHS-4 oil diffusion pump is used to evacuate the vacuum chamber; it is rated at 1200 liters/sec of air below 10^{-3} torr. The diffusion pump uses Convoil 20 pump oil and the boiler requires 300 cc of oil to fill it. The Varian VHS-4 is backed by a Sargent-Welch 1397 fore pump. The pump has a speed of 300 liters/minute from 10^{-2} to 10^{-4} Torr. The free air displacement is 500 L/min. It is an oil sealed machanical pump. The forepump uses a lubricating type highly refined mineral oil. Since this oil has a relatively high vapor pressure at high temperatures, it must be kept out of the diffusion pump boiler. To accomplish this, an activated alumina trap is placed between the fore pump and the diffusion pump. A valve in the foreline closes when power is turned off to the fore pump. This maintains the diffusion pump at low pressure until the quick cool on the diffusion pump has time to cool the oil, thus avoiding oxidation of the oil and backstreaming of pump oil into the high vacuum region.

All exhaust from vacuum systems is vented into a continuously pumped vent to an area not normally occupied by personnel. This venting keeps oil vapor and any toxic gases out of the laboratory. Fig. 2.1 shows a schematic of the vacuum system.

In order to protect the vacuum system and associated experimental apparatus from interruptions of power, water or the failure of equipment, an electrical interlock system

FIGURE 2-1 VACUUM SYSTEM

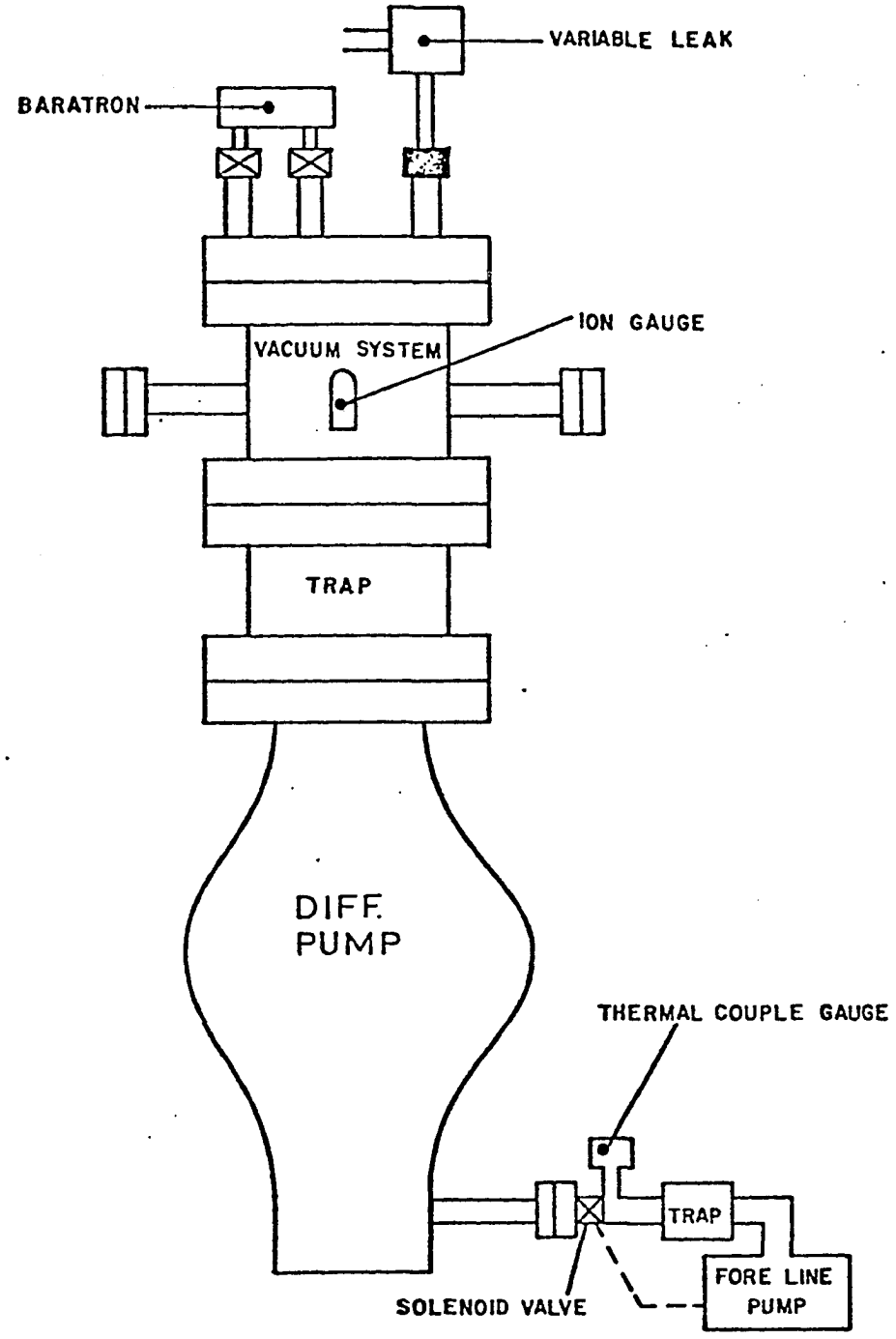

is wired to turn off the D.C. rack which powers the electron gun, to turn off the power to the diffusion pump heater and to cool the oil in the diffusion pump. The interlock wiring diagram is shown in Figs. 2-2 through 2-4.

Exposing the diffusion pump oil to atmospheric pressure while it is hot may cause the oil to break down or to ignite.[29] Prolonged operation of the pump at pressures above 10^{-3} Torr may cause excessive backstreaming of the oil into the high vacuum region. In order to avoid the above problems, the interlock system turns the diffusion pump heater power off and turns on the water into the quick cool lines whenever foreline pressure or vacuum system pressure rises above a certain level. This cools the hot oil in about 10 minutes. Operation of the interlock is described in detail in Table 2-1.

A pump down and bake out cycle is listed below. For proper operation and precautions in using the vacuum pumps, refer to the manufacturers' literature. A brief list of operating procedures follows.

Oil diffusion pumps must be protected from exposure to high pressure (greater than 1×10^{-4} Torr) for extended periods while the oil is hot. Heating up and cooling down times for a VHS-4 oil diffusion pump are 10 minutes. The quick cool line must be connected to the cold water supply during operation in order to have rapid cool down of the pump boiler in case of equipment failure.

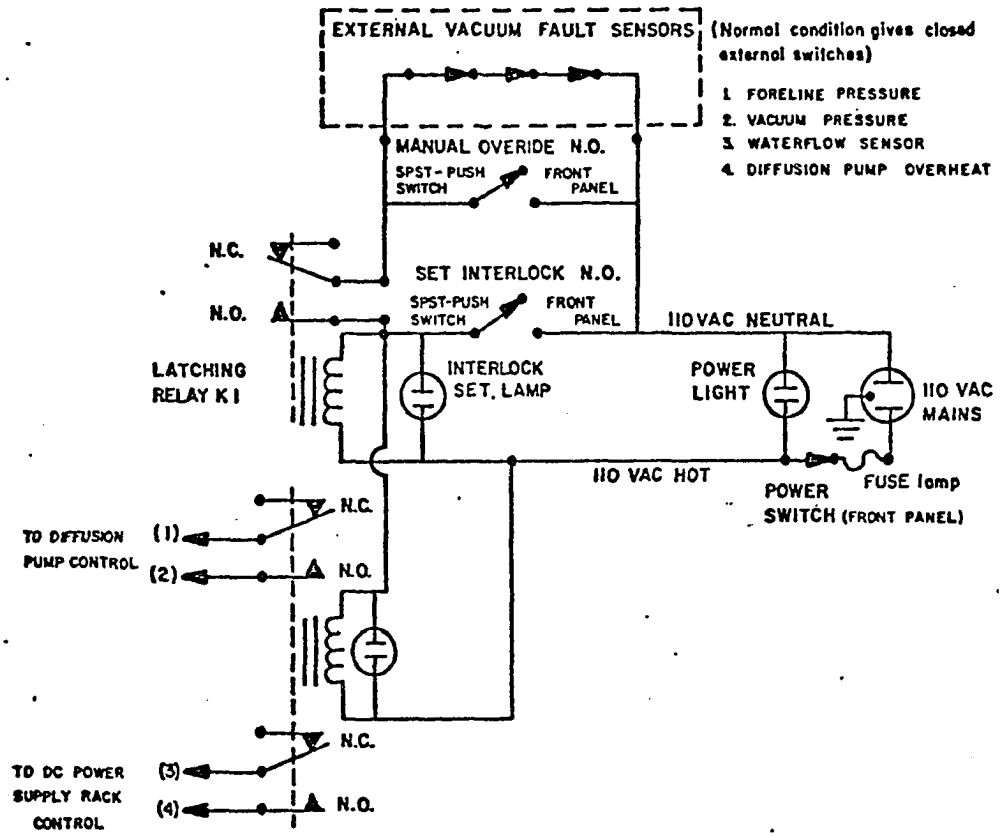

VACUUM SYSTEM INTERLOCK

FIGURE 2-2

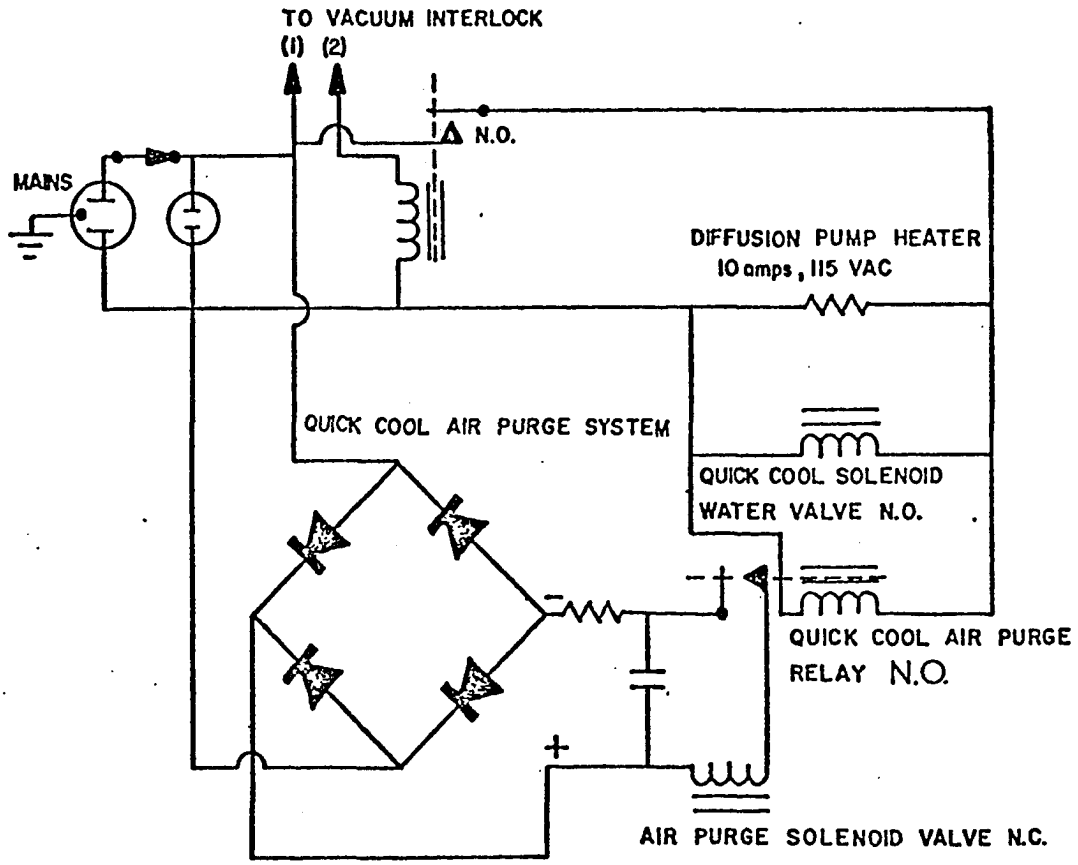

VACUUM SYSTEM INTERLOCK

FIGURE 2-3

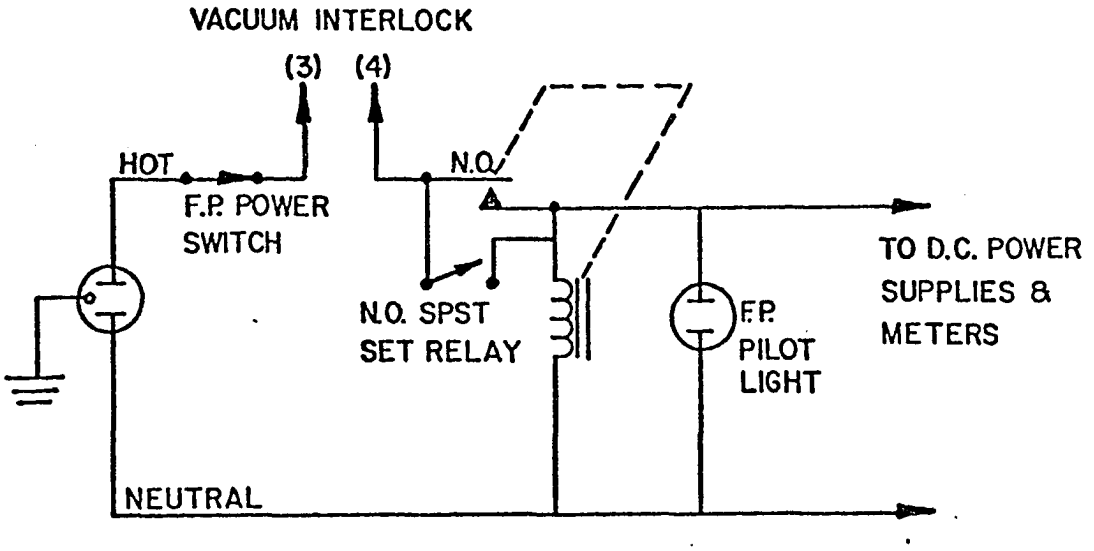

D.C. POWER SUPPLY RACK CONTROL

FIGURE 2-4

TABLE 2-1. Vacuum System Interlock Operation.

Sensor	Indication	Description of condition	Response
Triode ion gauge pressure reading	Reading less than 5 on chosen scale - set point variable 1 - 9	Normal condition	#1. None
Triode ion gauge pressure reading	Press. reading above 5 - any scale	Abnormal	#2. Turn off electron gun power rack. Turn off diff. pump. Turn on quick cool water.
Foreline pressure gauge readout	Foreline pressure less than 100 mTorr	Normal condition	Response #1 above
Foreline Pressure gauge readout	Foreline pressure greater than 100 mT (adjustable)	Abnormal	Response #2 above
Diff. pump overheat switch	Diff. pump boiler temp. less than approx. 300 C	Normal	Response #1
Diff. pump overheat switch	Diff. pump boiler temp. greater than approx. 300 C (adjustable)	Abnormal	Response #2 *consult factory before adjusting
Diff. pump water flow switch	Diff. pump cooling water flowing	Normal	Response #1
Diff. pump water flow switch	Diff. pump cooling water not flowing	Abnormal	Response #2

Table 2-1 (continued)

Sensor	Indication	Description of condition	Response
D.C. rack line power latch relay	110 VAC mains power interruption 100 ms or longer	Abnormal	D.C. rack turned off vacuum system
D.C. rack line power latch relay	Continuous 110 VAC mains power	Normal	Response #1
Interlock	Power pilot light off mains power interruption	Abnormal	Vacuum system will turn off-- when power returns only foreline pump will run

The oil sealed mechanical fore pump is designed to operate at higher pressures than the oil diffusion pump. Extended operation at 100-200 mTorr is acceptable with this type of pump. At higher pressure the pumps tend to lose oil from their crankcase. This lost oil must be replenished to avoid running too low on oil for proper lubrication. When pumping substances (mainly water) that can dissolve in the oil, the ballast valve must be opened during initial pump down for short periods to purge the oil of these condensable substances. Otherwise the pump oil may become permanently contaminated and must be replaced.

Initial pump down of the vacuum system may be done while leak checking is performed. After two days of pumping, the vacuum system pressure should reach 2×10^{-7} Torr if no large leaks are present. To find small leaks, two methods are utilized. The first method is to spray the suspected area with acetone or ethanol and watch for an increase in pressure on the ionization gauge. Note that only reagent grade chemicals are to be used for this step. The second and most sensitive method, although somewhat slower, involves tuning to the He peak on the mass spectrometer which has been previously pumped down to low pressure ($<10^{-5}$ Torr). Two techniques are then followed. A large plastic bag is placed around a section of the apparatus and filled with helium. An increase in output of the mass spectrometer

indicates that helium is entering the vacuum system through a leak and being detected in the mass spectrometer tube. The leak may then be located by probing the surface of the vacuum system with a small tube connected to a helium bottle with a regulator set for 10-30 cc/min flow. An indication on the mass spectrometer of He will indicate the location of the leak.[30,31] Another technique is utilized to find large leaks. They may be detected by the sound of hissing air entering the leak or with soap bubbles in the case of a pressurized system. The vessel with the leak may be pressurized with freon and a halogen flame detector used to probe the surface and locate the leak. Alternatively the vessel is evacuated with the halogen detector hooked to the exhaust of the fore pump. Freon is used to probe the suspected areas of the leak. A green color in the flame of the halogen detector indicates freon has entered a leak, been pumped from the vacuum system, exhausted from the fore pump and then detected.[32]

After leak checking and testing of all vacuum interlock circuits, the vacuum system may be baked out. High temperature bakeout is the process of pumping the system to low pressure at elevated temperature in order to remove surface contaminants from the vacuum system. A typical bakeout cycle is presented in Table 2-2.

Cleaning of the component parts is performed each time the vacuum system is opened and new parts installed or when

TABLE 2-2. Baking the Vacuum System

Elapsed Time hr	Main Vacuum System			Main Trap		Foreline Trap		Notes
	Power watts	Outer skin temp °C	Pressure torr	Power watts	Temp °C	Power watts	Foreline pressure mTorr	
0	0	20	2.5×10^{-7}	0	20	0	25	Initial pump down and leak check complete. Begin bakeout.
1	100	20	2.5×10^{-7}	0	20	0	25	Heat main vacuum system first. Keep traps cool until main vacuum up to full bakeout temp.
8	200	30	3×10^{-7}	*				Only changed items entered below
15	300	70	4×10^{-7}					
22	400	110	2×10^{-6}					
29		200						Main vacuum system up to full bakeout temp.
32			6×10^{-6}	50	20		25	Heat main trap first.
34				100	50		30	Keep temp below main vacuum system.
36				150	80		40	Water being pumped off main trap.
38				200	110		60	Highest press. reached.
40			1×10^{-5}	250	150		90	

Table 2-2 (continued)

Elapsed Time hr	Main Vacuum System			Main Trap		Foreline Trap		Notes
	Power watts	Outer skin temp °C	Pressure torr	Power watts	Temp °C	Power watts	Foreline pressure mTorr	
44							40	Drop in pressure indicates main trap now free of water
45						15	25	Main trap now to full bakeout temp.
47						30	100	Start heating foreline trap.
49						45	150	
51								Foreline trap losing water.
53						60	130	
59						60	60	Foreline trap at full bakeout temp.
83						60	50	Bakeout of both traps complete when foreline pressure stops increasing.
								Initial pressure.
89						0	50	Cool foreline trap.
113				0			40	Cool main trap.
119			1×10^{-7}		20		25	Bake main system only.
167								Start cooling main system.

Table 2-2 (continued)

Elapsed Time hr	Main Vacuum System			Main Trap		Foreline Trap		Notes
	Power watts	Outer skin temp °C	Pressure torr	Power watts	Temp °C	Power watts	Foreline pressure mTorr	
175	0		$5x10^{-8}$					Slowly over 8 hrs in 8 steps of power.
179		20	$5x10^{-9}$-$1x10^{-8}$					System cool.

*A blank space indicates item unchanged from last entry above.

surface discoloration indicates the need. Most cleaning techniques used are adapted from Rosebury.[32] Perhaps the most important cleaning technique is the copper etching process which will be covered in the section on the electron gun.

B. Pulsed Electron Gun

1. Introduction

The electron gun hook-up is schematically shown in Fig. 2-5 and a drawing of the gun (not to scale) is shown in Fig. 2-6. The basic construction and operating principles are described in Golden and Zecca.[33] It consists of a heated cathode in the Pierce configuration followed by a Pierce element[34] and an anode with a 0.040" aperture. The RPD monochromator, consisting of the system elements 2000, 3000, and 4000, is an electrically and geometrically symmetric arrangement. The outer apertured lenses are at 10-100 V. The lens 5000, 6000, and 7000 form a set of extraction optics which focus the image from the last Einzel lens (element 4000) aperture into the scattering cell or the Faraday cup. The energy of the electrons in the scattering region can be varied from about 0 to 110 eV. A Faraday cup with an inner collector and outer shield at the scattering cell potential collects that portion of the beam transmitted through the scattering cell.

The gun is constructed of OFHC copper tubes 1.5" O.D. with a 0.326" I.D. bore. The scattering region has three

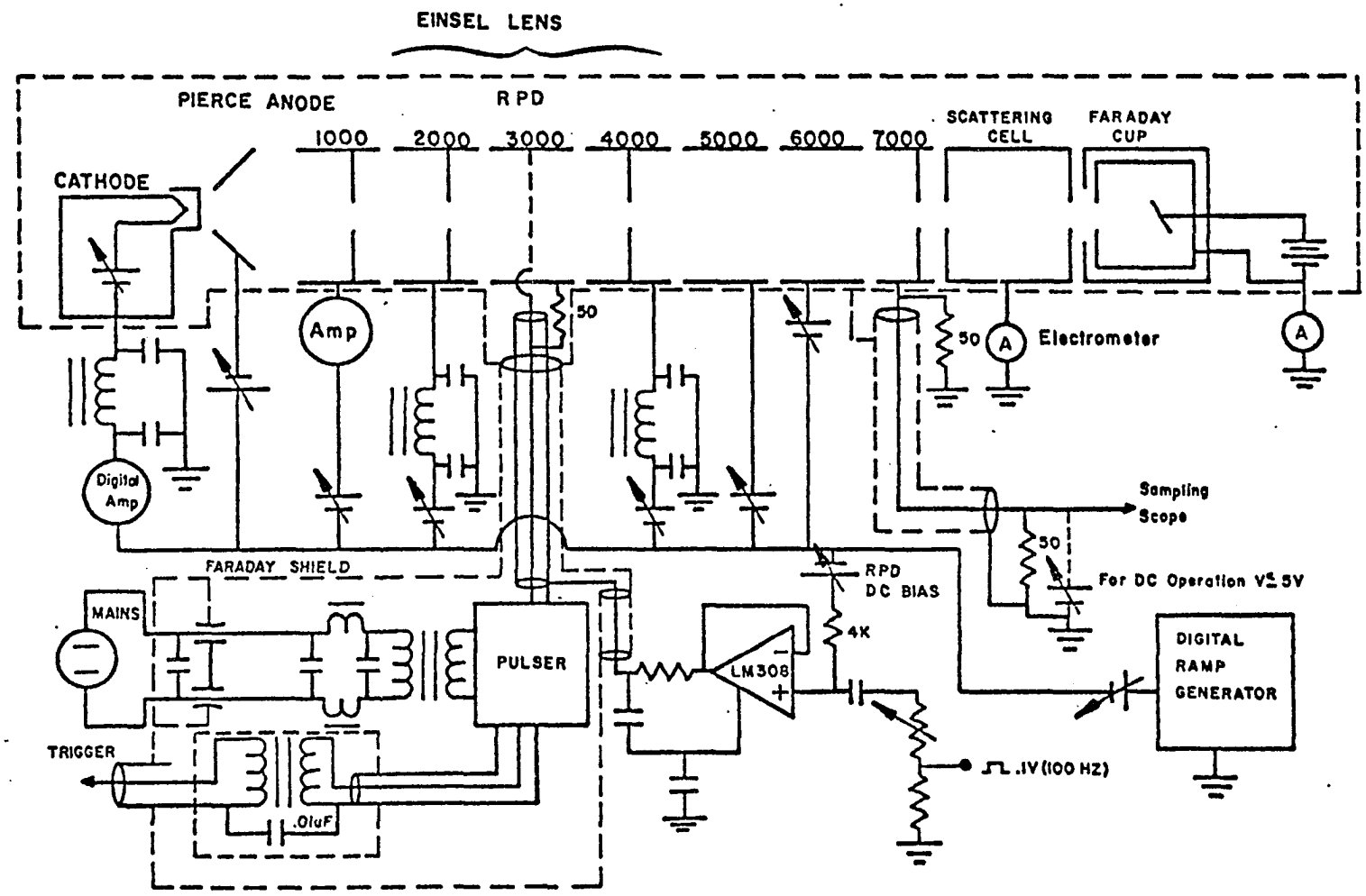

FIGURE 2-5 ELECTRICAL SCHEMATIC OF ELECTRON GUN

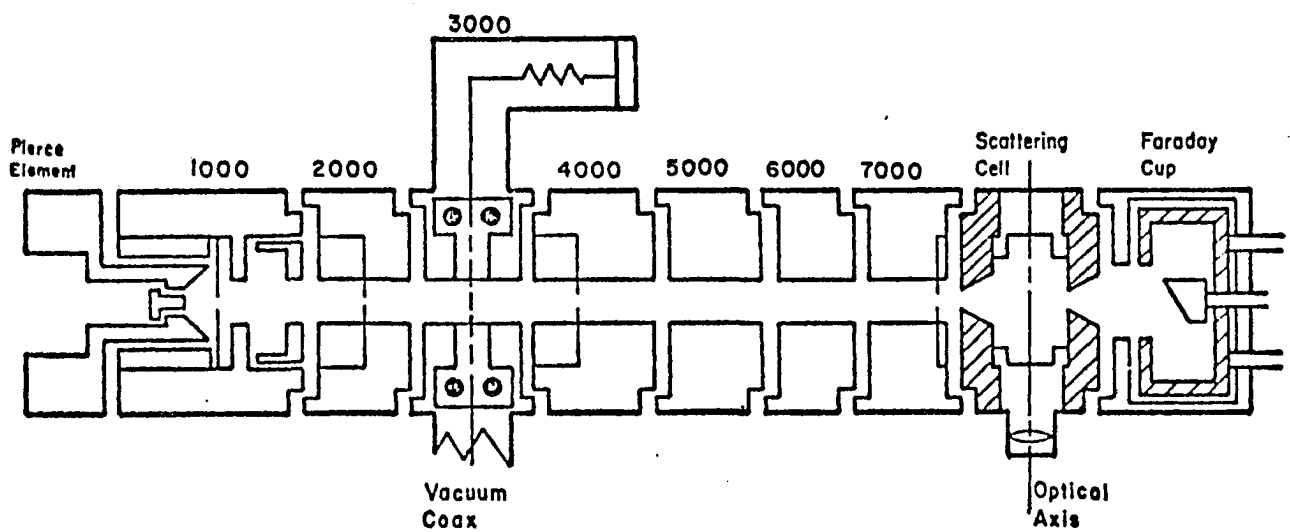

PULSED ELECTRON GUN - Cross-sectional view of elements.

FIGURE 2-6

0.040" I.D. apertures, two for the electron beam and one at a right angle to the beam for scattered electrons.

2. Cathode, Pierce, Anode System

The cathode and two following elements consist of a heated cathode, a Pierce element and an anode all in the Pierce geometry. First discussed by Pierce, the arrangement consists of a plane cathode, an equipotential surface (the Pierce element) at an angle of 67.5^{o} to the axis of the electron beam, and an anode with an aperture the diameter of which is small compared to the cathode to anode spacing. The Pierce element ideally is at potential zero with respect to the cathode, but actually provision is made to adjust this potential to account for differences in geometry due to construction tolerances and assembly. By changing the voltage of the Pierce element and using the focusing properties of the anode which is set at approximately 110 volts with respect to the cathode, the electron beam emerging from the anode aperture may be made parallel by the proper choice of electrode shapes and applied voltages. What is done in principle is to use the analytical solution for parallel flow of a beam of electrons between two planes to establish the potential distribution required to produce a parallel beam with no charge in the region outside the limits of the beam.[34,35] The Pierce element is placed between the cathode and anode. The shape of the element is that of the 0 volt potential

which makes an angle of 67.5° to the direction of the parallel electron beam.

In practice the angle on the Pierce element is usually made smaller than 67.5° to compensate for the diverging lens effect of the anode aperture as the beam emerges from the cathode-anode region. Thus it is possible to make a beam that is parallel and remains nearly so after leaving the anode aperture. The beam impinges on the aperture of the first element of the Einzel lens RPD monochromator.[33]

The cathode is an oxide coated nickel cup which is bonded to a ceramic disk about 1/2" O.D. The cathode is manufactured by RCA for operation in television picture tubes. The part number of the assembly is FKS623B-801F. The heater filaments are also made by RCA and have parts # MCH8004D and NEB261. The ceramic disk is clamped in a copper holder. The three electrical leads for the cathode and the insulated cathode heater are inside a 3/8" O.D. ceramic cylinder with four small holes running the entire length. The Pierce element is spaced as closely as possible to the cathode without electrically shorting to it. Usually this spacing is set at 0.020".

The cathode is capable of delivering 1.0 mA of current, but is generally set to deliver at from 200 μA to 450 μA of total cathode current. This current is monitored continuously by a Fluke 8000A digital meter placed in the cathode circuit.

The heater is operated at 7 to 8 watts of power which can be increased slightly as the cathode ages or to increase the beam current so that a particularly weak transition may be studied. The heater is a double coiled and insulated tungsten wire of about 1 ohm resistance at room temperature. One side of the heater is connected to the cathode to reduce back emission from the cathode.

The present electron gun is capable of delivering one to 2 μA of beam current inside the scattering cell at electron energies of 10 to 100 eV. At 15 eV the beam current is 2 μA in the scattering cell and about 25 nanoamp in the Faraday cup with no gas in the scattering cell.

3. RPD Monochromator

The principle of the RPD (Retarding Potential Difference) type monochromator has been discussed by Fox et al.[36] This type of monochromator has been used by several workers for the determination of various cross sections.[37,38,58] See Figs. 2-7 and 2-8 for the construction details of the RPD element and its electrical connection.

The RPD monochromator consists of an electrically and geometrically symmetric Einzel lens. The center 3000 element has a grid mounted in its center. The lens is also symmetric about a plane through the retarding grid. The parallel beam from the Pierce cathode arrangement impinges

RPD
LENS ELEMENT 3000

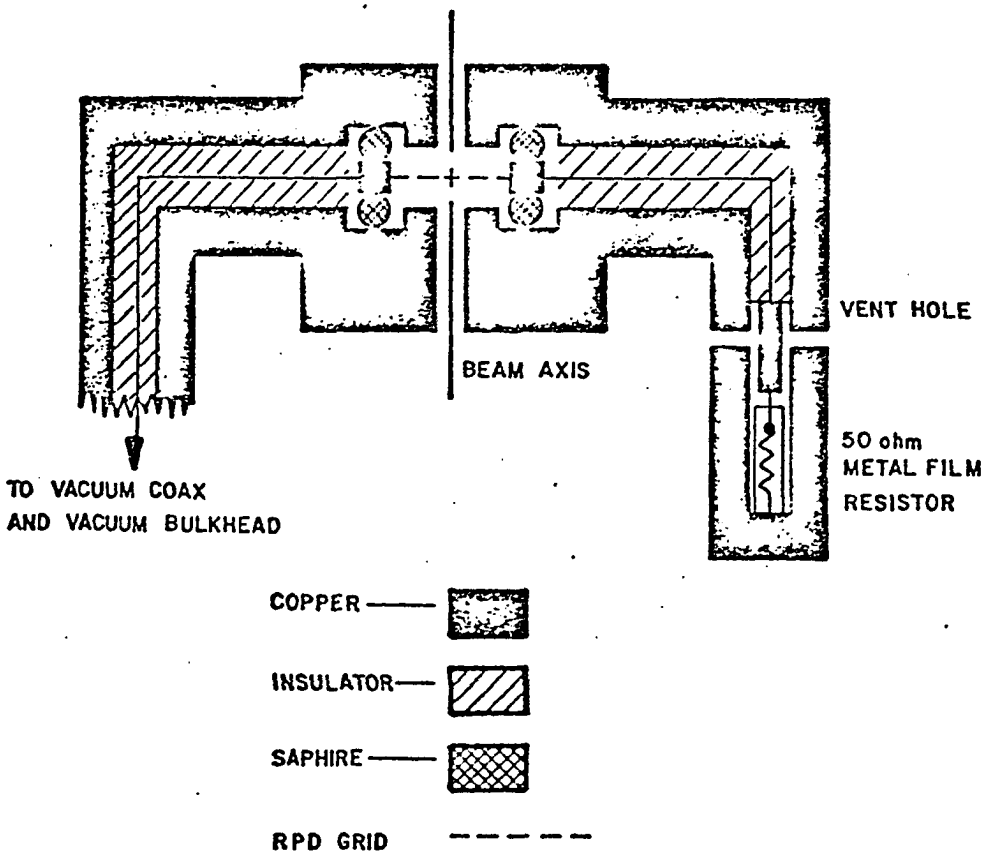

FIGURE 2-7

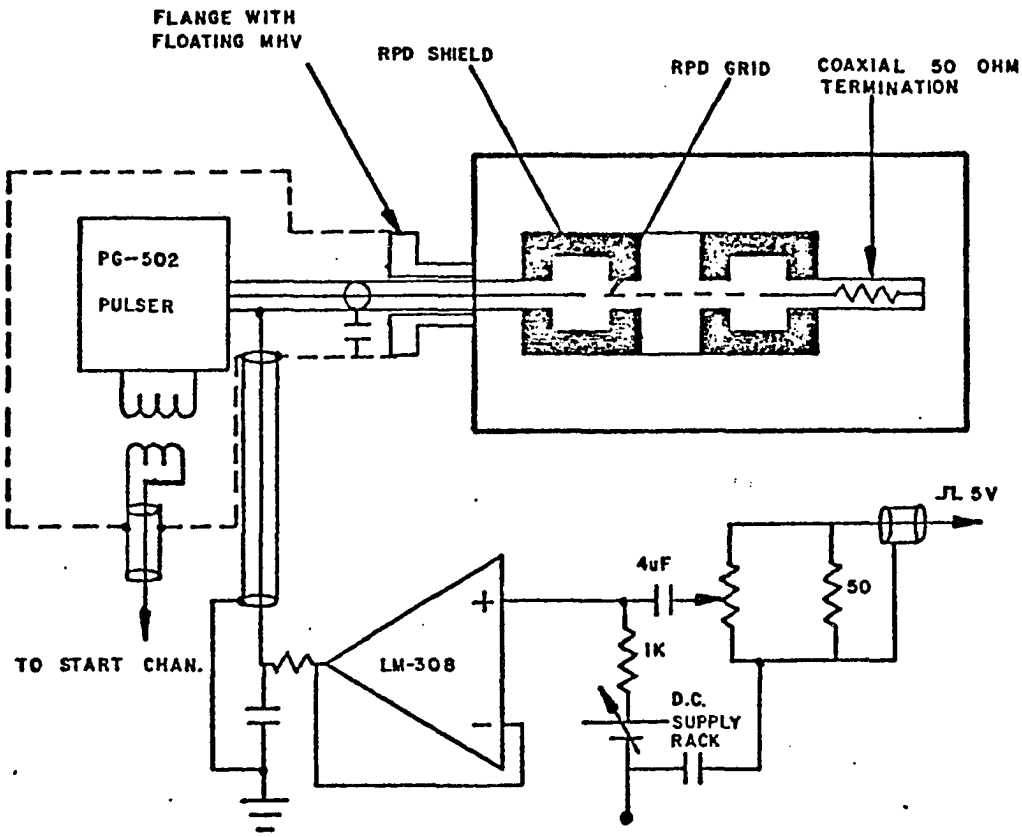

ELECTRICAL CONNECTION OF RPD

FIGURE 2-8

on the first Einzel lens aperture (element 2000). The beam is slowed as it passes into the region of the retarding grid and the beam expands. Due to the geometrical symmetry, only electrons that go through the first aperture and cross the retarding plane perpendicular to it will be imaged on the second aperture and allowed to pass through the monochromator. Since the field of the retarding grid is perpendicular to it, the grid will only act on the perpendicular velocity components of the electrons. This is the reason for the choice of geometries. For the best energy resolution, the electrostatic retarding field must act in the same direction as the total velocity of the electron. It is therefore important to have the electrons cross the grid perpendicular to it. The Einzel lens is configured to take an object at infinity (the parallel beam) and image it on the exit aperture. It does this for a wide choice of outer element voltages[39] as long as the outer Einzel elements are at the same voltage. The retarding grid is usually set at 1.5-3.0 volts with respect to the cathode. The grid is used to do the following things: A 100 kHz to 1.0 MHz square wave with a 1.0 nsec rise and fall time is applied to the grid to turn the electron beam off, and a low frequency (100 Hz) signal is applied with an amplitude of 0.1 to 0.3 V peak to peak amplitude which serves to modulate the electron energy distribution passed

by the retarding element when high energy resolution spectra are collected. The high frequency wave varies from 0 to 3 volts with respect to the outside of the RPD. The outside of the RPD is biased 1.5 to 3.0 volts D.C. with respect to the cathode. Thus it is possible by phase sensitive detection methods to detect a signal due to electrons in only a small energy region of the total energy distribution of electron beam.

The pulse applied to the RPD grid is supplied by a Tektronix PG502 pulser via a coaxial connector on the top flange of the vacuum system through a 50 ohm vacuum coax and into the cavity containing the RPD grid. The molybdenum grid is insulated from the outside OFHC copper shield of the RPD and is held in place inside the cavity by six sapphire balls which are 0.125" O.D. Opposite the constant impedance connector which attaches the coaxial line to the RPD is a coaxial 50 ohm terminator. The terminator is connected to the RPD grid by a constant impedance coaxial line and fittings. The 50 ohm resistor is a metal film 1% resistor with its epoxy coating stripped off, cleaned and vacuum baked for 24 hours before installing on the RPD.

The pulse from the PG502 has a rise time of 0.6-0.8 nsec measured on a Tektronix 555 oscilloscope with a 1S1 sampling unit. The 0 to -3 volt pulse is applied between the grid and the RPD shield. When the voltage is zero,

the RPD operates as described by Golden and Zecca.[38] It is only when the grid goes 3 volts negative with respect to the outside of the RPD that this operation is interrupted and the beam shuts off. The PG 502 pulser is operated in the back terminated mode (output impedance is 50Ω), and the RPD end of the coax is also terminated in 50 ohm. This reduces reflections from the ends of the cables to a minimum and improves the timing resolution of the apparatus.

4. Pulse Techniques

Proper termination of all coaxial lines is very important where fast rise time pulses are utilized, especiayly when switching an electron beams since they respond very rapidly.[41] The dimensions of a coaxial line for a given characteristic impedence may be calculated from the formula[42,43]

$Z_0 = (138/\sqrt{\varepsilon}) \log_{10}(D/d)$

d - diameter of inner conductor

D - inside diameter of outer conductor

ε - dielectric constant of dielectric media between two conductors.

For lengths of conductor less than 1/10 λmin where λmin is the shortest wavelength signal on a line, the conductor does not exhibit characteristics of a transmission line. However, for longer lengths the conductor should be made

into a transmission line terminated on both ends in its characteristic impedance.[44] When a transmission line is not terminated with its characteristic impedance, the pulses sent down the line will reflect off the end where the improper termination is connected. This will cause a series of reflections to be formed on the line which distorts the pulses and changes timing information contained in the pulses. If the termination is a complex impedance, the transmission line will have a reflection coefficient that is a function of frequency. To be specific, if a line is to be designed that will pass pulses with 1 nsec rise time with no distortion, the termination impedance should be equal to the characteristic impedance of the transmission line and should exhibit no reactive or capacitive components up to 1 GHz assuming a rise time (10%-90%) given by $T_r = 1/fmax$. In addition, no connecting wires which are not transmission lines can have lengths longer than

$$\frac{\lambda_{min}}{10} = \frac{c}{1\ GHz} = 3\ cm$$

assuming free space velocity where

$\lambda_{min} = c/f_{max}$ and $f_{max} = 1/T_r$

λ_{min} - shortest wavelength

f_{max} - maximum frequency used

c - velocity of wave in media

T_r - 10% to 90% rise time.

The effect of a mismatch in terminating a transmission line is described in many references[43,45] which consider how to determine the magnitude of the effects. There are two common ways to test a transmission line and termination system. With a fast rise time pulser and a wide band oscilloscope, pulses are applied to one end of the terminated line and examined on the other terminated end with the fast scope. The wave form of the pulses is examined for lengthened rise and fall times or any distortion which indicates reflections. If the transit time of the pulse down the entire length of the line is long compared to the width of the pulse, a series of pulses of diminishing amplitude will be observed if a mismatch exists. The quality of the impedance match may be estimated directly from the amplitude of the reflected pulses or the distorted rise and fall times.

Another way of measuring impedance matching is with a wideband A.C. noise bridge and a wideband oscilloscope. A noise bridge directly gives either the magnitude of the complex impedance or both its reactive and resistive components.

When a pure resistance terminates a transmission line, the voltage amplitude of the reflected wave as the fraction of the incident wave is given by the reflection coefficient, ρ, where

$$\rho = (R-Z_0)/(R+Z_0)$$

R - terminating resistance

Z_0 - characteristic impedance of line.

Note that if $R>Z_0$ than $0<\rho<1$ thus the voltage of the reflected pulse has the same phase as the incident pulse. If $R<Z$, then $-1<\rho<0$ thus the phase of the reflected wave's voltage is 180 degrees out of phase from the incident pulse. If $R = Z_0$, then the amplitude of the reflected pulse is zero there is no reflected signal and all the incident pulse is absorbed by the terminator R. In the case where $R = Z_0$, the transmission line appears to be infinitely long.

Two special cases will be considered:

1. $R = 0$, i.e. a short circuit

   $\rho = -1$, the reflected wave 180 degrees out of place and its voltage is equal to the incident wave. The two voltages add at the termination and the sum is equal to zero which is just the condition for a short circuit. No power is absorbed by R since $R = 0$.

2. $R \to \infty$, e.e. open circuit

   $\rho = 1$, the reflected wave is in phase and its voltage is equal to the incident wave. The sum of the voltages of the two pulses gives twice the voltage of the incident pulse. No power is absorbed by the load since the current is zero.

The quality of an impedance match may be expressed as a voltage standing wave ratio (SWR) or simply SWR.

$$SWR = R/Z_0 \quad \text{if } R>Z_0$$

$$SWR = Z_0/R \quad \text{if } R<Z_0$$

In the case of a complex terminating impedance Z, SWR is given by

$$SWR = Z/Z_0, \; Z>Z_0 \quad \text{where } \vec{Z} = R+iX$$

$$SWR = Z_0/Z, \; Z_0>Z \quad \text{and } Z = |\vec{Z}|$$

R - resistive component of Z

X - reactive part of Z.

The SWR is normally the quantity measured with electronic equipment such as reflectometers. Knowing this quantity, the reflection coefficient, ρ, may easily be calculated.

$$\rho = (SWR-1)/(SWR+1)$$

Typical SWR encountered in the range 50 to 1000 MHz are 1.5 to 2.0. A SWR of less than 1.2 is to be considered quite good for most applications, since a SWR of 1.2 corresponds to a voltage reflection coefficient of only $\rho = 9.1\%$.

The 50 ohm terminator and vacuum coax for the RPD have been tested as outlined above using pulses from a Tektronix PG502 pulser which have 0.6-0.8 ns rise and fall times between 10% and 90%. The pulses were observed on a Tektronix 555 scope with a 1S1 sampling unit. The pulse fall times are recorded for the pulse on a 50 ohm coaxial Textron terminator and then applied to the RPD with the probe placed near the 50 ohm terminator. The probe used

in both cases was a 2' length of RG-58 coax with the outer shield folded back over itself exposing about 1/8" of the center conductor. By comparing the waveform of the pulses before and after being applied to the RPD it was found that no noticeable difference in the wave forms existed on a 0.5 nsec/cm scale and that no reflections occurred on longer time scales. From this test the impedance match of the RPD and coax is determined to be acceptable.

Tests with an Omego-T[46] extended bandwidth noise bridge confirm the above results. The noise bridge used has a frequency response from 1 MHz to 300 MHz and measures a 60 ohm impedance which corresponds to a SWR of 1.2 and a reflection coefficient of 9.1%. Most of the impedance mismatch probable orginates from the capacitive load of the RPD grid inside the RPD shield. There is error in the vacuum coax geometry, since the wire was .021" O.D., while the holes in the fish spine beads which were the dielectric media were almost .060". The problem that reflected components could cause is to turn the electron gun on after the time at which the gun is supposed to be cut off. This would repopulate the states involved and severely distort the photon time spectra. Since the RPD square wave pulse amplitude was 0 to -3.0 volts, the reflected component would be apprximately 0.3 volts for a total voltage RPD grid to shield of -2.7 volts. D.C. measurements made by

monitoring the Faraday cup current showed that when the RPD grid to RPD shield voltage was greater than -2 volts, no detectable current reached the Faraday cup. It was concluded that the reflected component would not turn the beam back on.

5. Extraction Optics

The extraction optics lens elements 5000, 6000, 7000 focus the image of 4000 lens element aperture into the scattering cell. The 7000 element has two other functions. It acts as a shield for the scattering cell so that electrostatic fields will not penetrate inside the scattering cell. The last element, the 7000 element, has a .035" aperture mounted 0.10" from the entrance aperture of the scattering cell. The purpose of this aperture is to collect that part of the beam that would otherwise strike the region around the entrance aperture on the outside of the scattering cell. This reduces the zero pressure current collected by the scattering cell and thus makes measurements of scattered current more sensitive when gas is added to the cell. In either case, it is possible to measure the scattered electron current, but with the aperture in the 7000 element, the scattered current is a much larger fraction of the total scattering cell current. The great flexibility in focusing the image into the scattering cell is somewhat limited by the addition of the

aperture since, it is advantageous to keep the scattering cell aperture to 7000 element aperture lens weak by setting both elements at the same voltage. This constrains the 7000 element voltage to be nearly equal to the scattering cell voltage. This requires careful tuning of the gun voltages in order to keep the beam current nearly constant as the electron energy is swept. However, it poses no problem for lifetime measurements, since in this case the gun is tuned at a constant energy and operated at that point for the entire collection time.

A schematic of the electron gun element is shown in Fig. 2-5. Not detailed in the diagram are Π filters on 2000, 4000 cathode elements to reduce high frequencies. The schematic of the Π filters is shown in Fig. 2-9. They reduce all observable noise components to less than 5 mV peak to peak. The filters are contained in well shielded metal boxes to reduce stray noise pick-up.[52]

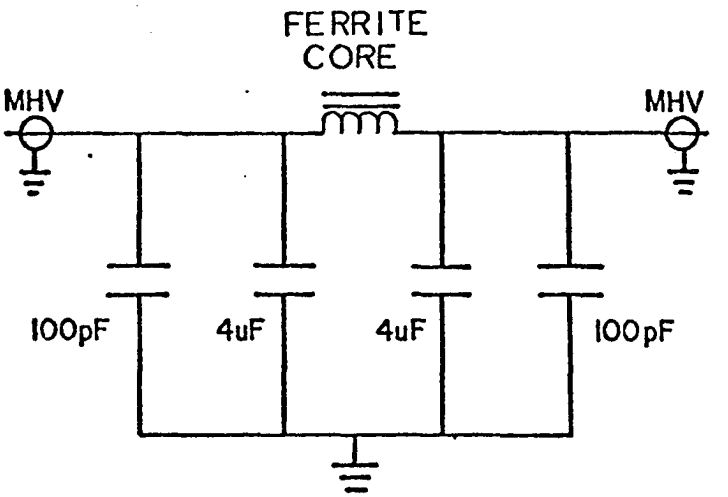

PI FILTERS

FIGURE 2-9

C. The Scattering Cell

The scattering cell is designed to contain the sample gas at pressures from 1 to 50 mTorr. One aperture on the beam line allows the beam to enter the cell and another on the axis allows the unscattered portion of the beam to continue on and be collected in a shielded Faraday cup. A third aperture allows electrons scattered at 90 degrees and photons to leave the scattering cell. The optical axis at 90 degrees to the electron beam allows study of photons produced due to the decay of excited molecules. A quartz window on the optical axis allows light out of the scattering cell. A lens is attached to the scattering cell to focus the U.V.-visible light towards a fast photon detector outside the vacuum system. A quartz window on a 8" sidearm flange completes the optical path.

The scattering cell is 1.62" long (inside) and 0.7" I.D. The three apertures are 0.040" I.D. Two apertures are on the beam line, and the third is on the optical axis opposite the 1" O.D. U.V. grade quartz window which is epoxied into the copper scattering cell with Varian TORR SEAL$_{TM}$. The quartz window is shielded from the scattering region by two 95% transmission copper grids spaced 1/16" apart by a copper ring and all grounded to the scattering cell. Two end caps on the cell which each carry one aperture are demountable to allow thorough cleaning of the cell.

Two 1/8" copper gas lines are attached to the cell. One is a static line which runs to a BARATRON capacitance manometer outside the vacuum system. The other line runs to the top flange and is connected to a 1/2" O.D. SS tube outside which is connected to a Granville Phillips leak valve. Both gas lines have Corning MACOR breaks for electrical insulation. The breaks are 3/4" long cylinders 5/16" O.D. which have a hole in them for gas flow. The copper lines are epoxied with TORR SEAL to the MACOR breaks.

The electrical isolation of the gas cell allows the scattered electron current to be measured by connecting an electrometer to the scattering cell lead. The other side of the electrometer is grounded.

The apertures in the gas cell allow it to run at a relatively high pressure (10^{-2} Torr), while the electron gun is operated in a lower pressure region ($2x10^{-5}$ Torr). By keeping the electron gun at lower pressures, the gun operating parameters are much less influenced by the pressure in the scattering cell. However, in spite of this pressure differential, each time the scattering cell pressure is changed it was found necessary to retune the voltages on the electron gun. The interaction of the background gas and the electron gun probably occurs mainly in the cathode-anode region. Changing the background gas pressure by changing the scattering cell pressure affects the cathode temperature and

therefore the cathode emission. More importantly, the gas pressure affects the space charge in the cathode-anode region by influencing the amount of ionized gas in this region.

D. Faraday Cup

Electrons that are transmitted through the scattering cell are collected in a shielded Faraday cup. The inner collector is biased 50-90 V with respect to the Faraday cup in order to collect low energy secondary electrons emitted from the collector surface. The Faraday cup is at the scattering cell potential. Its entrance aperture is 0.10" I.D. and is spaced approximately 0.20" from the Faraday cup shield. The Faraday cup shield is at the same potential as the scattering cell and it has an entrance aperture of 0.60" I.D. The outer shield serves as a mount for all Faraday cup parts which are insulated from it by $MACOR_{TM}$ spacers. It also serves to shield the scattering region from the collector voltage. The front surface of the collector is at a 45 degree angle to the beam line which causes most of the electrons scattered off the surface to travel in directions off the beam line. The secondary electrons have a cosine distribution as they are emitted from the surface.[47] The 45 degree inclination tends to reduce the number of secondary electrons emitted along the

beam line. Those electrons that hit the collector tend to stay in the back of the Faraday cup and off the beam axis until they are collected. To decrease the probability that an electron which is incident on the collector will scatter through the entrance of the Faraday cup, the solid angle that the entrance aperture subtends at the collector is made as small as possible.

Another constraint on the entrance aperture is that it admits the total amount of transmitted beam. The efficiency of the Faraday cup assembly can be checked as a function of beam energy by monitoring currents to the Faraday cup, shield and collector by increasing the collector bias voltage. A point is reached beyond which little improvement in collector efficiency is gained. Measurements indicate that the shield collects very small amounts (1%) of current compared to the Faraday cup and collector. This indicates that the Faraday cup is getting most of the beam and that secondary electrons are being efficiently collected.

The signal from the Farday cup is utilized in two operating modes of the electron gun. Then the gun is used in the pulsed mode but with no energy selection by the RPD lens system, the D.C. current to the Faraday cup is used to tune the voltages on the gun lens elements. When the current in the Faraday cup is maximized by tuning each lens voltage at a given electron energy of the scattering cell,

the focus of the electron beam is in the center of the scattering cell and the gun is tuned for maximum transmitted beam through the scattering cell averaged over the entire electron energy distribution emitted by the hot cathode.

If the voltage on each gun element is set to maximize the scattering cell current, the focus of the electron beam is set at the entrance aperture of the scattering cell. All the above tuning procedures are done with D.C. current measurements. This technique sets the beam geometry for an average over the entire electron beam energy distribution. By applying a low frequency signal to the RPD element and modulating the electron beam, a signal that is due to a narrow energy band of electrons in the energy distribution may be detected at the Faraday cup by a phase sensitive detector (PAR). By retuning the gun voltages, the focus region for a narrow distribution of electron energies may be chosen. The location of the energy slice chosen is set by the D.C. bias on the RPD element. The photon signal may also be used to tune the gun. As might be expected this signal is closely related to the scattering cell current.

E. Assemby and Cleaning of Electron Gun

After assembly of the electron gun, several checks are made to insure proper operation. An electricl diagram is drawn for the apparatus, and each element is checked for possible shorts to all other elements or to ground. Each element lead is checked for continuity from the element to the connector on the outside of the vacuum system. Also each connector is tested for high resistance leaks to ground which can upset sensistive electrometer readings.

As each element is spaced on the preceding element (0.020" to 0.030") and bolted in place, care must be taken to insure that the ceramic rods do not dig into the soft copper and cause the axis of the element to not be colinear with the axis of the other elements. A small light shining between the copper element and either or both ceramic rods will reveal this incorrect assembly. In other words, each element should touch both ceramic rods along the entire length of the element.

The Pierce element is so constructed that it shorts to the anode when the spacing on the O.D. of both elements is 0.016". Thus, if an anode to Pierce spacing at the beam line of 0.020" is desired, there should be 0.032" between the Pierce and anode elements on the outside surface. All the elements should be spaced so that there will be no optical path from the beam line to any insulators. The

closest insulator present is usually the ceramic rods upon which the gun elements are mounted. A x10 scale drawing of the cross section of two adjacent elements was made, and it was found that at a spacing of approximately 0.038" an optical line of sight just grazes the edge of the elements before intercepting the electron beam. Therefore, the elements are always mounted closer than 0.038". The effect of decreasing the interelement spacing is to make the electron lens between the elements stronger.[35]

Due to the heat generated by the cathode heater, the end of the gun near the cathode is at a higher temperature than the scattering cell and Faraday cup. Thus, the mounting bolts for the elements on the end of the gun near the cathode must be tightened more than those farther away. The extra tightness of the mounting nuts at the cathode end will insure that the elements do not slip even during temperature cycling caused by turning the power to the cathode heater on and off.

The alignment of the apertures on those elements that have them is accomplished by inserting a machined stainless steel guide into the bore of the element. The pin of the guide is inserted into the aperture and will insure correct alignment of the aperture and the axis of each element.

After all elements have been bolted in place but before the cathode assembly is installed on the Pierce element, the aperture alignment may be inspected by eye or with

a bore scope mounted on a x-y rotating table.

The cross hairs of the scope are centered on the first and last aperture made visible by a light shining on them and checking the location of the cross hairs on each aperture in turn as the bore scope focus is set on one and then on the other. Apertures should have no misalignment greater than 1/8 their diameter and much less is desirable. Considerable care is required in this step since any misalignments of the apertures will result in a drastic reduction of the beam intensity. Several apertures will not be directly illuminated due to the construction of the gun elements, so careful focusing is required to insure that each aperture is properly examined. Note that an aperture may be examined by either front light or back light. In case of the latter, a disk of light surrounded by a sharp black ring will be observed.

The RPD and 7000 element should be tested for proper high frequency operation in addition to D.C. checks. The element impedance measured from the coaxial fitting on the top flange should be 50 ohm when measured with a VOM and 50 ohm when measured by a wide band A.C. noise bridge.

The cleaning procedure described here has been adopted from that of Sutcliffe[48] and that of Rosebury.[32] The copper cleaning consists basically of an acid etch and several

rinses to leave the etched surface clear and free of any cleaning material. The following are the steps used in cleaning:

Clean container each time solutions are renewed with detergent. Rinse with tap water five times and then rinse using distilled water five more times.

1. Clean with abrasive pad and detergent in tap water to remove scale, oxide and grease. Rinse and scrub at same time to remove detergent.
2. Acetone dip - degrease.
3. Mix formic acid HCOOH 10% by volume, and hydrogen peroxide H_2O_2 5% by volume, and 85% distilled water. Use solution at room temperature. Small bubbles should form over entire surface of work. Leave in solution until surface shows a uniformly fine etch. Depending on condition of surface, this step takes 5-15 minutes. Replace solution when it turns dark blue or a dark residue is formed on work.
4. Distilled water rinse 20 seconds.
5. Methanol rinse and agitate 20 seconds.
6. Distilled water rinse and agitate 20 seconds.
7. Mix HCl 10% by volume and distilled water 90% by volume. Rinse and leave work in solution 5 to 10 minutes longer if finished pieces darken and turn red to yellow when exposed to air.

8. Distilled water rinse and agitate vigorously.
9. Acetone (reagent grade) rinse and agitate with ultrasonic cleaner 10 to 15 minutes. Change every 3 to 4 hours of use. Keep covered at all times.
10. Repeat step 9 above.
11. Remove piece from last acetone rinse. Rinse entire piece with clean acetone from squeeze bottle, especially bolt holes, corners and residue from last acetone rinse. Immediately blot drops and pools that form in cracks, crevices, and holes with a clean KIMWIPE$_{TM}$ towel and blow dry.
12. Store clean copper wrapped in KIMWIPE$_{TM}$ in a lined covered metal box.
13. Handle pieces only with chemically clean plastic gloves.

F. Photon Channel

The photon channel consists of U.V. grade quartz windows on the vacuum system and focusing optics, a monochromator, a cooled photomultiplier tube (PMT),[57] amplifiers, and a fast timing electronics.

A U.V. grade quartz lens is attached to the scattering cell; it has a 1" focal length and a diameter of 1". This lens takes a f/1.0 cone of light and projects it parallel to the optical axis as a 1" O.D. cylinder. The monochromator intercepts the light in the front slit of the Bausch

and Lomb High Intensity monochromator. No condenser lens was used. The monochromator has a reciprocal dispersion of 76 Å/mm. Its main feature is the large throughput of light possible with this instrument. At the blaze angle of 3000 Å the efficiency of the monochromator is 40% with a U.V.-visible grating of 1200 lines/mm designed to operate from 8000 Å to 2000 Å. The entrance optics of the monochromator are f/2.5 and the exit f/3.5 and uncollimated.

The advantages of the grating monochromator over band pass filters in the wavelength region of 2000 A to 3500 A are high efficiency, freedom from fluorescence that many dyes display, and convenient selection of the wavelength of light.

A trade off between intensity and spectral resolution has to be made with any optical instrument. This has limited the spectral resolution to 20 Å for all of this work. Other monochrometers are available for use on the experiment, one a 1/4 meter Jarrell-Ash with 33 Å/mm, the other a 16 Å/mm 1/2 meter Jarrell-Ash. Both are fine instruments, but the low current to the scattering cell has so far limited any use of them.

The photomultiplier tube (PMT) is an RCA type C31034A-02 with a Galleum Arsenide photocathode. This tube must be cooled to -20° C to reduce the noise generated by the

photocathode when it is at room temperature. The PMT has a wavelength response of 2200 Å to 8000 Å. The extended red response is due entirely to the cathode and the short wavelength response to the U.V. grade front window of the PMT. The time jitter associated with a PMT is due mainly to transit time differences as the group of electrons travel down the dynode chain. Also variations in pulse height contribute to uncertainties in timing pickoff electronics which trip at a certain voltage level. PM tubes also exhibit timing changes with wavelength and timing distortion when high background light levels are present.[49]

The particular PMT in use presently is rated at 1460 volts for a gain of 10^6 and 10 noise counts per second at a cathode temperature of -30 C. The noise count rate is very important since it sets the signal/noise ratio in a counting experiment for a given counting time. The main noise source in a counting experiment is the PMT, since electronic noise can be electrically discriminated against. It is not possible, however, to discriminate against dark counts that originate in the PMT, especially those from the photocathode, since they have nearly the same amplitude as the ones produced by light signals on the cathode. The rise time of pulses from the PMT is 2.5 nsec (10% to 90%). A device shuch as a PMT must be considered a wide band very

high gain detector not only wide band in wavelength of light but also in the output signal.[51] Thus all signal leads from the PMT must be well shielded coaxial transmission lines terminated on both ends. Amplifiers must be placed as close as possible to the detector (at least the first preamplifier). These amplifiers must be wide band impedance matched pulse amplifiers well shielded so as not to radiate spurious emissions back into the PMT circuitry. Finally the PMT must be well shielded from stray light, electrostatic and magnetic fields, and R.F. fields. Criteria for RFI/EMI shielding are given by METEX.[52]

The PMT is installed in a Products for Reserch cooler. This cooler, in addition to cathode cooling, provides magnetic shielding, R.F. shielding, shielding from moisture (it is hermetically sealed), and stray light. The magnetic shielding was checked with a Rawson-Lush[53] rotating coil gauss meter. This instrument utilized a synchronously detected signal from a rotating coil, the rotation of which is phase locked to the detector. The attenuation of the earth's magnetic field provided by the magnetic shield in the PMT holder was greater than 100.

Signals from the PMT leave the holder by a BNC connector. The signals are terminated at the BNC with a coaxial 50 ohm terminator. These signals at this point have a rise time of approximately 2.5 nsec and an amplitude of

-5 to -10 millivolts. A 4" long piece of RG58 A/U foam coax connects the PMT to an Avantek[54] preamp which has a 3 decibel bandwidth of 1 MHz to 1.5 GHz. This amplifier is A.C. coupled and has excellent frequency response with a 30 decibel gain. Since it is A.C. coupled, care must be taken that high count rates do not cause D.C. base line shifts, since this amplifier is designed for microwave C.W. service and has no base line restoration, as do many nuclear instrumentation type amplifiers. D.C. base line shifts must be avoided, since they will cause an effective change in the discriminator level setting. Even constant fraction type discriminators will be affected, because the shifts are D.C. in nature and cannot be detected by constant fraction mode circuitry.[70]

Exposure of the PMT to room lights tends to cause high dark count rates when the tube is returned to the dark and turned on. This extra dark noise is due to fluorescence of the glass envelope. Sunlight and fluorescent lights are expecially efficient in causing this phenomenon. Exposure of the tube only to a photographer's darklight will avoid the fluorescence in the glass due to the low levels of U.V. light from this type light. Of course, the PMT should never be operated when exposed to room light levels (C31034A-02 maximum anode current 100 nanoamp). The tube will be destroyed rapidly if this maximum anode

current is exceeded. Extended red response cathodes will, in addition, lose some of their red sensitivity after prolonged exposure to high levels of light in the red region of the spectrum. Some of the sensitivity returns after a time when the tube is stored in the dark with no voltage applied.[50,51]

G. Fast Timing Electronics

Optical Emission Functions:

Refer to Fig. 2-10 for the schematic for recording optical emission functions.

The high efficiency U.V. visible monochromator picks out a band of wavelengths to be detected by the PMT. Fast negative pulses from the PMT are amplified by two amplifiers and the polarity of the pulses is reversed by a Vari-L wide band pulse transformer.[55] The constant fraction discriminator generates a fast negative -0.5 volt timing pulse when the input pulse reaches 60% of its full amplitude. This pulse is the stop pulse for the ORTEC Time Amplitude Converters 467 (TAC) after being delayed a variable amount by a gate and delay generator.

The start pulses are generated by the trigger output of the Tektronix PG-502 pulser. The PG-502 is D.C. isolated from earth ground by means of a mains isolation transformer, a wide band pulse transformer, and low pass filters

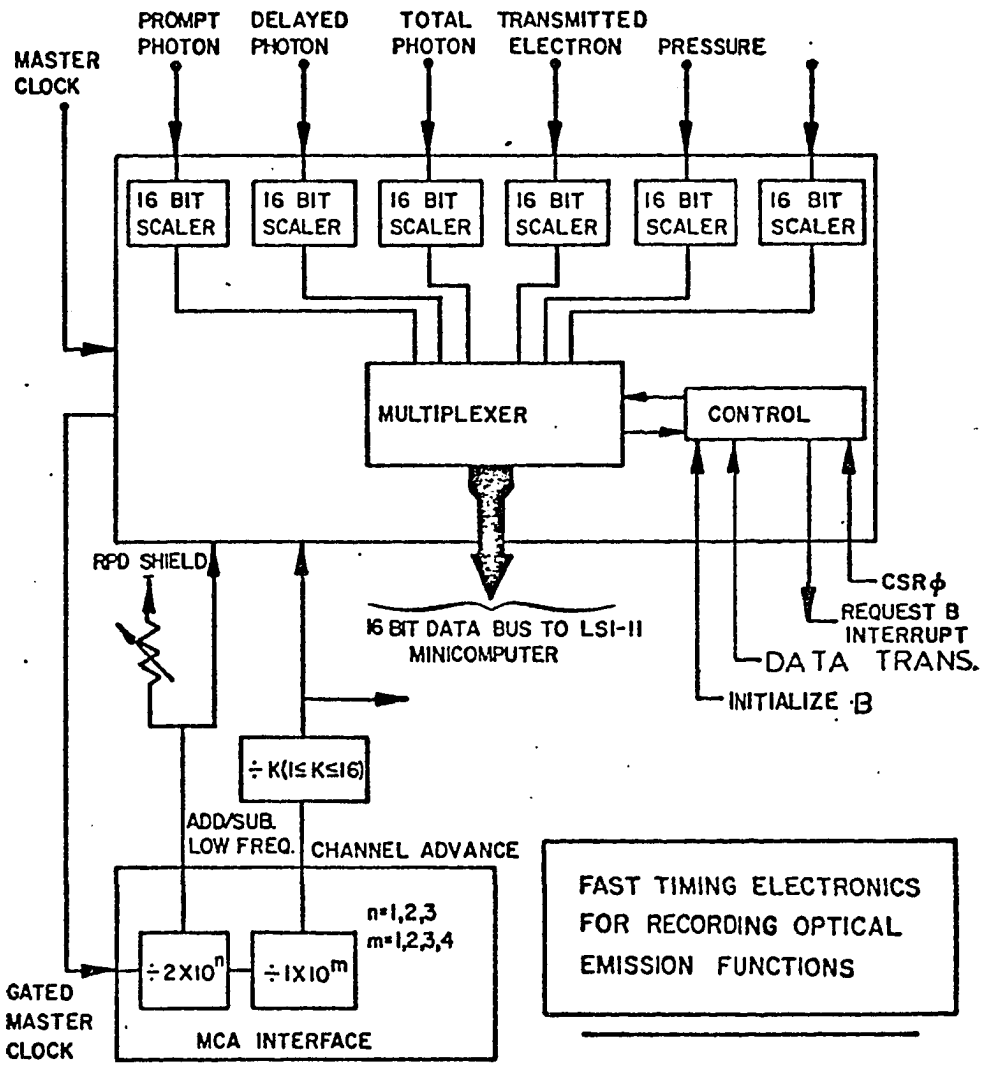
PROMPT PHOTON
DELAYED PHOTON
TOTAL PHOTON
TRANSMITTED ELECTRON
PRESSURE
MASTER CLOCK
16 BIT SCALER
16 BIT SCALER
16 BIT SCALER
16 BIT SCALER
16 BIT SCALER
16 BIT SCALER
MULTIPLEXER
CONTROL
RPD SHIELD
16 BIT DATA BUS TO LSI-11 MINICOMPUTER
CSRϕ
REQUEST B INTERRUPT
DATA TRANS.
INITIALIZE B
÷K(1≤K≤16)
ADD/SUB. LOW FREQ.
CHANNEL ADVANCE
n=1,2,3
m=1,2,3,4
÷2X10^n
÷1X10^m
GATED MASTER CLOCK
MCA INTERFACE
FAST TIMING ELECTRONICS FOR RECORDING OPTICAL EMISSION FUNCTIONS

FIGURE 2-10

on the A.C. mains to the pulser. A timing processing chain of timing filter, amplifier, constant fraction discriminator similar to the stop channel provides the start pulse to the TAC.

The photon signals are time sorted according to the upper and lower level discriminator settings on the single channel analyzer integral with each TAC. Time regions of interest are as follows: the delayed region long after cut-off of the electron gun, the prompt region just as the electron gun turns off, and total photon signal which is the entire range of the TAC. The delayed region emphasizes excitation processes with long lifetimes (>200 nsec), while the prompt region emphasizes mainly processes with short (<100 nsec) decay constants which consequently build up excited states faster than processes in the delayed region.

Each time the interface generates a channel advance pulse the computer locks all scalers and stops the experiment by locking the gated master clock out. The computer reads each scaler, stores the result in memory, zeroes the scalers, advances the digital ramp one channel and restarts the experiment by turning on the Gated Master Closk. The data collection is halted at the end of a preselected number of channels. Up to six scalers are available for recording data with the ultimate capability of the interface to handle 16 scalers.

The computer may also be gated by the add/subtract signal to alternately add and subtract the signals in the scalers. At the same time, a variable amplitude modulation is applied to the RPD and thus modulates the electron beam. Thus, the RPD monochromator is utilized to generate a synchronously detected signal that is stored in a scaler.

Lifetime Spectra:

In order to record time spectra, to measure excited state lifetimes, MCA (multichannel analyzers) are connected to the time amplitude converter (TAC) or TPHC (time to pulse height converter) (see Fig. 2-11). The MCA are set to record in the pulse height mode. The energy of the electrons in the scattering cell is fixed at some appropriate energy and time spectra collected. If two MCA are available, one is connected to TAC with a time scale x10 of the other. The purpose of this step is twofold. The short time scale spectra gives a record of the electron gun cut-off, while the longer time scale data allows observation of much slower collisional excitation processes that may be taking place. Fig. 2-11 shows a schematic of only the TAC and MCA, as all other instruments are the same as when emission functions are collected except that the digital ramp, computer and its interface are not in the circuit.

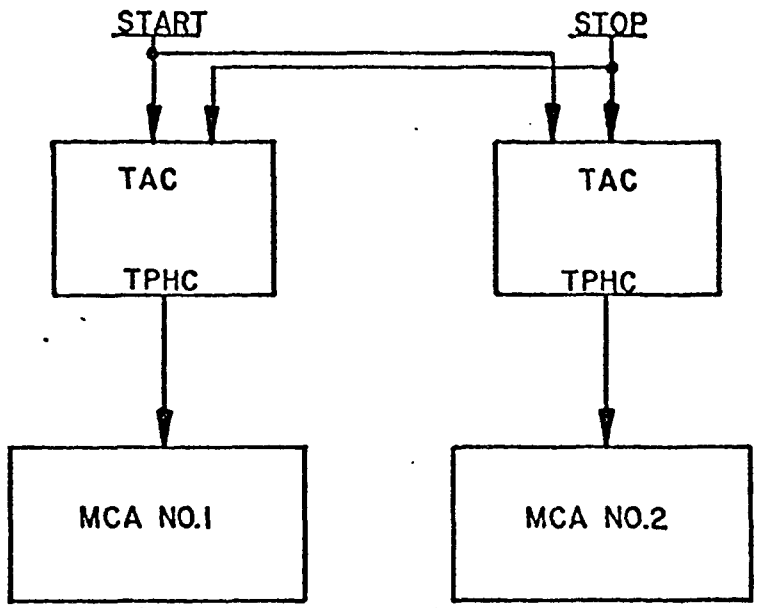

FAST TIMING ELECTRONICS FOR RECORDING LIFETIME SPECTRA.

FIGURE 2-11

H. Magnetic Shielding

The entire electron gun, gas cell and Faraday cup are surrounded by a magnetic shield. The attenuation of the earth's magnetic field provided by this shield is a factor of 150 measured by a Rawson-Lush rotating coil gauss meter. The shield is made of 0.10 thick molypermalloy and has been commercially hydrogen fired to give the shield its excellent magnet properties. The shield is a cylinder 18" long by 6" in outside diameter. It has two tightly fitting end caps by which it is mounted to the electron gun mounts. Holes are punched in one end cap to permit wires, cables and gas plumbing to exit. Holes along the O.D. of the cylinder permit light to exit along the optical axis. Provision has been made to look through the scattering cell along the optical axis through another hole in the side opposite the photon exit hole. The entire shield is degaussed with a degaussing coil each time the experiment is reassembled. The magnetic shield may be cleaned by mild detergent solution followed by several distilled water rinses and acetone rinses.

The shield must be protected from sharp blows, dropping and rough handling since these will tend to magnetize it. During any machining process, steps should be taken to keep the shield material cool as heating and work hardening will destroy the shielding properties of the material.

I. Gas Handling System

The gas handling system is constructed of all stainless steel. It consists of a high vacuum system and a high pressure system. Refer to Fig. 2-12 for a schematic diagram of the apparatus. The high vacuum system is bakeable and capable of reaching pressures of 10^{-6} Torr upon initial pumpdown. The high vacuum system is all stainless steel and bakeable to 150 C. The temperature is limited by Viton "0" rings in the Varian UHV valves. The high vacuum system consists of 2" O.D. stainless steel tubing and tees connected by 2-3/4" conflat flanges (Varian). The system is pumped by means of a Varian 2" oil diffusion pump which is trapped from the main system by a liquid nitrogen cooled trap made by Granville Phillips to reduce the backstreaming of diffusion pump oil. The oil diffusion pump is backed by a 1397 Welch foreline pump. The foreline has an activated alumina trap to reduce fore pump oil contamination of the diffusion pump oil.

A triode ion gauge allows measurement of low pressures 10^{-4} to 10^{-7} Torr. The ion gauge is also used for leak detection by means of acetone or alcohol sprayed on the outside of the vacuum system at the location of suspected leaks.

FIGURE 2-12 GAS HANDLING SYSTEM

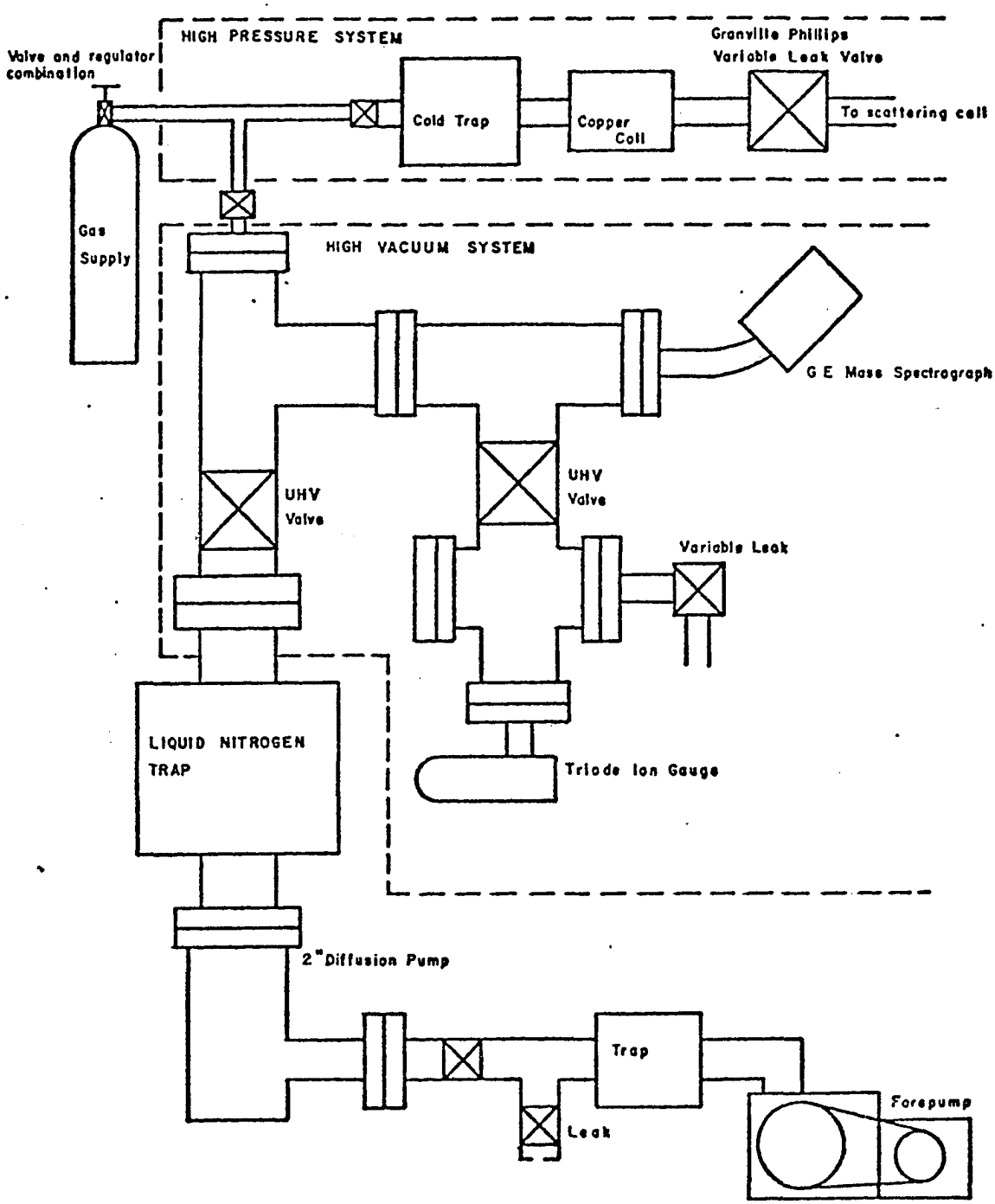

A General Electric mass spectrograph is used to pinpoint small leaks by tuning it to the He peak and spraying He on the surface of the vacuum system by a small tube. The variable leak (Granville Phillips) allows small amounts of He to be leaked into the system in order to allow precise adjustment of the mass spectrograph on the He peak.

The high pressure system is designed to operate from 5 to 200 psi. The pressure is supplied by a stainless steel high purity Matheson regulator (3500-580) with a teflon diaphragm which is connected to a supply tank at 1800 psi of high purity gas. In the case of CO, the supply tank is made of aluminum to avoid the formation of iron carbonyls which readily form at pressures above 500 psi.[56] All valves in the high pressure region are welded bellows valves. Fittings are Swagelock type 316 stainless steel. Tubing used in the high pressure system is stainless steel type 304 seamless 1/2" O.D. tubing except for a 10" piece of 1/4" O.D. copper tubing which is formed into a 5" O.D. coil for strain relief.

The cold trap is formed by a 3' long section on 1/2" O.D. stainless steel tubing mandrel bent in a "U" shape. The cold bath is methyl alcohol chilled to -90 C by a freon cold finger and held in a 4 liter dewar. The freon cooler is capable of cooling to a temperature of -90 C and is a cascaded freon compressor machine. The cold trap removes

condensable materials, including any carbonyls that may be present. The cascaded cooler must only be operated with the cold finger in the alcohol bath to avoid damage to the freon compressors.

The fore line trap can be baked out at a temperature up to 120 C, but the temperature is limited by a viton O-ring in the body of the trap. After baking for 1-2 days, the fore line trap is cooled and ready for service. Initial pumpdown to 10^{-6} Torr takes approximately 1-2 hours after the system has been open to air. The system is leak checked with acetone and the triode ionization gauge or the mass spectrograph each time the high pressure system has been opened or at more frequent intervals, if deemed appropriate.

FIGURE 2-13
FAST TIMING ELECTRONICS FOR RECORDING OPTICAL EMISSION FUNCTIONS

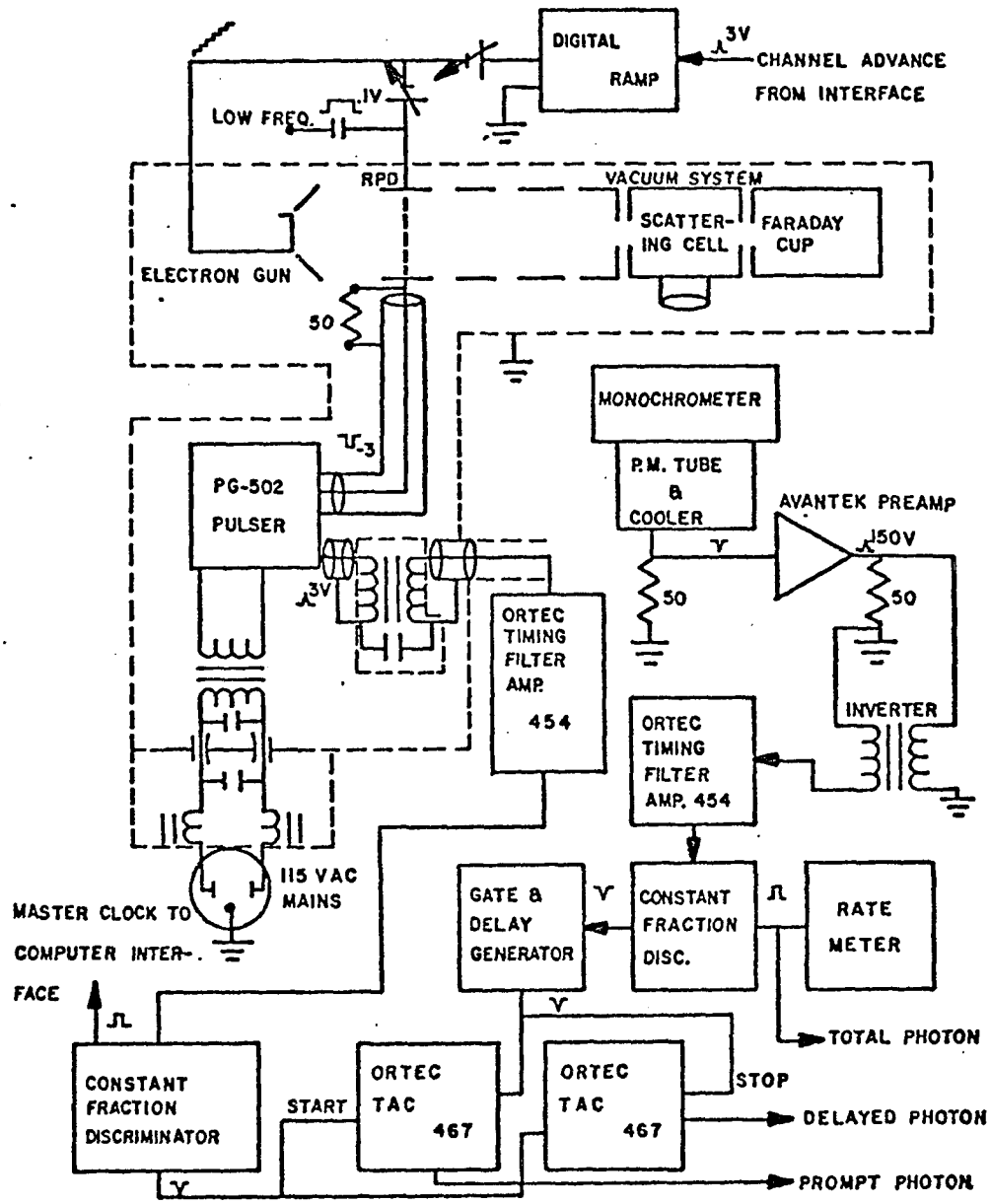

CHAPTER III

THEORY

This section presents the solutions to the rate equations that govern the population densities of the states under study. The population of the $b^3\Sigma^+$ ($v'=0$) level (refer to partial energy level diagram Fig. 3-1) under electron impact is determined by the electron impact across section for excitation to the $b^3\Sigma^+$ state as well as by any cascades from higher levels and by perturbations by near lying high vibrational levels of the $a'^3\Sigma^+$ level.[12,59-63] The theory will be set up in a general way and later applied to the measurement of the lifetime of the $b^3\Sigma^+$ ($v'=0$) level of CO.

If a beam of electrons is directed into a region containing ground state molecules, some of the molecules will be excited to higher energy levels. The population of the Kth level in Fig. 3-2 is monitored optically by observing light emitted when the molecule makes the transition K→L. Level L can be the ground state or another level of the molecule.

The population of the J and K levels is governed by the equation

CO

ENERGY LEVELS

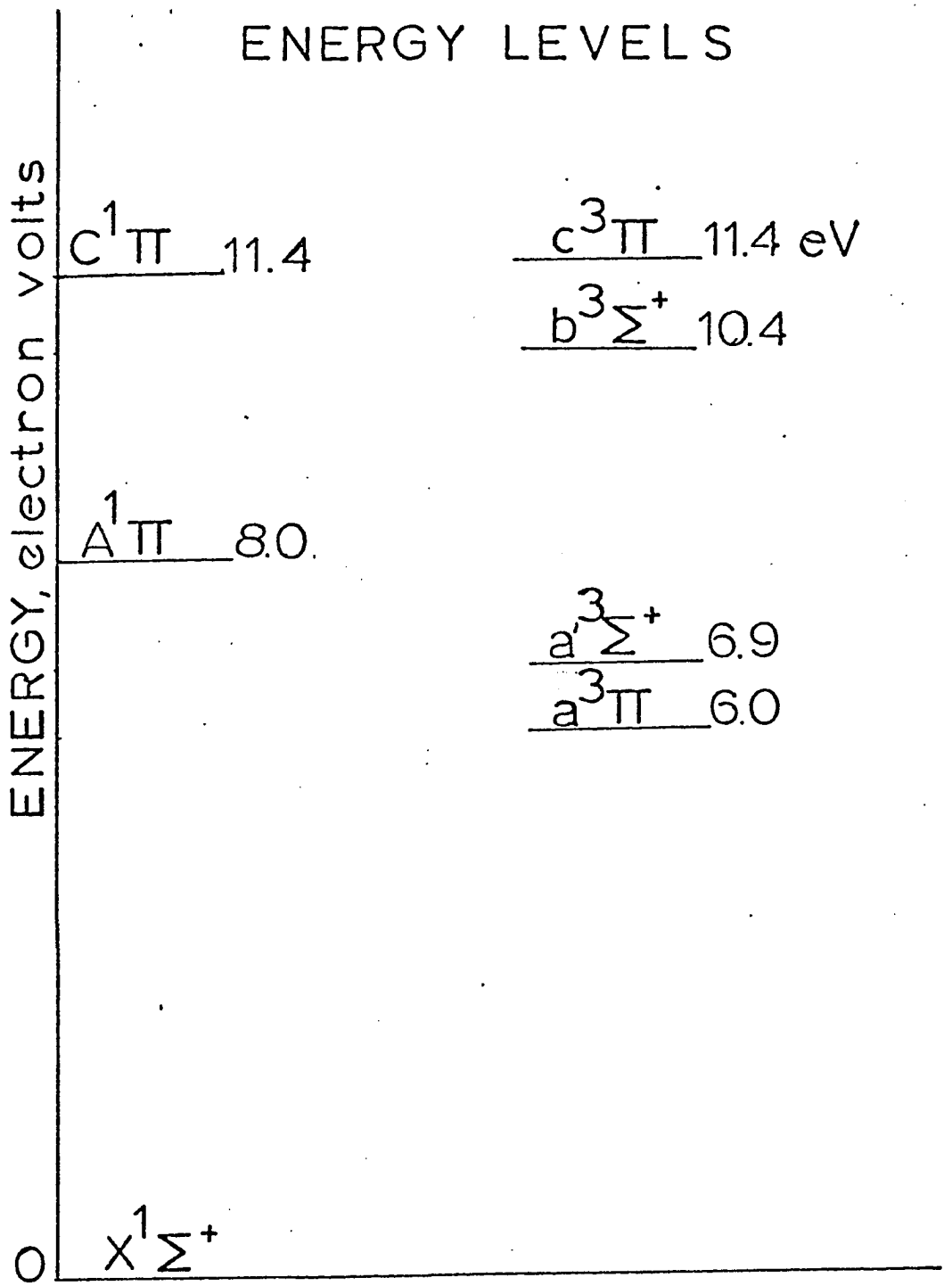

FIG. 3-1

THREE LEVEL

ONE CASCADE DECAY

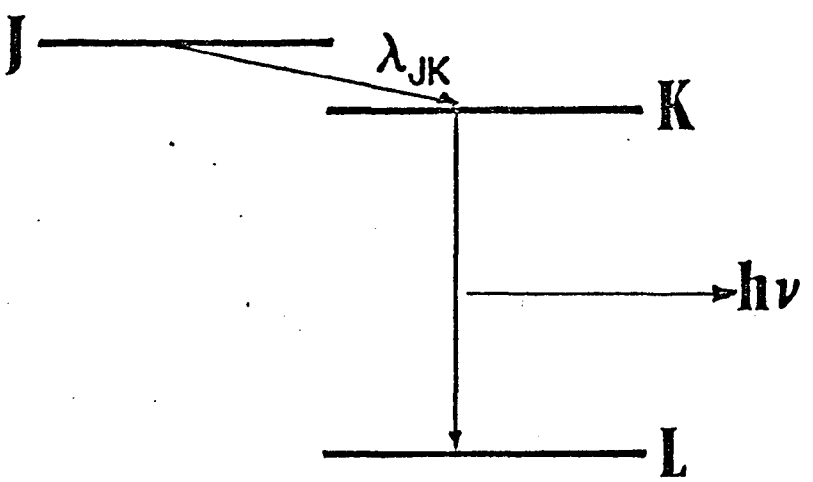

FIG. 3-2

$$\frac{dN_J}{dt} = \text{(rate of population of J level) - (rate of depopulation of J level)} \qquad (3\text{-}1)$$

In expanded form Eq. (3-1) becomes

$$\frac{dN_J}{dt} = nQ_J I_O - A_J N_J$$

$$\frac{dN_K}{dt} = nQ_K I_0 - A_K N_K + A_{JK} N_K \qquad (3\text{-}2)$$

where

n - density of ground state molecules mol/cm^3

Q_J - cross section for excitation of level J, cm^2

Q_K - cross section for excitation of level K, cm^2

I_0 - electron beam particle current, electrons/sec

A_K - total transition probability of level K, sec^{-1}

A_J - total transition probability of level J, sec^{-1}

N_K - number density of molecules in K level per length of the scattering region, molecules/cm

N_J - number density of molecules in J level per length of the scattering region, molecules/cm

A_{JK} - Einstien transition probability for dipole transitions from state J to state K, sec^{-1}

$A_J = \sum_{K<J} A_{KJ}$; A_J reciprocal lifetime of level J.

The effects of collisions can be taken into account by assuming that the effect of collisions are described by the Stern-Volmer equation[9,64] which gives the effective reciprocal lifetime at some pressure P as

$$\lambda_J(p) = A_J + K_J P. \qquad (3\text{-}3)$$

K_J - the collisional quenching coefficient of the level J for the gas at pressure p in units of $sec^{-1}/mTorr$

K_J describes the increase in the total effective transition probability, λ_J, due to collisions. A plot of $\lambda_J(p)$ vs. p extrapolated to p=0 gives A_J (which includes any effects of diffusion).[65] Extending pressure effects to the transfer of excitation, we can write

$$\lambda_{JK} = A_{JK} + K_{JK}p \tag{3-4}$$

where

A_{JK} - the Einstien transition probability for (J→K) a dipole transition, sec^{-1}

K_{JK} - collisional excitation transfer coefficient, $sec^{-1}/mTorr$

p - pressure, mTorr

Incorporating this pressure dependence Eq. (3-2) can be written[65]

$$\frac{dN_J}{dt} = nQ_J I_0 - \lambda_J(p)N_J$$

$$\frac{dN_K}{dt} = nQ_K I_0 - \lambda_K(p)N_K + \lambda_{JK}(p)N_J(t) \; . \tag{3-5}$$

At equilibrium for times long compared to any lifetime involved, N_K has saturated so that the rate of gain and loss are equal.

$$\frac{dN_K}{dt} = 0 \qquad \frac{dN_J}{dt} = 0 \qquad \text{for } t \to \infty$$

and

$$N_K^0 = \frac{nQ_K I_0 + \lambda_{JK} N_J}{\lambda_K} \qquad N_J^0 = \frac{nQ_J I_0}{\lambda_J} \quad . \tag{3-6}$$

The solution to Eq. (3-5) during the time when the electron beam is "on" is given by the following:

$$N_K(t) = \frac{\lambda_{JK} N_J^0}{(\lambda_K - \lambda_J)} (1 - e^{-\lambda_J t}) + \{N_K^0 - \frac{\lambda_{JK} N_J^0}{(\lambda_K - \lambda_J)}\} (1 - e^{-\lambda_K t})$$

$$N_J(t) = N_J^0(1 - e^{-\lambda_J t}) \quad . \tag{3-7}$$

The above equation assumes that the electron beam is turned "on" at time zero and instantly reaches its full current I_o. This equation describes the build up of the population in the J and K state and finally the reaching of equilibrium values for the $t >> \lambda_J^{-1}$ and $t >> \lambda_K^{-1}$ when the values of N_K and N_J become the following:

$N_J(t) = N_J^0$ for $t >> 1/\lambda_J$

and

$t >> 1/\lambda_K$

$N_K(t) = N_K^0$ for $t >> 1/\lambda_J$

and

$t >> 1/\lambda_K$.

If the electron beam is turned off at some time and instantly goes to $I(t) = 0$, the rate equation for the process is

$$\frac{dN_K}{dt} + \lambda_K(p)N_K = \lambda_{JK}N_J(t) \text{ and } \frac{dN_K}{dt} + \lambda_J N_J = 0 . \qquad (3\text{-}8)$$

The solution for these equations after the beam is turned off at time t=0 are

$$N_J(t) = N_J^0 e^{-\lambda_J t}$$

$$N_K(t) = \frac{\lambda_{JK} N_J^0}{(\lambda_K - \lambda_J)} e^{-\lambda_J t} + \{N_K^0 - \frac{\lambda_{JK} N_J^0}{(\lambda_K - \lambda_J)}\} e^{-\lambda_K t} . \qquad (3\text{-}9)$$

The number of molecules in level K which make a transition to level L per second with the emission of a photon is:

$$I_{KL} = A_{KL} N_K(t).$$

Thus, if light of wavelength corresponding to the transition $K \rightarrow L$ is monitored, the fluorescence decay will be the sum of two exponentials. If λ_J and λ_K are sufficiently different (say, a factor of two), then the fluorescence decay curve can be analyzed and the two exponentials can be deconvoluted from the data. The analysis will give the amplitude and decay constants of each exponential. Thus, the lifetimes and quenching coefficients of the level being monitored and the cascade components can be determined.

And if sufficient information is at hand concerning the states from which the cascades originate, i.e. the cross section, then the excitation transfer and the collisional excitation transfer coefficients A_{JK} and K_{JK} can be determined.

For the more general case of two cascades components feeding the Kth state, the rate equations for the energy levels in Fig. 3-3 are given below. This type of analysis has been extensively covered by Copeland,[66] Paske[67] and Fowler.[68]

This is the case for the $b^3\Sigma^+$ (v=0) level where two long lived cascade components feed the $b^3\Sigma^+$ state. The rate equations for the population of levels I, J and K are given below.

$$\frac{dN_I}{dt} + \lambda_I N_I = nQ_I I_0$$

$$\frac{dN_J}{dt} + \lambda_J N_J = nQ_J I_0 + \lambda_{IJ} N_J(t) \qquad (3\text{-}10)$$

$$\frac{dN_K}{dt} + \lambda_K N_K = nQ_K I_0 + \lambda_{IK} N_I(t) + \lambda_{JK} N_J(t)$$

For an excitation pulse width long compared to the characteristic times of the processes involved, the levels I, J, K assume their equilibrium values as follows:

FOUR LEVEL

TWO CASCADE DECAY

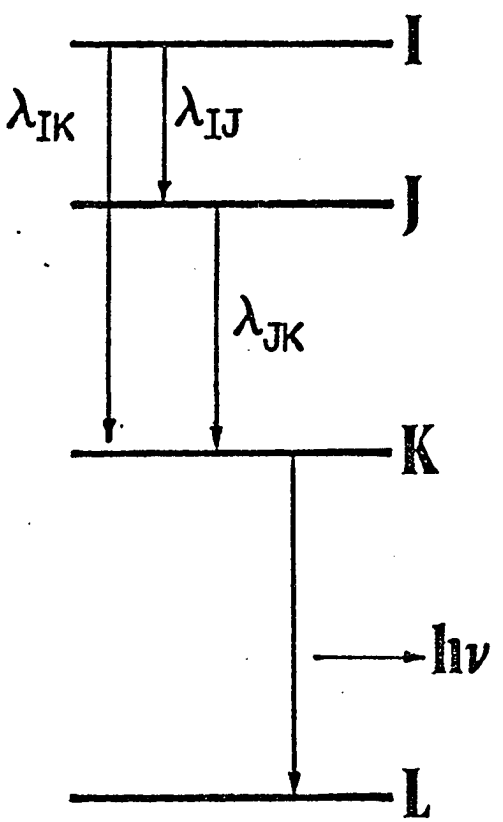

FIG. 3-3

$$N_I^0 = \frac{nQ_I I_0}{\lambda_I}$$

$$N_J^0 = \frac{nQ_J I_0 + \lambda_{IJ} N_I^0}{\lambda_J}$$

$$N_K^0 = \frac{nQ_K I_0 + \lambda_{JK} N_J^0 + \lambda_{IK} N_I^0}{\lambda_K} \quad .$$

The solutions to the set of coupled differential equations (3-10) is given below following the work of Copeland.[66]

$$N_I(t) = N_I^0 \, e^{-\lambda I t}$$

$$N_J(t) = \{N_J^0 - \frac{\lambda_{IJ} N_I^0}{(\lambda_J - \lambda_I)}\} \, e^{-\lambda_J t} + \{\frac{\lambda_{IJ} N_I^0}{(\lambda_J - \lambda_I)}\} \, e^{-\lambda_I t} \quad .$$

and finally for level K which is the population that will be monitored.

$$N_K(t) = N_I^0 \{\frac{\lambda_{IK}}{(\lambda_K - \lambda_I)} - \frac{\lambda_{JK}\lambda_{IJ}}{(\lambda_K - \lambda_I)(\lambda_J - \lambda_I)}\} \, e^{-\lambda_I t}$$

$$+ \{\frac{\lambda_{IJ} N_J^0}{(\lambda_K - \lambda_J)} - N_I^0 \frac{\lambda_{JK}\lambda_{IJ} N_I^0}{(\lambda_K - \lambda_J)(\lambda_J - \lambda_I)}\} e^{-\lambda_I t}$$

$$+ |N_K^0 - \{N_J^0 \frac{\lambda_{JK}}{(\lambda_K - \lambda_J)} - N_I^0 \frac{\lambda_{JK}\lambda_{IJ}}{(\lambda_K - \lambda_J)(\lambda_J - \lambda_I)}\} - N_I^0 \{\frac{\lambda_{IK}}{(\lambda_K - \lambda_I)}$$

$$- \frac{\lambda_{JK}\lambda_{IJ}}{(\lambda_K - \lambda_I)(\lambda_J - \lambda_I)}\}| \, e^{-\lambda_K t} \qquad (3\text{-}11)$$

It can be seen that the analysis of the amplitudes for N is very complicated. Some of the difficulty is handled by considering ratios of the amplitudes of the exponentials. In that case, the pressure, electron gun current, time of data run and detector efficiencies cancel out as well as other experimental parameters (see Methods section). In most cases, in order to make the expression for $N_K(t)$ tractable, it is necessary to find regions where one amplitude is nearly zero and thus negligible compared to the other decay components. This is the route taken in later chapters where one of the exponential amplitudes is negligible when the electron gun energy is chosen near the threshold for electron impact excitation of $b^3\Sigma^+$ ($v'=0$).

CHAPTER IV

EXPERIMENTAL PROCEDURE

A. Tuning of the Electron Gun

The tuning of the electron gun proceeds in two parts. First, the tuning of the electron monochromator (including the cathode, Pierce and anode elements, elements 2,3 and 4) and second, the adjustment of the output optics, elements 5, 6 and 7, to focus the beam into the desired region either the scattering cell or the Faraday Cup. A phase sensitive detector (PAR) is connected to the Faraday cup and set to detect the 50 Hz modulation of the electron beam produced when a 0.1 V peak to peak square wave modulation is applied to the 3000 or RPD element. (See RPD principle section C). The choice of anode voltage is within limits arbitrary. A voltage between 50 and 110 V works well. If more beam current is needed then the anode voltage can be increased up to 200 V. It has been found that the higher anode voltages require larger negative voltages on the Pierce element to maximize the Faraday cup or scattering cell current. Along with the higher anode voltages, there was an apparent decrease in the energy resolution noted in those optical emission functions (those taken without the RPD operating,

i.e. the low energy resolution mode) taken with the gun tuned with high (200 V) anode voltage compared to the low anode voltage mode (50V). Although no exhaustive study of this effect has been made, it has been estimated that the resolution changes from 240 meV to 400 meV when the anode voltage is increased from 50 to 200 V. The cause of this may be the need of increasing the Pierce element voltage as the anode voltage is increased in order to maximize the current in the interaction region. This effect has been discussed by Sutcliffe.[48] The Pierce element voltage is adjusted to produce a D.C. current at the scattering cell which is set between 10 and 20 V (all voltages are measured with respect to the cathode unless otherwise specified). The cathode current should not rise above 200-300 microamps in this last adjustment.

Next, the D.C. voltage on the RPD is set between 1.7 and 3.9 V, while V_{2000} and V_{4000} are both set to the same voltage between 20 and 100 V. The elements 5, 6, 7 are set to 50 V, 100 V and 15 V respectively, and V_{Anode} is set as discussed above. A D.C. current should now be detected at the scattering cell. The voltages on all the elements except the RPD are set to maximize the current on the scattering cell, I_{SC}. The PAR is set on its most sensitive scale while V_{RPD} is adjusted until the PAR detects a signal (PAR adjusted according to manufacturer's instructions).

Since the time constant of the PAR is about 1 sec, this adjustment must be made slowly to avoid missing the peak PAR signal.

Once the signal is detected on the PAR by any combination of lens voltages similar to those above, tuning of the gun proceeds routinely. The Pierce and RPD voltages are set to maximize the PAR signal and the voltages on the 5, 6, 7 elements are adjusted to maximize the PAR signals. A modification of the gun including connecting a 50 ohm terminating resistor and coax to the 7 element effectively connected the scattering cell to the 7 element and fixed the 7 element voltage. Various combinations voltages on the 2 and 4 elements may now be sudied to determine the voltage that gives the best resolution and lens transmission function as the beam energy is varied. This is judged by examining electron transmission spectra with and without gas in the scattering cell. By scanning the scattering cell voltage through regions containing resonances of known energy and width, the performance of the gun may be determined. The measured width of known resonances may be compared to the width determined by high resolution differential cross section measurements. The desired result of the tuning procedure is a large throughput of the electron optics in the energy interval of interest along with a resolution sufficient to resolve any structure to be studied. The 5, 6, 7 elements

may be adjusted to focus the beam in the scattering cell or into the Faraday Cup after the above adjustments have been made without upsetting the operation of the RPD monochromator. The location of the focus is determined by the type of experiment performed, e.g. either optical emission function or transmitted electron measurements.

B. Adjustment of the Optical Detection System and the Timing Electronics.

Optical Alignment:

Initial optical alignment was accomplished before assembling the vacuum system by shining a small beam of light through the scattering cell aperture. The monochromator slits were opened to 1 mm and the optics adjusted until the light fell on the axis of the PMT holder. Fine adjustment is performed after the vacuum system is assembled and the electron beam turned on. The fine adjustment includes the focusing of the optical system aligning the axis of the optical system to go through the center of the scattering cell, setting the slit of the monochromator so that it is parallel to the electron beam and focusing of the light from the quartz condensing lens so it falls onto the monochromator entrance slit. After the above adjustments have been made, the PMT is rotated in its holder to maximize the photon rate. Finally, the slits are closed down to the desired resolution, and a final check of the alignment is made.

The optical system design for this light scattering system follows the suggestions of Gilbert.[69]

Monochromator Adjustment:

After wavelength calibration and sine bar adjustments are made using a Hg source, the monochromator is mounted onto the optical bench (following manufacturer's directions). The optical monochromator is adjusted by the following procedure. With the electron beam set to an appropriate energy, a scan of the wavelength interval of interest is made. By comparing the position of known lines with the wavelength reading at which they appear, the calibration of the monochromator wavelength dial may be checked. The proper slit size is determined by the optical resolution desired. The reciprocal dispersion of the monochromator times the exit slit width gives the wavelength spacing at which two lines will just be resolved. The front slit is chosen for optimum intensity for a given monochromator. This assumes that the light source is properly focused on the monochromator with the condensing lens matching the f-number of the monochromator and the entrance slit filled with light.

All lifetime measurements of the $b^3\Sigma^+(v'=0)$ state were made with a 0.25 mm exit slit and a 0.75 mm entrance slit on the Bausch and Lomb high intensity monochromator. A 0.50 mm entrance is the optimum slit for a 0.25 mm exit slit, but it did not give a high enough signal intensity.

Photomultiplier Tube (PMT) Installation and Cooling:

The PMT housing and tube base is placed in an evacuated bell jar and held at 100 microns for 24 hours before installing the PMT to remove any trace of water. All surfaces of the tube base are cleaned with reagent grade acetone and blown dry before installing the tube. The RCA C31034A02 PMT, which is to be handled in total darkness at all times, is wrapped with black insulation tape at the factory. The tape is not to be removed nor should any device which exerts pressure on the tube except for the tube base be utilized to hold the tube in place in the PMT cooler housing. The PMT is pushed straight into the tube base (in total darkness) with gloved hands and installed in the cooler after the air is purged from the interior for at least 10 seconds by dry nitrogen. The quartz window and lens set that matches the monochromator to be used is installed in the cooler, and the cooler is turned on. After about two hours of cooling the PMT cathode is cooled to the selected temperature.

Initial Powering of PMT:

After the housing is securely attached to the monochromator and any possible sources of light leaks are covered by Apiezon Q, an electrometer set on the 100 nanoamp scale is connected to the anode of the PMT and voltage is applied to the PMT in 100 volt steps. Each time the voltage

is increased, the electrometer is checked to insure that the maximum 100 nanoamp, averaged over any 30 second time period, is not exceeded.[50] If the current is low enough, the voltage to the PMT may be incremented by the next 100 V. In the case of excessive anode current, the voltage must be immediately decreased until the anode current is less than 100 nanoamp or until the voltage is turned off. Initially, the PMT voltage is increased up to that voltage specified on the tube specification sheet supplied by the manufacturer when the tube is purchased. By choosing the rated voltage, the dark current and PMT gain will be known and any excess counts may be attributed to amplifier noise, light leaks or electrical discharge on the tube base. The PMT anode pulses are next examined by connecting the PMT to a fast (300 MHz band width) oscilloscope using a terminated 50 ohm coax. The light level can be increased slightly by uncovering the monochromator front slit to make viewing on the scope trace easier as long as the maximum anode current of 100 nanoamps is not exceeded. The anode pulses will be negative, going with rise and fall times of approximately 2.5 nanosec and an amplitude of -5 to -10 millivolts. The presence of larger amplitude signals with widths much larger than 5 nsec will indicate the presence of discharges around the resistor chain or tube base. Continued cooling of the PMT with voltage applied for 10-30 hours will sometimes remove water from the base. The water is pumped to the colder

surfaces of the PMT cooler from warm region around the dynode resistor chain and the tube base. Extremely large discharges around the PMT must be eliminated right away, since the light from these discharges may easily overcurrent the last dynode stages and anode of the PMT, resulting in serious if not permanent damage.

Light leaks are detected by covering the front slit and noting any decrease in dark count rate as the room lights are turned off. Light leaks are eliminated by taping, covering with Apiezon Q, installing baffles, covers or sheet metal housings. When the dark count rate reaches the rate specified by the manufacturer at the operating temperature of the PMT cathode, adjustment of the amplifiers and discriminators is performed. After exposure to room light during installation, the dark counts of the PMT will slowly decrease while the tube is in operation for the next 1 to 3 days. The tube should never be exposed to room level lights while power is applied to the dynode resistor chain.

A constant light signal from the scattering cell is used for checking the signal to noise ratio of the photon channel. By varying the PMT voltage, amplifier gain, and discriminator setting, the signal/dark count rate is maximized. Generally, the best operating point is found by using a higher than normal voltage on the PMT to increase its gain within the maximum allowable PMT cathode to anode voltage and installing a low noise wide band preamp on the

output of the PMT. It was found that the C31034A02 performed best with 1660 V into a low noise preamp[54] with the discriminator set as low as possible. The coax used in this channel is RG-58 with polyethylene foam dielectric for low loss. A PMT anode pulse height spectrum was used to adjust the discriminator levels. This spectrum shows that the electronic noise occurs at low pulse height level and may be easily discriminated against. The total number of counts in the spectrum minus the noise will indicate the signal rate that should be observed on a rate meter connected to the photon channel. Adjustment of the Constant Fraction Discriminator is made until the proper signal rate is reached, that is, the rate where the noise is excluded.

For pulses with constant amplitude, leading edge timing may be used and will give good results. However, PMT anode pulses have various pulse heights, and constant fraction timing will give less timing jitter than leading edge timing.[70] In the case where pulses with slow rise times are present with the anode pulses, slow rise time reject will discriminate against these pulses. Pulses with slow rise time leading edges may be caused by electrical discharges on and around the dynode chain.[51]

The TAC time range is selected along with the repetition rate and waveform to observe the desired time region. The single channel analyzers in each TAC select counts that

occur in a selected time region and inhibit the counting of others outside this selected time interval.

C. RPD Principle

The RPD is a high resolution electron energy analyzing device that operates by applying a low frequency modulation to a retarding element.[38,40,58] The retarding element is a grid which is perpendicular to the electron beam and is installed in the center element (the RPD element) of an Einzel lens which makes up the RPD monochromator. The RPD monochromator selects a small slice of the thermal electron distribution that is emitted by the cathode. This slice of the energy distribution selected by the RPD allows detection of signals that are due to electrons whose energy falls in the selected energy interval. However, those electrons with energies higher than the selected interval are still allowed to pass the RPD monochromator and enter the scattering cell. The RPD technique only allows one to electronically select the high resolution signal.

To aid in tuning this important element of the gun, a brief analytical description of the RPD is given below.

Referring to Fig. 4-1, assume that the low frequency is applied such that the RPD is at retarding voltage, V_1, then all electrons with energy less than $E_1 = eV_1$ are stopped and those with energy greater than E_1 are transmitted through the RPD grid. Now let the applied modulating signal change so that a voltage, V_2, is applied to the RPD.

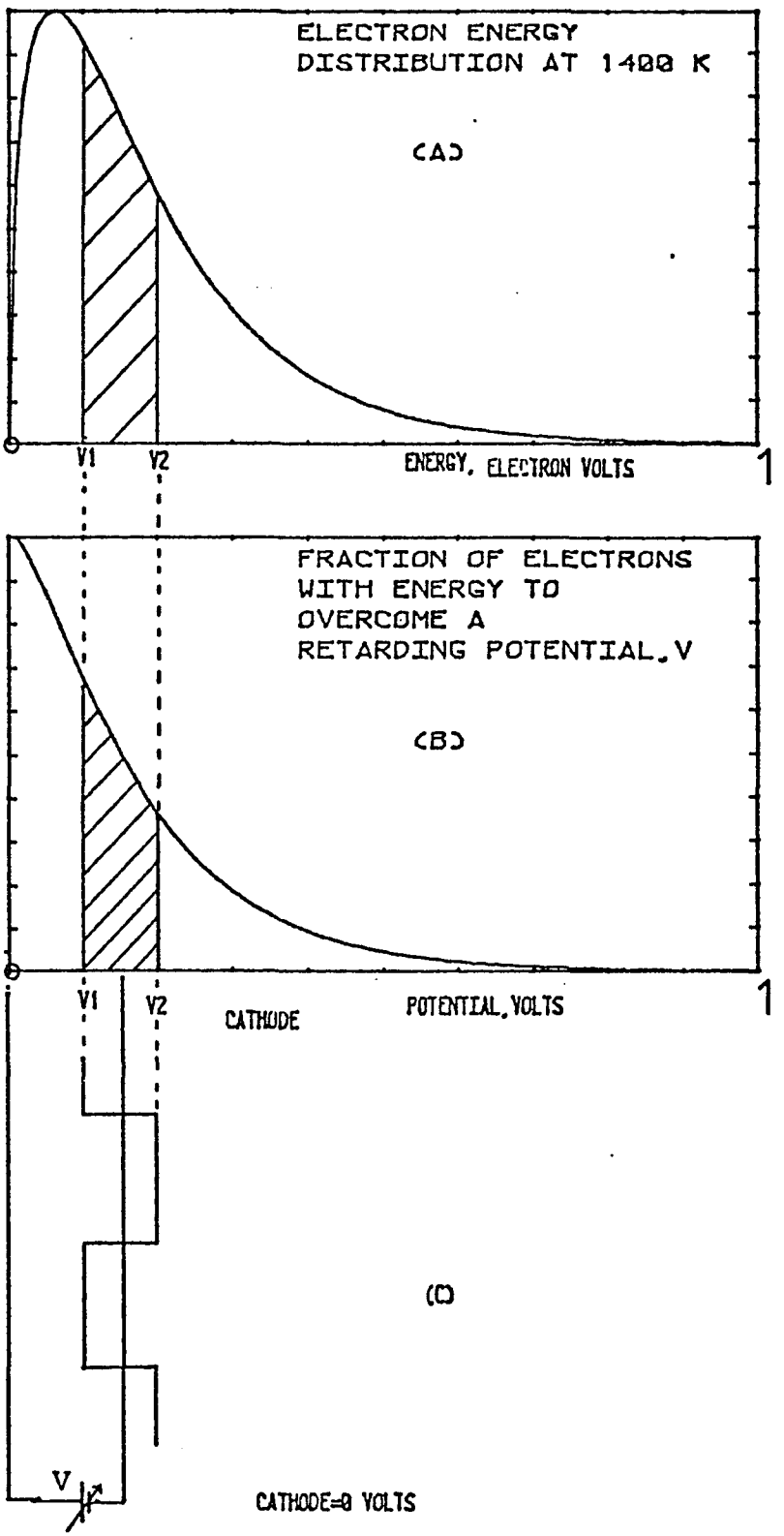

Fig. 4-1: RPD TECHNIQUE

Electrons whose energy is lower than $E_2 = ev_2$ are repelled by the RPD, and those with energy greater than E_2 are transmitted by the RPD. If the detection electronics are set up to alternately add and subtract synchronously with the low frequency modulation, the difference signal thus detected is due only to electrons in the selected energy interval from E_1 to E_2. This subtraction is done by analog and digital circuits.

In the present experiment, the subtraction for the Faraday Cup signal is by analog circuits in a phase sensitive amplifier. The subtraction process for the photon channel is done by synchronously gating up/down counters in the digital scalers to alternately add and then subtract the photon signal.

The fraction, $\rho(\varepsilon)d\varepsilon$, of molecules in an ideal gas that have an energy ε to $\varepsilon+d\varepsilon$ is given by a Maxwell-Boltzmann distribution[13,14]

$$\rho(\varepsilon)d\varepsilon = 2\pi\left(\frac{1}{\pi KT}\right)^{3/2} e^{-\varepsilon/KT}\sqrt{\varepsilon}\, d\varepsilon \qquad (4\text{-}1)$$

Boltzmann's constant $k = 8.6529\times10^{-5}$ electron volt/K

absolute temperature T, Kelvin

It was shown by Richardson that electrons that are emitted from a hot metal surface also have a Maxwellian velocity distribution.[71,72] Assuming the reflection at the surface of the metal of the electrons to be negligible $\rho(\varepsilon)$ for emitted electrons, it takes the form

$$\rho(\varepsilon)d = A(T)\exp(-\varepsilon/KT)\sqrt{\varepsilon}\,d\varepsilon \qquad (4\text{-}2)$$

where A(T) is a function of the condition of the metal surface and work function of the metal, and

$$\int_0^{+\infty} \rho(\varepsilon)d\varepsilon = 1.$$

An example of this function is shown in Fig. 4-2 for T = 1700, K. If a retarding voltage is applied to the RPD element, the fraction of electrons that will overcome the retarding voltage V_1 is given by (Fig. 4-1A)

$$R(V_1) = A(T)\int_{V_1}^{+\infty} \sqrt{\varepsilon}\exp(-\varepsilon/KT)\,d\varepsilon \qquad (4\text{-}3)$$

where the energy ε_1 at v_1 is $\varepsilon_1 = +eV$ and the potentials are measured with respect to the surface of the cathode from which the electron was emitted.

The form of this curve (Fig. 4-1b) is easy to determine at v = 0 (i.e., $R(v_1) = 1$), the slope is zero. All the electrons pass the RPD. At large retarding potentials, no electrons pass the RPD and $R(v_1) = 0$. At the peak of $\rho(\varepsilon)$ (Fig. 4-1a) the integrated curve has an inflection point. See Golden and Bandel[73] for an experimentally determined set of these curves for momentum selected electron distributions.

If the voltage V_1 is now modulated (i.e., alternately set at v_1 and v_2) with a square wave voltage (Fig. 4-1c) of

amplitude $V = V_1 - V_2$, and its D.C. value with respect to the cathode surface is set at V, the RPD element may be tuned by varying V and noting the difference current detected (Fig. 4-1).

When the RPD voltage is set at V_1 the fraction of the current that crosses the RPD is $R(V_1)$ and at V_2 the fraction is $R(V_2)$. If the difference current in the Faraday cup is detected by a phase sensitive amplifier, it will detect a signal that is proportional to the difference $R(V_1) - R(V_2)$ which is represented in Fig. 4-1b by the crosshatched area. The tuning of the RPD is accomplished by changing the voltage V until the detected signal reaches a maximum. By referring to the graph of $R(V_1)$, it is seen that the shaded area will be the largest when $V_1 = 0$. When the RPD is tuned as described above, the electrons cross the RPD with the same energy distribution as they had when they were emitted from the hot cathode surface. Thus, the RPD grid operates as a virtual cathode. This above argument neglects lens effects, loss of electrons from the beam due to collection on the electron gun surfaces and electrostatic field penetration into the region of the RPD.

Fig. 4-2

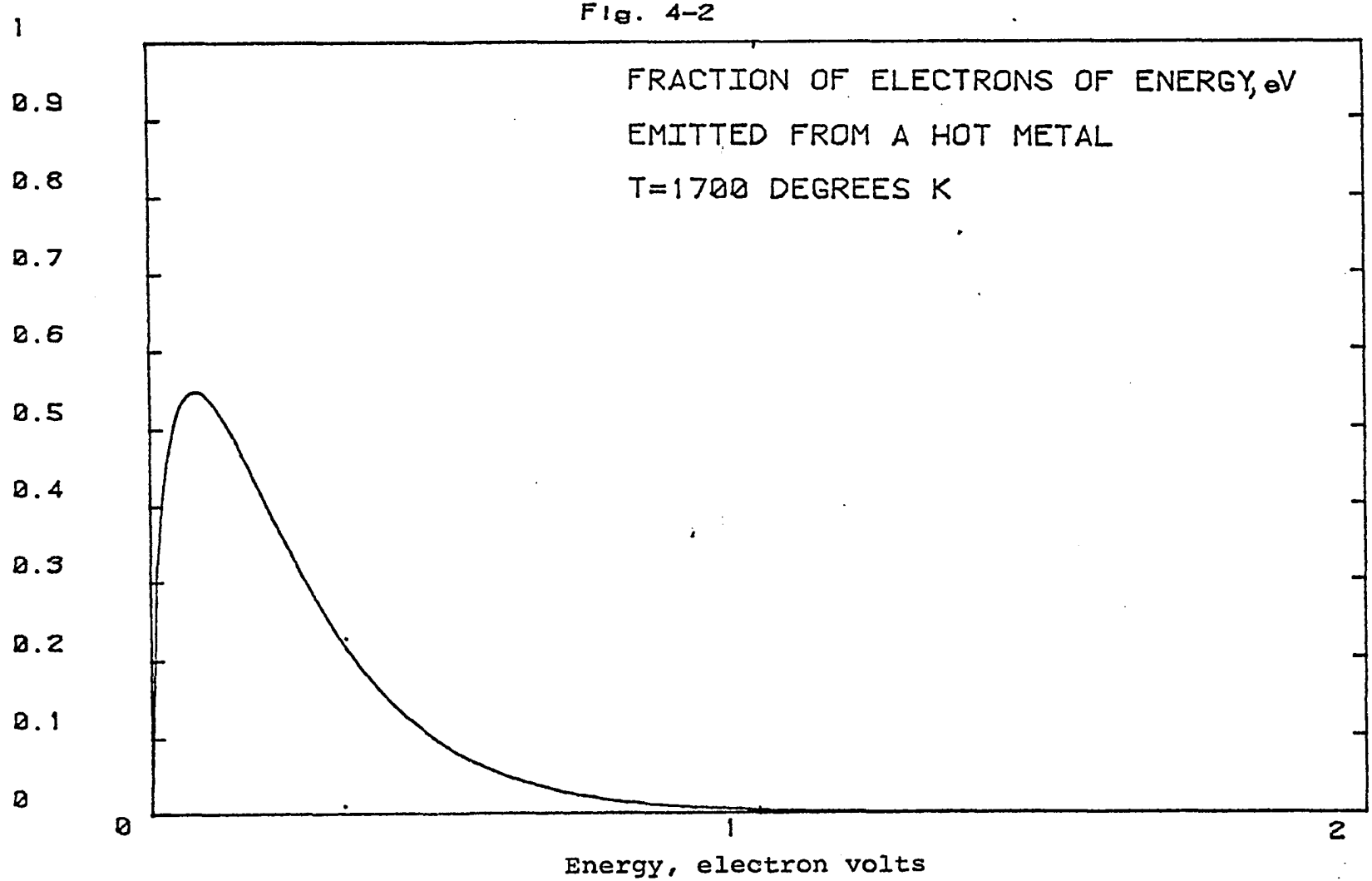
FRACTION OF ELECTRONS OF ENERGY, eV
EMITTED FROM A HOT METAL
T=1700 DEGREES K
1
0.9
0.8
0.7
0.6
0.5
0.4
0.3
0.2
0.1
0
0
1
2
Energy, electron volts

Fig. 4-3

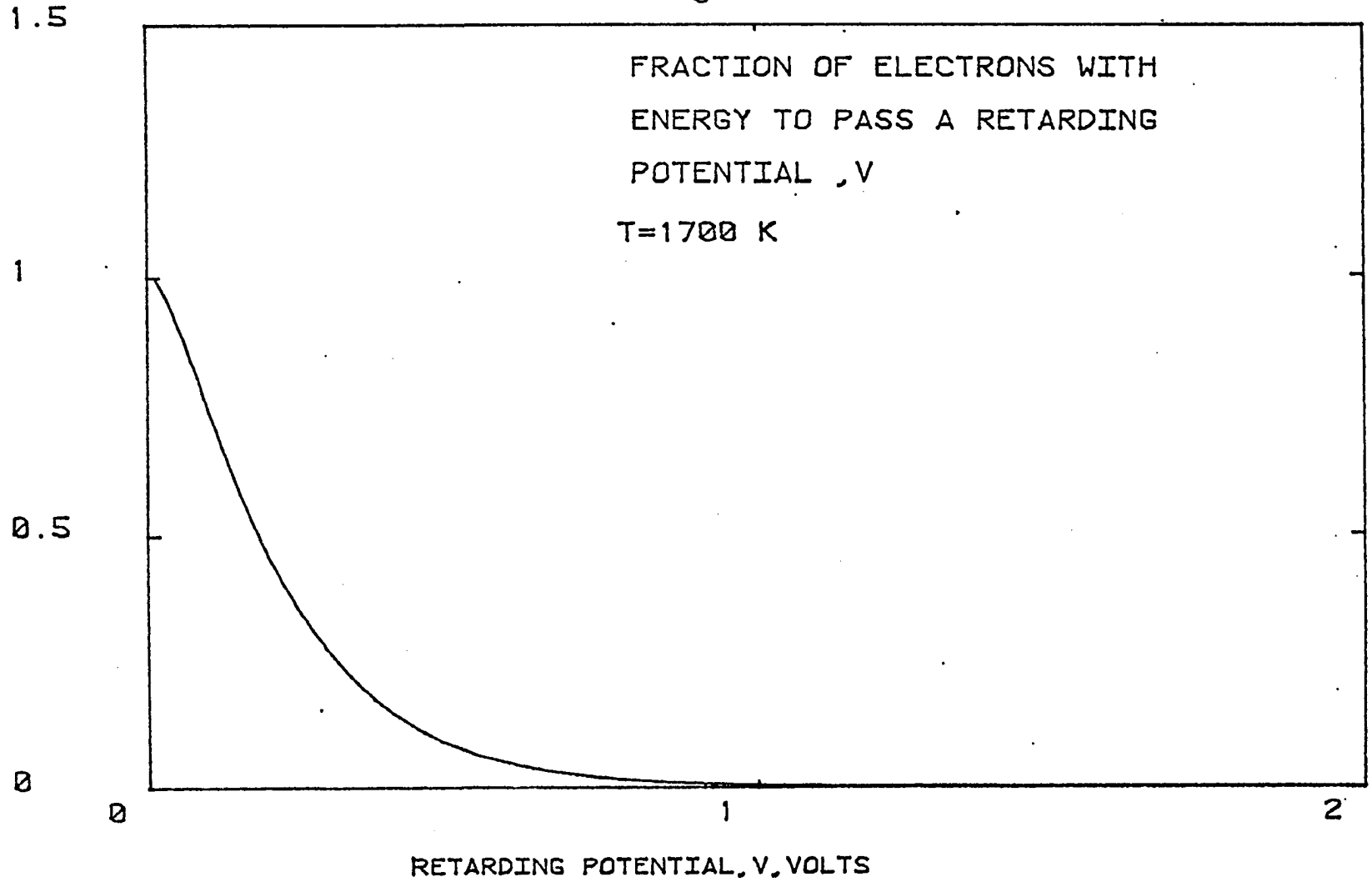
1.5
1
0.5
0
0
1
2
FRACTION OF ELECTRONS WITH
ENERGY TO PASS A RETARDING
POTENTIAL ,V
T=1700 K
RETARDING POTENTIAL, V, VOLTS

D. Decay of Electron Beam

The electron gun must be tuned such that the electron beam will turn off as rapidly as possible. The decay of the electron beam is an important parameter in lifetime measurements, since it can bias lifetime results if not properly accounted for. When attempting to measure lifetimes whose decay constants are nearly equal to the decay constant of the electron gun, multiexponential deconvolution of the detected signal becomes very difficult. To stress this point, the contribution to the detected signal of the electron gun after cutoff is discussed below.

Let the decay of the electron beam after the electronics start turning the beam off be described by $I = I_0 e^{-t/\tau}$ where τ = decay constant of beam, I_0 = steady state current of beam (electron/sec) and cutoff of the beam begins at time $t = 0$ sec.[68] Consider some excited state J which decays to K and lower states. The rate equation describing the population of the Jth state is given by

$$dN_J/dt = \text{(rate of molecules into level J)} - \text{(rate of molecules out of level J)} \qquad (4\text{-}4)$$

$$dN_J/dt = I(t)Q_J n - A_J N_J \qquad (4\text{-}5)$$

$I(t)$ - electron beam current, electrons/sec

Q_J - cross section for excitation of the Jth level, cm^2

n - density of ground state molecules, molecules/cm^3

A_J - Einstein A coefficient for spontaneous emission from the J level to all lower allowed levels, (sec^{-1}) (also called the reciprocal lifetime)

N_J - number of molecules in Jth level per cm of beam length.

Substitute $I = I_0 e^{-t/\tau}$ into Eq. (4-5) (4-6)

$$\frac{dN_J}{dt} + A_J N_J = A_J n I_0 e^{-t/\tau} \quad . \tag{4-7}$$

The solution to (4-7) is given by

$$N_J(t) = \frac{Q_j n I_0}{(A_J - \frac{1}{\tau})} \; e^{-t/\tau} + Ce^{-A_J t} \tag{4-8}$$

at t = 0 just before the beam is cut off assume $N_J(t)$ has reached its equilibrium population or

$$\frac{dN_J}{dt} = 0 \quad : \quad N_J^0 = \frac{Q_J n I_0}{A_J - \frac{1}{\tau}} \tag{4-9}$$

where N_J^0 is the equilibrium population of the Jth level. Evaluate C in Eq. (4-8)

$$C = N_J^0 \; \frac{-1/\tau}{(A_J - \frac{1}{\tau})} \tag{4-10}$$

Substitute (4-10) into (4-8) and write in a more compact form

$$N_J(t) = N_J^0 \frac{A_J}{(A_J - \frac{1}{\tau})} e^{-t/\tau} + N_J^0 \frac{-1/\tau}{(A_J - \frac{1}{\tau})} e^{-A_J t} . \quad (4\text{-}11)$$

In the case of a three level system (see Chapter 3), the number of molecules in the Jth level is given by one Cascade Three Level System

$$N_J(t) = \frac{\lambda_{IJ}}{(A_J - \lambda_I)} N_I^0 e^{-\lambda_I t} + \{N_J^0 - \frac{\lambda_{IJ}}{A_J - \lambda_I} N_I^0\} e^{-A_J t} \quad (4\text{-}12)$$

where $\lambda_{IJ} = A_{IJ} + K_{IJ}P$

A_{IJ} - excitation transfer coefficient (sec^{-1}) $A_J = \sum_{I<J} A_{JI}$ transition probability of level J,

K_{IJ} - collisional excitation transfer coefficient (sec^{-1} $mTorr^{-1}$)

P - pressure (mTorr)

$\lambda_I = \sum_{J<I} \lambda_{IJ}$.

N_I^0 and N_J^0 are the equilibrium populations of the I and J levels. Comparing (4-12) to (4-11), it is seen that in the case that a transition is free of cascades, the effect of a finite decay of the electron beam is to add a feed mechanism after cutoff (t=0) that resembles a cascade from a higher energy level. If the beam decay time is shorter than the lifetime of the J level $\tau_J = 1/A_J$ then the feed exponential has a negative amplitude. This negative amplitude feed exponential has the effect of causing the first few channels after cutoff to have a rounded shape rather than a sharp

corner. See Fig. 4-4 and Fig. 4-5. In Fig. 4-4 a single level decay is shown with no feed from the electron gun. Fig. 4-5 shows rounding at cutoff due to feed from the gun of the observed state.

There are several ways to properly account for the finite decay of the electron beam. One method is to start the analysis several electron beam decay constants (lifetimes) after the cutoff. Another method used was to add another exponential in the fitting function. In the case of the $b^3\Sigma^+(v'=0)$ state, this meant fitting to four exponentials. There was not any significant difference in the decay constants extracted for the $b^3\Sigma^+(v=0)$ state using the two methods.

An attempt was made to directly view the decay of the electron beam by placing a .035" ID aperture on the 7 element just in front of the scattering cell entrance aperture. A 50 ohm vacuum coax was connected to the 7 element and the coax terminated at the element by a 50 ohm metal film resistor. The terminating resistor had been previously cleaned and vacuum baked as described elsewhere. The other end of the vacuum coax was connected to a MHV connector on the top flange. Observation of the pulse signal from the 7 element on a 1S1 sampling oscilloscope which had a rise time of 350 psec, showed two things about the signal. The signal was swamped with switching noise primarily because the 7 element

Fig. 4-4

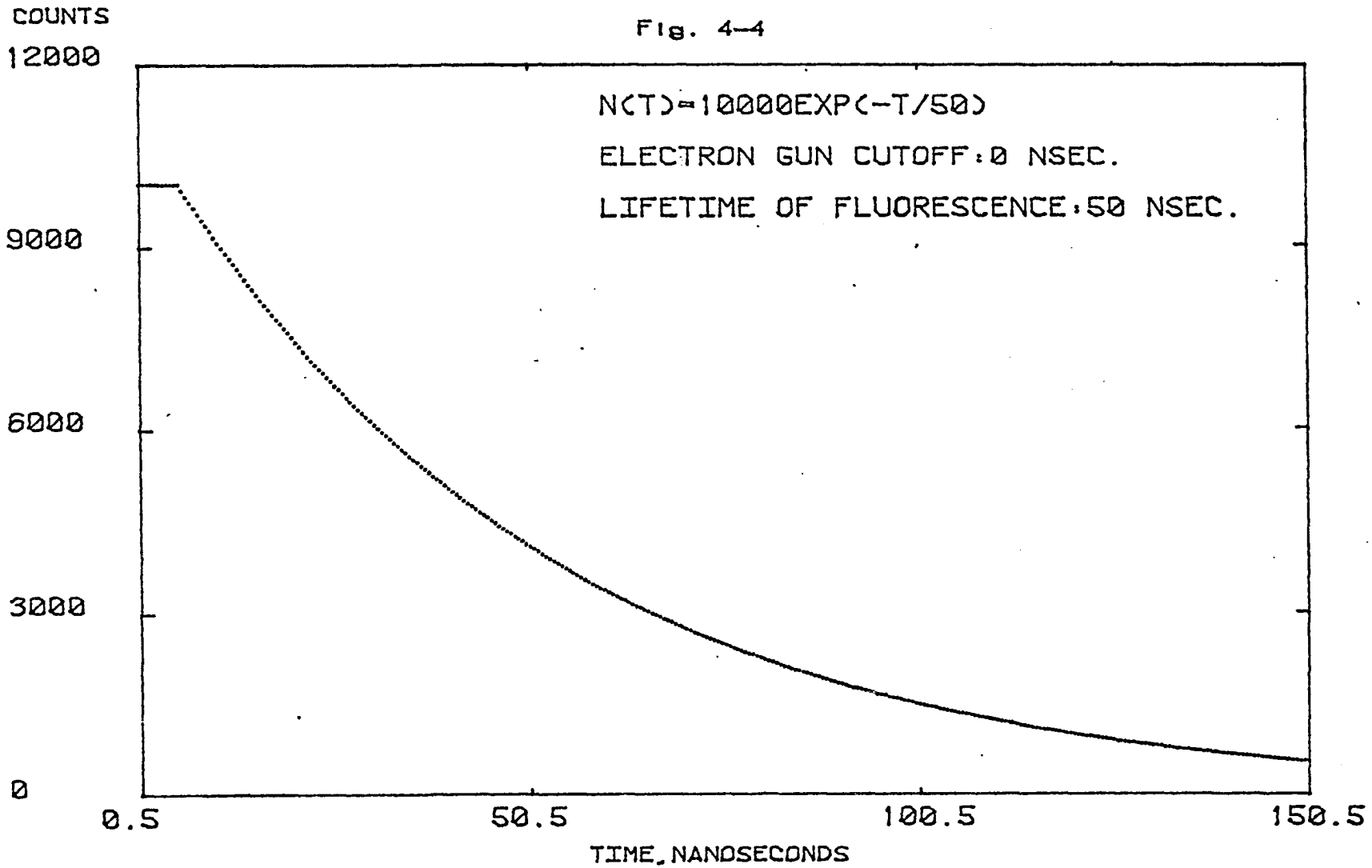
COUNTS
12000
9000
6000
3000
0
N(T)=10000EXP(-T/50)
ELECTRON GUN CUTOFF:0 NSEC.
LIFETIME OF FLUORESCENCE:50 NSEC.
0.5
50.5
100.5
150.5
TIME, NANOSECONDS

Fig. 4-5

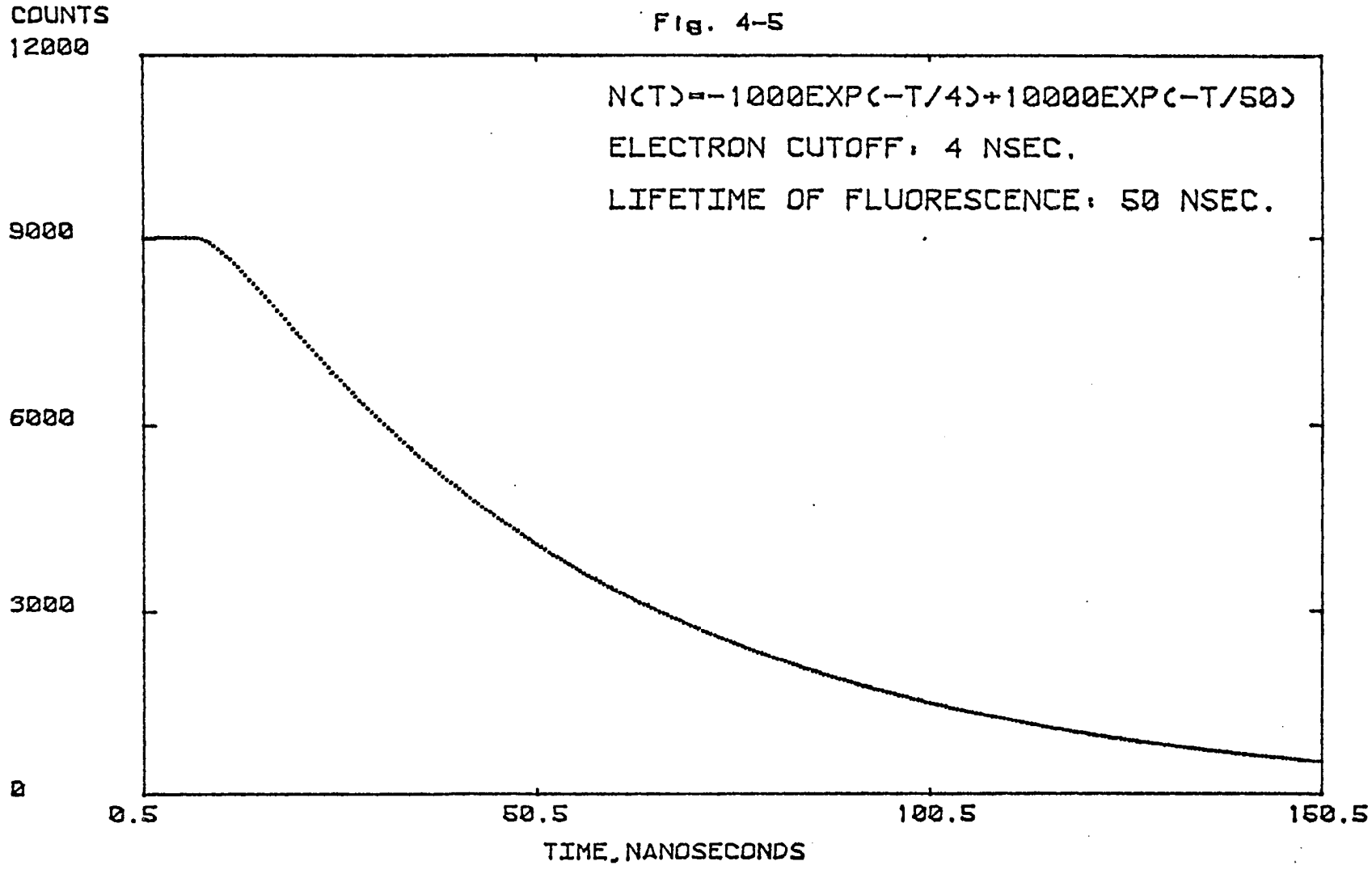
COUNTS
12000
9000
6000
3000
0
N(T)=-1000EXP(-T/4)+10000EXP(-T/50)
ELECTRON CUTOFF: 4 NSEC.
LIFETIME OF FLUORESCENCE: 50 NSEC.
0.5
50.5
100.5
150.5
TIME, NANOSECONDS

with aperture is not shielded. By a rough estimate, it was determined that the fall time of the signal on the 7 element (90% to 10% of full amplitude) was 15-25 nsec. This was 3-5 times longer than the shortest exponential found by computor fits to typical data. The probable cause of this lengthened fall time of the 7 element signal is the large capacitance of the element to nearby elements. The solution for this problem would be to hollow out the 7 element in a similar manner to the RPD and set the aperture inside but insulated from the body of the 7 element. This has not been pursued to date, but may be a possible future solution to direct viewing of the electron beam cutoff.

Another approach would be to place a moveable silver target in the scattering cell inclined 45^0 to the beam and the optical axis and oriented so that the region of the target that the electron beam strikes could be viewed by the optical detector. The production of transition radiation[74] as the electrons penetrate the metal surface could be used to determine the apparatus response function. This response function could be put in the multiexponential fitting function in place of the fastest exponential. This would offer the advantage of fitting the electron beam decay to the actual response function of the apparatus rather than some assumed idealized function.[75]

E. Lifetime Measurements

Delayed coincidence experiments can suffer from several kinds of systematic errors in addition to random experimental errors. For an extensive discussion of these errors see Corney,[76] Imhof and Read,[77] and Kharallah and Smith.[49]

The following sources of error were determined to apply to the present experiment, time calibration of the MCA time spectra, count rate distortion in the time spectra, effect of finite time width of TAC channels, spectral overlap in the optical spectra, cascades, finite electron beam decay and data analysis.

Time Scale Calibration:

Fluorescence decay curves were accumulated in a multichannel analyzer (MCA). The channel of the recorded count is proportional to time, and the height of the histogram is the number of counts detected at that time. The time per channel was calibrated before each lifetime measurement by an ORTEC 462 time calibrator. The TAC and MCA did not show more than one channel drift in 1024 channels during the time that the data was collected (60 days) for a full scale of 5.0 microsec.

Count Rate Distortion:

The probability p(I) of registering an event in channel I of the MCA in one on-and-off cycle of the electron gun as

given by Read and Imhof[77] and Egbert[78] $p(I) = q\{1 \rightarrow (I-1)\}p(I)$, since only one photon can be counted per cycle where $q\{1 \rightarrow (I-1)\}$, is the probability of not registering an event in channel 1 to channel (I-1). p(I) is the probability of registering an event in the Ith channel, and q and p(I) depend on the specific decay curve being measured. Assume that q and p are random in nature and not correlated to the start pulses. In this case, we can use Poisson statistics to recalculate the probability, p_n, of observing n counts in a time Δt when the average number of counts during t is μ where $p(n) = \mu^n e^{-\mu}/n!$ $\mu = R\Delta t$, R - average count rate, Δt - time duration of measurement, the probability of zero counts is $p(0) = e^{-\mu}$ and for one count $p(1) = \mu e^{-\mu}$, the probability of zero counts in channels 1 to (I-1)

$$q\{1 \rightarrow (I-1)\} = e^{-(I-1)\mu} \quad . \tag{4-12}$$

Thus, the probability of a count in the Ith channel is

$$p(I) = \mu e^{-\mu}$$

or, since $\mu = R\Delta t$,

$$p(I) = R\Delta t \; e^{-IR\Delta t}$$

expanding Eq. (4-13) in a Taylors series gives

$$p(I) = R\Delta t - IR^2 (\Delta t)^2 + \ldots \tag{4-14}$$

Equation (4-14) shows that if $R\Delta t >> IR^2\Delta t^2$ (4-14) becomes $p(I) = R\Delta t$ and the probability of registering a count in any channel I is the same and equal to $R\Delta t$. However, if $IR\Delta t \gtrsim 1$, then higher order terms in the expansion must be included and the probability of registering a count becomes a function of the channel. This probability decreases as the channel number is larger. In other words, the data is biased to shorter times which has the effect of decreasing the measured lifetimes.

The distortion of the probability is typical of high count rates and large total time periods, T

$$T = \sum_{I=1}^{N} I\Delta t$$

N number of channels utilized. To insure that this distortion is not an important consideration, the inequality

$$N_I R\Delta t << 1 \tag{4-15}$$

must be satisfied. What is done in practice is to make the stop pulse rate two orders of magnitude smaller than the start pulse rate.[77] These are not severe restrictions in the present experiment giving allowable stop rates of 1 kHz and 100 Hz for start rates of 100 kHz and 1 kHz respectively.

The distortion of the time spectra described above is due to the use of a measurement technique that only measures one event per operating cycle and ignores all those following events. The MCA spectra were checked at selected count rates for distortion at typical full scale times ($N\Delta t$) of the TAC using random pulses in the stop channel supplied by the PMT with the electron gun in the unpulsed mode and start pulses at 100 kHz supplied by the pulser. The time spectra are free of any obvious distortions from a straight line with zero slope on the 5 microsec scale at a stop count rate of 1kHz (see Fig. 4-6, Dark Count Spectra and a Start Count Rate at 100 kHz), and on to 10 microsec scale at a count rate of 1.0 kHz (see Fig. 4-7, Dark Count Spectra and a Start Count Rate of 100 kHz).

Spectral Overlap:

Spectral overlap due to the finite resolving power of the optical monochromator is an important factor in any optical measurement. Blended lines can sometimes mistakenly be interpreted as cascades and spectral overlaps can be an important consideration in the study of molecular systems where vibrational band systems may overlap each other.

Wavelength scans were made in the region of interest 2000 to 3500 $\mathring{A}$ to determine if the transitions monitored were free of spectral overlap. In addition, a survey of

Fig. 4-6

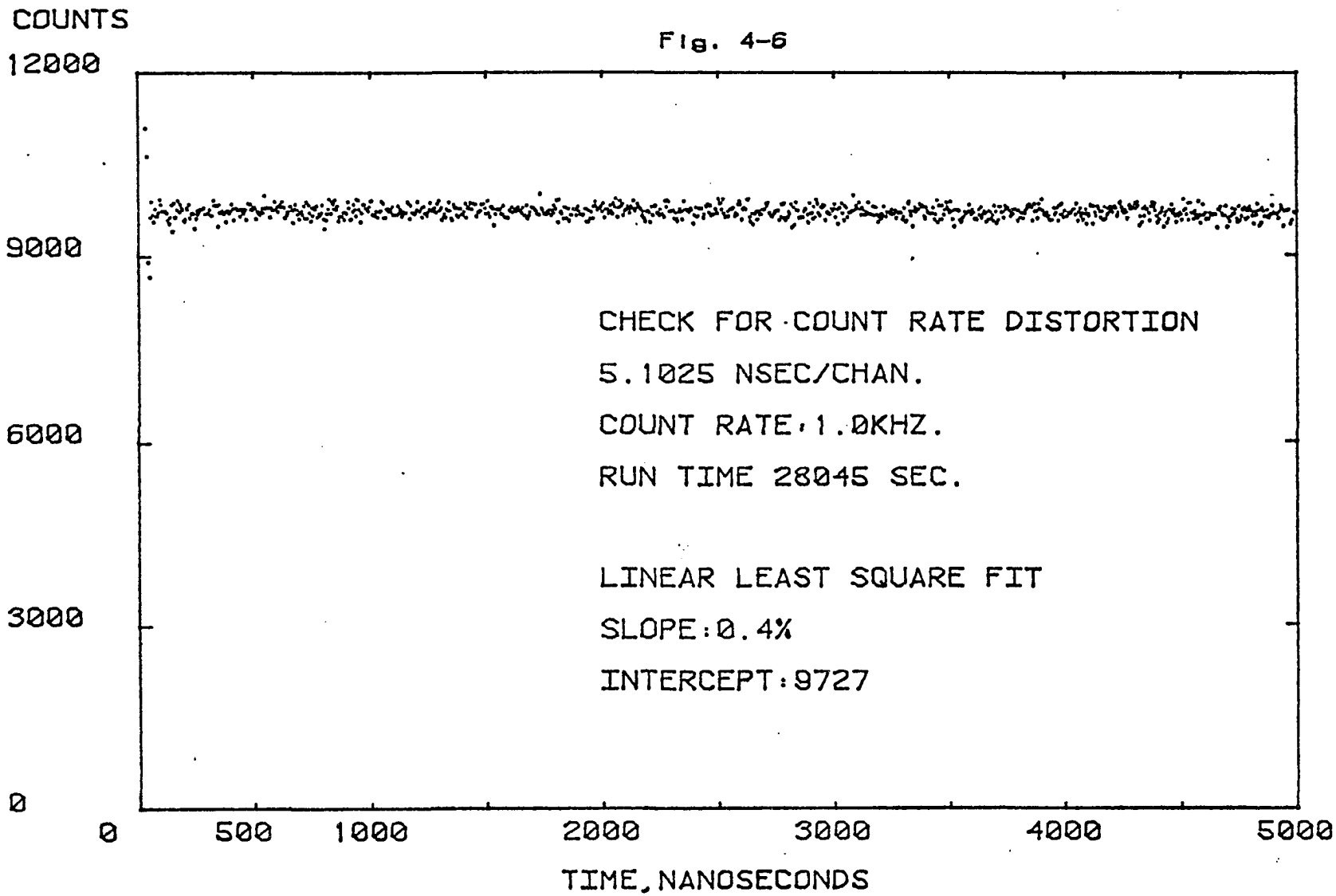
COUNTS
12000
9000
6000
3000
0
0
500
1000
2000
3000
4000
5000
TIME, NANOSECONDS
CHECK FOR COUNT RATE DISTORTION
5.1025 NSEC/CHAN.
COUNT RATE: 1.0KHZ.
RUN TIME 28045 SEC.
LINEAR LEAST SQUARE FIT
SLOPE: 0.4%
INTERCEPT: 9727

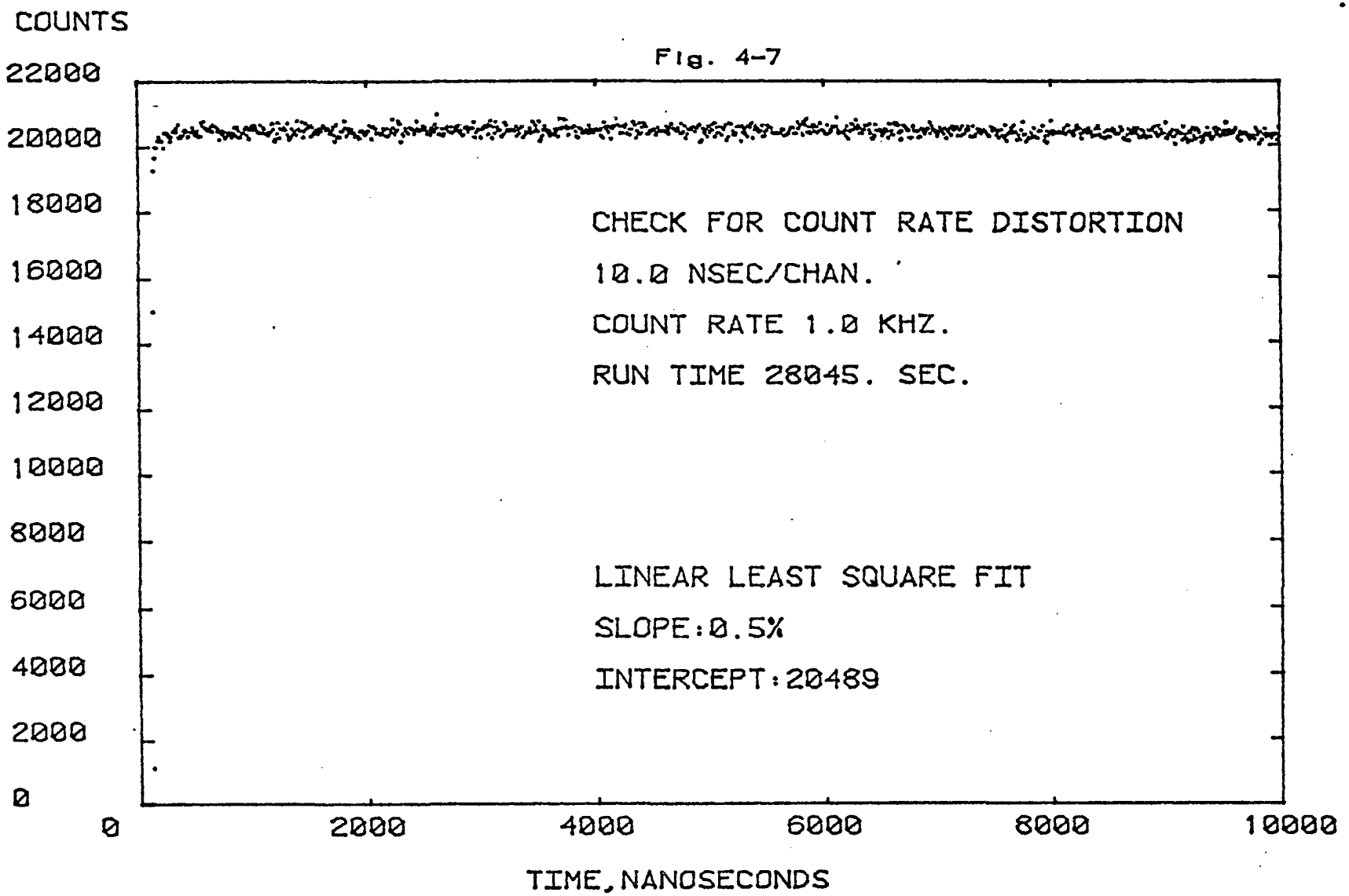
COUNTS
22000
20000
18000
16000
14000
12000
10000
8000
6000
4000
2000
0
0
2000
4000
6000
8000
10000
TIME, NANOSECONDS
CHECK FOR COUNT RATE DISTORTION
10.0 NSEC/CHAN.
COUNT RATE 1.0 KHZ.
RUN TIME 28045. SEC.
LINEAR LEAST SQUARE FIT
SLOPE: 0.5%
INTERCEPT: 20489

Fig. 4-7

the spectroscopic literature Suchard,[61] Rosen,[60] Pearse and Gaydon,[62] Krupenie[12] was undertaken to check for line blending that the optical monochromator would not resolve. The wavelength spectra were obtained with 20 Å resolution and electron beam energies of 10-20 eV. See Fig. 4-10 (wavelength-spectra). For the optical resolution used in this work, no spectral overlap was found for the third positive system for electron energies up to a few tenths of an electron volt above the $b^3\Sigma^+$ ($v'=0$) threshold (10.39 eV). The $b^3\Sigma^+$ ($v'=0$)→$a^3\Pi$($v''=1$) transition at 2977 Å is nearly overlapped by the b^3 + ($v'=0$)→$a^3\Pi$($v''=1$) transition at 2930 Å. However, the 2930 Å line is expected to be weak due to the small excitation cross section of the $b^3\Sigma^+$ ($v'=1$) level. The $b^3\Sigma^+$ ($v'=0$) → $a^3\Pi$($v''=0$) transition at 2833 Å has an adjacent line at 2799 Å, due to the $A^1\Pi$($v'=0$)→ $X^1\Sigma^+$($v''=22$). The lines were resolved in the present case. The 3134 Å line $b^3\Sigma^+$($v'=0$) → $a^3\Pi$($v''=2$) is overlapped by a line at 3138 Å $C^1\Sigma^+$($v'=0$) → $a^3\Pi$($v''=2$). However, by keeping the electron energy set at the peak of the $b^3\Sigma^+$($v'=0$) excitation cross section, the $C^1\Sigma^+$($v'=0$) state will not be populated, since its threshold is 0.7 eV above the energy at the peak (10.7 eV). In addition, since this is an intercombination line, it is expected to be weak.

The relative optical excitation function, as well as the lifetime of the $b^3\Sigma^+$($v'=0$) level, were measured by

studying the 2833 Å (0,0), 3134 Å (0,2) and 2977 Å (0,1) lines with electron energy resolution of 0.3 eV. These lines suffer from spectral overlap above the 16.5 eV threshold of the $A^2\Pi$ from the Comet tail bands ($A^2\Pi \rightarrow X^2\Sigma^+$) of CO^+ and above the 19.7 eV threshold of the $B^2\Sigma^+ \rightarrow X^2\Sigma^+$).

The Bausch and Lomb high intensity optical monochromator used for all $b^3\Sigma^+$ lifetime measurements had a 0.25 mm exit slit. The optimum entrance slit was approximately 0.50 mm, but a 0.75 mm slit was used to increase the detected light intensity. The optical resolution in this configuration is approximately 20 Å. Cascades have been avoided as much as possible by keeping the electron gun energy near the peak of the $b^3\Sigma^+(v'=0)$ cross section at 10.7 eV. It should be noted that this is just above its threshold of 10.39 eV.

Analysis of data sets collected on a 0.5 μ sec full range time scales indicated the existence of weak long lived components in the decay of the $b^3\Sigma^+(v=0)$ state, even when near threshold excitation was used. This necessitated lengthening the TAC time range to 5.0 μsec in order to provide accurate analysis of these long lived components. It also required a computer fit to the well known sum of exponentials,

$$n(t) = D_I \exp(-\lambda_I t) + D_J \exp(-\lambda_J t) + D_K \exp(-\lambda_K t) + D \qquad (4\text{-}16)$$

where $\lambda_I = A_I + K_I p$

A_I - transition probability for the Ith level (sec^{-1}) extrapolated to zero and including any diffusion effects

K_I - pressure quenching coefficient (sec^{-1}/mTorr)

p - pressure (mTorr)

D - a constant background due to detector and electronic noise.

D_I, D_J, D_K are the amplitudes of each exponential and contain cross sections and transfer coefficients, as well as probabilities of the various levels. The specific form depends on the specific decay scheme chosen with which to model the system.

No dipole allowed transitions ending on the $b^3\Sigma^+(v'=0)$ level have been found in the literature,[12,59-62] although at least two cascade components have been observed. In addition to fitting cascade components, it is possible to find the electron gun cutoff by multiple exponential deconvolution if the TAC range is sufficiently short. (See Chapter 3 for one level with a feed mechanism.) In this way, the cutoff of the electron gun was found to be approximately 3 nsec with the 0.040 apertures in the 2 and 4 elements and 5-8 nsec without the apertures. See Figs. 4-8 and 4-9 for typical data from which the gun cutoff was obtained.

The data in Fig. 4-8 is the $b^3\Sigma^+(v'=0) \rightarrow a^3\Pi(v''=1)$ transition at 2977 Å. The best fit to this data was

$$N(t) = -1429\exp(-t/3.55) + 28133 \exp(-t/53.78) + 389 \quad (4\text{-}17)$$

where N(t) is the total counts at time t in nanoseconds. The above fit was made to a record length of 445 channels for a channel width of 0.21786 nsec/chan at an energy of 11.8 eV. The first exponential in Eq. (4-17) corresponds to the a gun cutoff with a 3.55 nsec lifetime and the second is the prompt decay of the $b^3\Sigma^+(v=0)$ level. The lifetime here is 53.78 nsec, significantly longer than the lifetimes determined on longer time records in this work. The reasons for this discrepancy are discussed later in Chapter 5, but are related to ignoring long lived components which add to the background and distort the shorter lifetimes. This effect has been discussed by Carlson et al.[9] for the case of CO.

The data shown in Fig 4-9 is the $c^3\Pi(v'=0) \rightarrow a^3\Pi(v''=0)$ transition at 2295 Å. The best fit to the data for a record length of 550 channels is represented by the formula

$$N9t) = -366 \exp(-t/3.25) + 6109 \exp(-t/11.57) + 609 \exp(-t/93.8) + 1848 \quad (4\text{-}18)$$

giving a reduced chi square of 1.0295.

Fig. 4-8

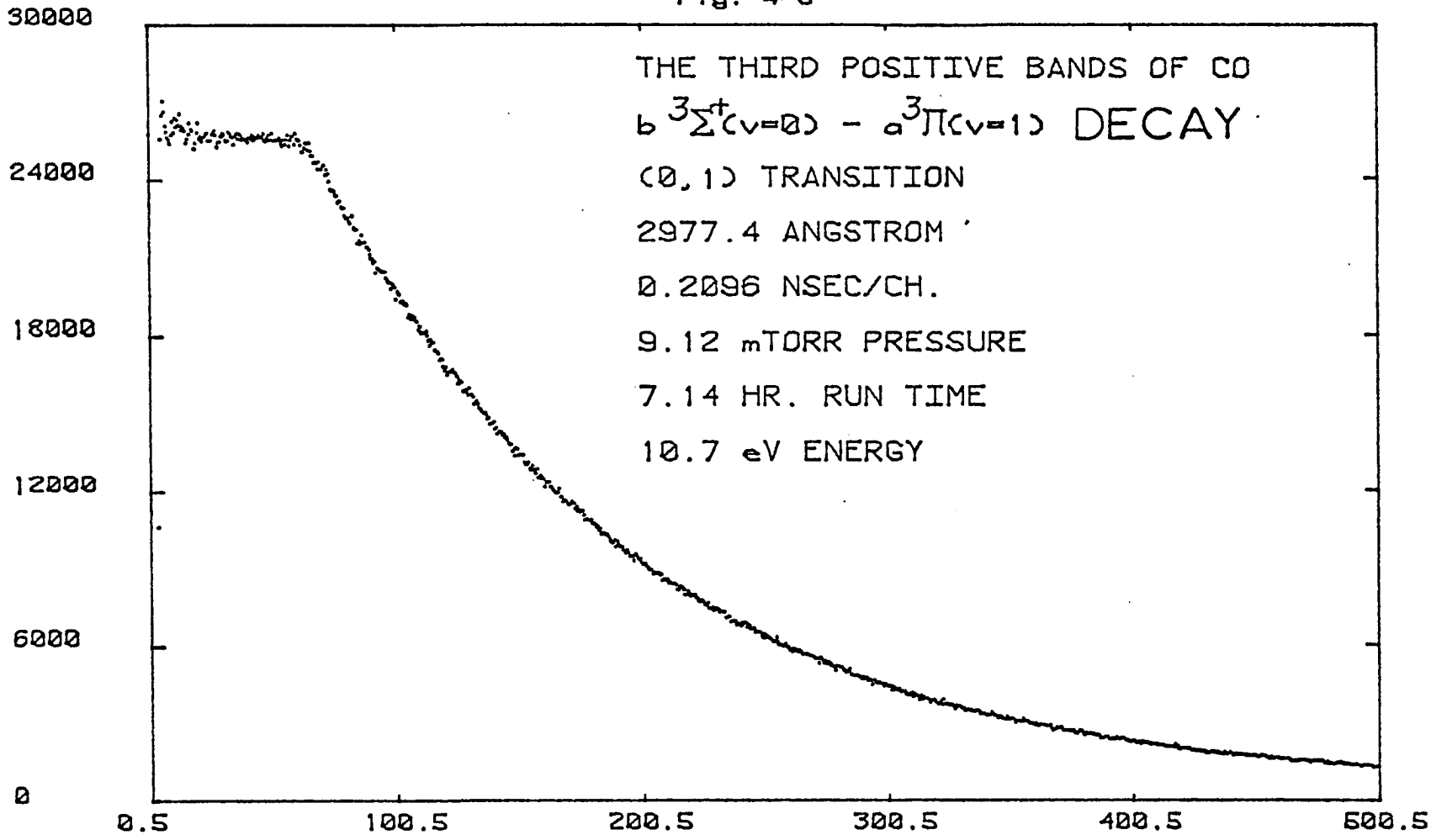
30000
24000
18000
12000
6000
0
0.5
100.5
200.5
300.5
400.5
500.5
THE THIRD POSITIVE BANDS OF CO
b $^3\Sigma^+$(v=0) - a $^3\Pi$(v=1) DECAY
(0,1) TRANSITION
2977.4 ANGSTROM
0.2096 NSEC/CH.
9.12 mTORR PRESSURE
7.14 HR. RUN TIME
10.7 eV ENERGY

As in Fig 4-8, the 3.25 nsec component is the electron gun cutoff. The 11.57 nanosec component is the prompt decay of the $c^3\Pi(v'=0)$ level and the weak component at 93.8 nanosec is due to spectral overlap from the $A^1\Pi \rightarrow X^1\Sigma^+$ bands at 2332, 2311, 2286, 2273 Å. The lifetime of the $c^3\Pi(v=0)$ state has been determined to be 16±2 nsec by Van Sprang et al.[1] By fitting to only one exponential we obtain 13.46 nsec, which for a single measurement is in reasonable agreement with Van Sprang et al. The remainder of the discrepancy is probably due to fitting procedures used by Van Sprang et al.[1] and discussed in another section. The gun cutoff parameter seems to be well determined by these two measurements using different wavelengths and states.

The apertures were removed to provide more beam current to study weaker systems. The amplitude of the gun cutoff exponential also increased with the apertures removed, as expected for the larger beam current.

A computer program, RTLASL, was used to extract lifetimes and amplitudes from the data.[67,79] The program fit the data by the technique of non-linear least squares. The usual analysis procedure called for fitting one, two and, if needed, three exponentials to improve the fit to the data. In those cases where the gun cutoff was desired to be examined, a fourth exponential was added to the fitting function.

Fig. 4-9

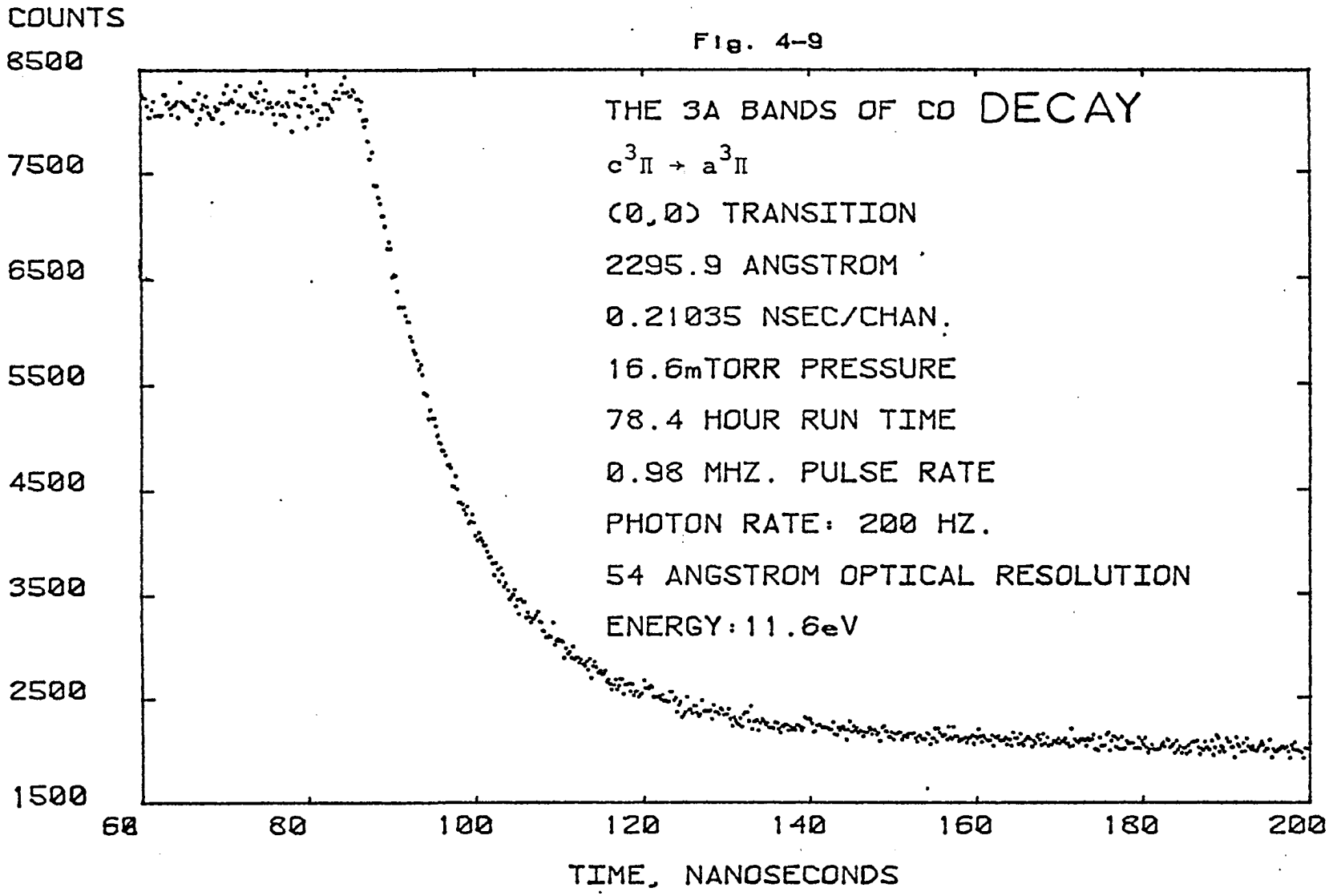
COUNTS
8500
7500
6500
5500
4500
3500
2500
1500
60
80
100
120
140
160
180
200
TIME, NANOSECONDS
THE 3A BANDS OF CO DECAY
$c^3\Pi \rightarrow a^3\Pi$
(0,0) TRANSITION
2295.9 ANGSTROM
0.21035 NSEC/CHAN.
16.6mTORR PRESSURE
78.4 HOUR RUN TIME
0.98 MHZ. PULSE RATE
PHOTON RATE: 200 HZ.
54 ANGSTROM OPTICAL RESOLUTION
ENERGY:11.6eV

Fig. 4-10

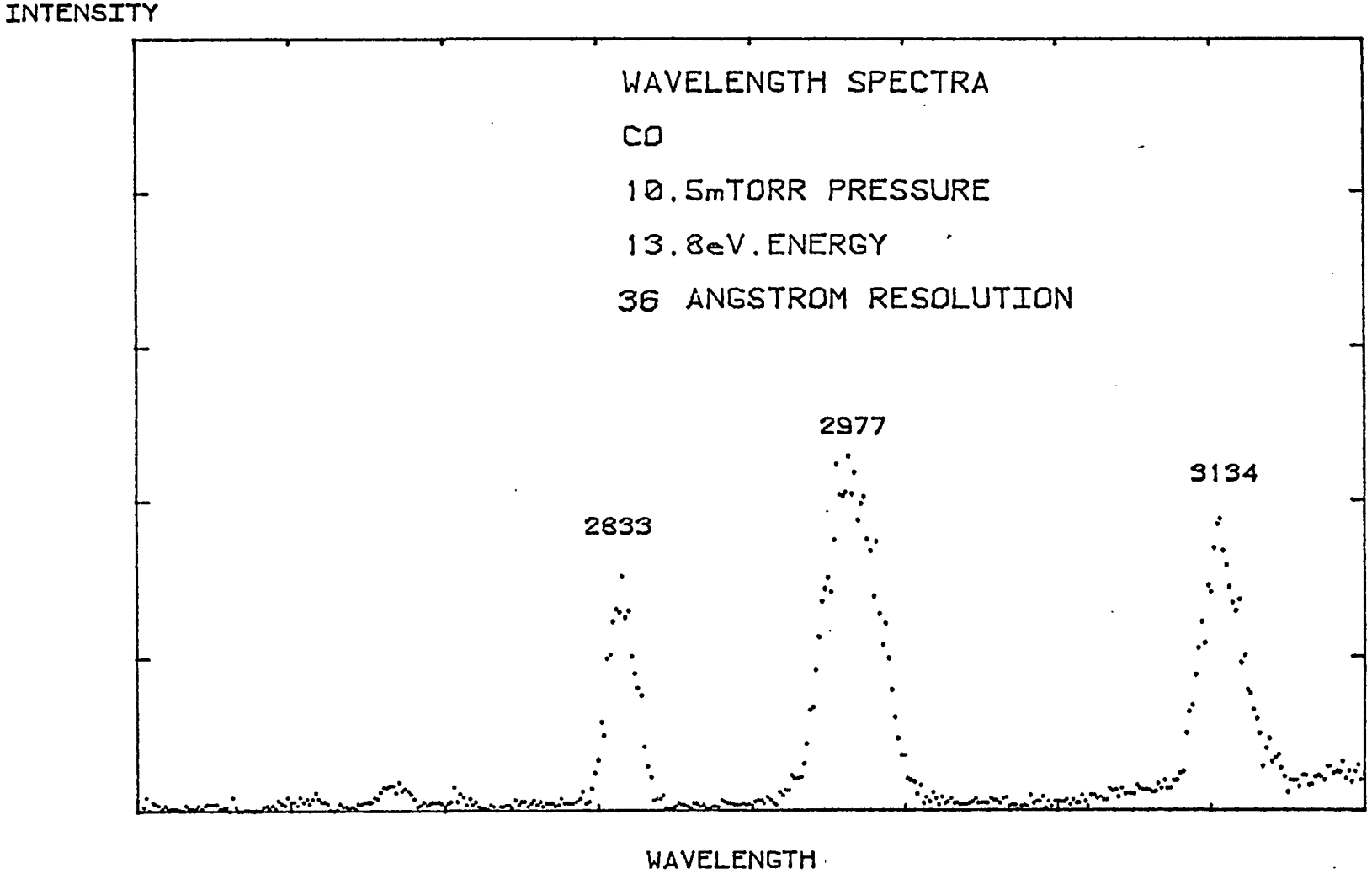
INTENSITY
WAVELENGTH SPECTRA
CO
10.5mTORR PRESSURE
13.8eV. ENERGY
36 ANGSTROM RESOLUTION
2977
3134
2833
WAVELENGTH

In all data analysis, the first and last channels included in the analysis were varied to ascertain if another component which has not been identified or accounted for in the fitting function was distorting the lifetimes.

F. Quenching Coefficients

The pressure in the collision region was varied from 1 to 20 mTorr in order to measure the quenching coefficients. The lifetimes were measured at each pressure, while the electron energy was set at 10.7 eV. Using the relation $\lambda_I = A_I + K_I p$, a plot of $\lambda_I(p)$ vs. p was made and extrapolated to zero pressure. The slope of the line yields a value for K_I, and the intercept is the zero pressure transition probability, A_I, which can indlude the effect of diffusion.[65,81] The pressure data were fit by the technique of weighted linear least squares.[80] Cascade components, which have lifetimes comparable to the diffusion time of the excited molecules out of the viewed portion of the collision region, will have a substantial distortion to A_I. No correction for long lifetimes was made for diffusion, but Curtiss et al.[82] have worked out the details and established that it is theoretically possible in a number of cases to make this correction with excellent results. Another possible approach to the problem of diffusion of metastables from the viewed region is to vary the extent of this region for the longer lifetimes by suitable

arrangement of the optical system. The calculation of the geometry of the viewed region is an involved function of the light gatering optics and the specific optical monochromator geometry which all may vary as a function of the wavelength of the light detected. The approach taken has been to include all the above effects in the zero pressure transition probability. This will have the effect of decreasing the zero pressure lifetime of the state under study and could affect excitation transfer coefficients as well. The estimated diffusion time for this apparatus is 5 μsec. This was estimated by using thermal velocities of the CO molecule and estimating the field of view of the optical system to be on the order of 2 mm.

G. Excitation Transfer Rate Coefficients

Assume a system that has one cascade component (level J) feeding another level K. The level K decays via a prompt transition K-L and corresponds to the wavelength that is monitored. Such a system is shown schematically in Fig. 3-2. The transition K-L is monitored with the appropriate wavelength and resolution selected by the monochromator and associated detectors. The expression for N (t), the number of molecules in the Kth level as a function of time after the beam turnoff is given by

$$N_K(t) = \{N_K^0 + \frac{\lambda_{JK}N_J^0}{(\lambda_K-\lambda_J)}\} \exp(-\lambda_K t) + \frac{\lambda_{JK}N_J^0}{(\lambda_K-\lambda_J)} \exp(-\lambda_J t) \quad (3\text{-}9)$$

where it has been assumed that we can neglect the reverse transition K→J, since if these reactions were large it is doubtful that the effect of J→K would be seen at all. N_K^0 and N_J^0 are defined as follows.

$$N_K^0 = \frac{nQ_K I_0 + \lambda_{JK}N_J^0}{\lambda_K}$$

$$N_J^0 = \frac{nQ_J I_0}{\lambda_J} \quad . \quad (3\text{-}6)$$

The ratio of the amplitudes of the exponentials will now be calculated along with the finite channel width correction.

Effect of Finite Channel Width:

Consider a fluorescence decay that consists of one cascade of reciprocal lifetime A_J and amplitude C_J with a prompt component of reciprocal lifetime A_K and amplitude C_K. The number of molecules in the K level, as a function of time after the electron beam is turned off, is

$N_K(t) = C_J e^{-A_J t} + C_K e^{-A_K t}$.

The photon flux due to molecules that decay from level K to L by a dipole allowed transition, emitting a photon of wavelength λ is

$$I_{KL}(t) = A_{KL}N_K(t) \tag{4-17}$$

where A_{KL} is the transition probability for the K,L transition and the signal detected by the optical detector is

$$S_{KL}(t) = G(\lambda)A_{KL}N_K(t) \tag{4-18}$$

where $G(\lambda)$ is the geometric factors and detection efficiency of the detection system which may be a function of λ. If the time histogram is recorded by a TAC in a MCA with time channels of width Δt and the experiment is run for a total time T, the number of counts recorded in the Ith channel is[49,67]

$$C_n(I) = TG(\lambda)A_{KL}\int_{i\Delta t-\frac{1}{2}\Delta t}^{i\Delta t+\frac{1}{2}\Delta t} \{C_K \exp(-A_K t) + C_J \exp(-A_J t)\}dt \tag{4-19}$$

carrying out the integration

$$C_n(I) = TG(\lambda)A_{KL}\{\frac{C_K}{A_K} e^{-I\Delta tA_K}(e^{\frac{1}{2}\Delta tA_K} - e^{-\frac{1}{2}\Delta tA_K}) + \frac{C_J}{A_J} e^{-I\ tA_K}$$

$$x\ (e^{\frac{1}{2}\Delta tA_J} - e^{-\frac{1}{2}\Delta tA_J})\}$$

by expanding the exponentials in the parenthesis and keeping only terms up to $(\Delta A_J)^2$

$$C_n(I) = TG(\lambda)A_{KL}\{\Delta t(1+\tfrac{1}{4}\Delta t A_J)C_J e^{-A_J I\Delta t} + \Delta t(1+\tfrac{1}{4}\Delta t A_K)C_K e^{-A_K I\Delta t}\}.$$

If we assume that $\frac{1}{4}\Delta tA \ll 1$ then the expression becomes

$$C_n(I) = TG(\lambda)A_{KL}\{\Delta tC_J \exp(-A_J\Delta t) + \Delta tC_K \exp(-A_K I\Delta t)\}. \quad (4\text{-}20)$$

In the case where $\frac{1}{4}\Delta tA_J \ll 1$, the number of counts in the Ith channel is just the count rate at the center of the channel multiplied by the channel width and the run time and other constants. If $\Delta tA_J \geq 1$, then the amplitudes of the cascades are distorted depending on their lifetimes.

Eq. (4-20) represents the data that will be collected ignoring the constant background counts for now. Once the time spectra is analyzed, the lifetimes and amplitudes of the spectra stored in the MCA and represented by Eq. (4-20) will be obtained.

Let

$$D_K = TG(\lambda)A_{KL}\Delta tC_K$$

D_K - the amplitude of the prompt component and

$D_J = TG(\lambda)A_{KL}\Delta tC_J$.

If we make several runs at various pressures and calculate the ratio of $D_K(p)/D_J(p)$ at each pressure, we will obtain an experimental curve describing the form of unknowns in the equation

$$\frac{D_K(p)}{D_J(p)} = \frac{C_K(p)}{C_J(p)}$$

where $C_K(p)$ has been written to explicitly show the pressure dependence of the original amplitudes $C_K(p)$ and $C_J(p)$. It is useful to note that in taking the ratio, the run time, detection efficiency and geometric terms, time width of the channels and A_{KL}, the transition probability cancels out. In effect, this ratio is not dependent on the run time or detection efficiencies or even the lower transition, L, used to monitor the fluorescence

$$T(p) = C_K(p)/C_J(p).$$

The ratio of the prompt amplitude divided by the delayed is given by the following using Eq. (3-9)

$$T(p) = \{N_K^0 - \frac{\lambda_{JK}N_J^0}{(\lambda_K-\lambda_J)}\} / \{\frac{\lambda_{JK}N_J^0}{(\lambda_K-\lambda_J)}\} = \{\frac{(\lambda_K-\lambda_J)N_K^0}{\lambda_{JK}N_J^0}\} - 1$$

substituting for the equilibrium population densities N_K^0, N_J^0:

$$T(p) = \frac{(\lambda_K-\lambda_J)}{\lambda_{JK}} \frac{\{nQ_KI_0+\lambda_{JK}(nQ_JI_0/\lambda_J)\}\ (1/\lambda_K)}{(nQ_JI_0/\lambda_J)} - 1$$

$$T(p) = \frac{(\lambda_K-\lambda_J)\lambda_J}{\lambda_{JK}\lambda_K} \left\{\frac{Q_K + \lambda_{JK}\frac{Q_J}{\lambda_J}}{Q_J}\right\} - 1 \qquad (4\text{-}21)$$

rearranging terms, we are left with

$$T(p) = \frac{(\lambda_K-\lambda_J)\lambda_J}{\lambda_{JK}\lambda_K} \frac{\{Q_K + (\lambda_{JK}/\lambda_J)Q_J\}}{Q_J} \qquad (4\text{-}22)$$

In the case of the $b^3\Sigma^+(v'=0)$ state, we can make the approximation $\lambda_K > \lambda_J$

$$T(p) + 1 \tilde{\sim} \lambda_J\{Q_K + (\lambda_{JK}Q_J/\lambda_J)\}/\lambda_{JK}Q_J$$

which can be simplified to give

$$T(p) = \frac{\lambda_J}{\lambda_{JK}} \frac{Q_K}{Q_J} \; . \qquad (4\text{-}23)$$

This formula shows that the ratio of the experimentally determined amplitudes $T(p) = D_K(p)/D_J(p)$ as a function of pressure is independent of the electron gun current as well as the previously mentioned parameters. T(p) only contains cross sections, quenching and excitation transfer coefficients. If sufficient data concerning the Jth state and the Kth state is available, then the other unknown parameters can be determined by a curve fitting procedure to the experimental data.

Even in the present case of two cascades, if an electron energy can be found where one cascade is sufficiently weak, the data can be analyzed ignoring the weakest component. This was done by setting the electron energy at 10.7 eV and measuring lifetime spectra at several pressures. The long lived cascade is not zero even at this low electron energy, but it is sufficiently weak so as to introduce only about 10% error in the amplitude of the medium component error by ignoring it.

H. Time Resolved Optical Emission Function

Time resolved emission functions are useful when the cascade components on a particular state have lifetimes very much different from the state studied. By pulsing the electron beam, the various components (having different decay constants) may be studied. A time interval is selected in which all components but one have decayed away. By counting photons which occur only in the selected region and sweeping the beam energy, an emission function for one excitation process is measured.[28] The time regions are referred to as the prompt, delayed and total. The prompt region is that time region just after cutoff or turn-on of the electron gun and is due to molecules that have been excited into the K state and decay with its decay constant of τ_K (see Figs. 3-1 and 3-2). The delayed region

starts at $8\tau_K$ or $10\tau_K$ after cutoff of the beam and stops just before the next turn-on of the beam. The delay region corresponds to long lived processes from the J level with decay constant τ_J. These remarks assume a three level system. Similar remarks apply in the case of a two cascade component system (Fig. 3-3) except that the separation into prompt and delay now gives a delayed region that includes two long lived components.

Example:

Lifetime spectra at some energy is analyzed and shows a fluorescence to be of the form

$$N(t) = D_J \exp(-t/\tau_J) + D_K \exp(-t/\tau_K) + D$$

a typical set of decay parameters similar to those found for the $b^3\Sigma^+$ state (ignoring the weak second cascade)

D_K = 10000 counts $\qquad$ D_J = 300 counts

τ_K = 50 nsec $\qquad$ τ_J = 400 nsec

D = 200, background counts

where D_K and τ_K are prompt amplitude and lifetime and D_J and τ_J are delayed amplitude and lifetime.

$$N(t) = D_K \exp(-t/50) + D_J \exp(-t/400) + 200$$

Calculate the ratio

$$R(t) = D_K \exp(-t/50)/D_J \exp(-t/400)$$

at various times after cutoff of the beam. This ratio is the number of molecules in the K level due to direct excitation to that level divided by the number due to cascade processes as a function of time after the electron beam cuts off. The ratio R(t) is the ratio of intensities measured at a time t due to prompt process versus the delayed process. The value of R(t) at t=0, $8\tau_K$ and $10\tau_K$ are given below.

$R(0) = 33.3$

$R(8\tau_K) = 0.03$

$R(10\tau_K) = 0.005$

The preceding example demonstrates that a delayed to prompt lifetime ratio of $\tau_J/\tau_K = 8/1$ is very favorable for separating the two decay components since ten prompt lifetimes τ_K after the beam cutoff, 99.5% of the remaining radiation present is due to the process with the 400 nsec lifetime. At time t=0, most of the fluorescence from the J level is due to the short lifetime component and only about 3% is due to the long lived decay. Thus, by first analyzing lifetime spectra, it is possible to choose time regions that will emphasize long lived processes over shorter lived ones. By collecting a series of lifetime spectra at different electron energies, the variation of the amplitudes of the prompt and cascade components will be obtained. By studying the functional dependence of the

amplitudes on energy, it is possible to select one amplitude to be negligibly small with respect to the others. Thus, one cascade component can be almost entirely eliminated from the optical emission functions and time spectra. All delayed emission functions have been taken with the lower level discriminator (LLD) of the TAC set at $8\tau_K$ or $10\tau_K$ as noted. That is, the LLD is set to discriminate against pulses that do not occur after the selected time from the beam cutoff.

When studying long lived states, the electron gun must remain on for a time that is long enough to allow the excitation processes of the states to saturate before the electron gun is cut off, and the gun must remain off long enough to allow significant numbers of these excited long lived molecules to decay and be detected. To satisfy these requirements, the beam is pulsed with a square wave of period $10\tau_I$ where τ_I is the longest lifetime present. In the case of the $b^3\Sigma^+(v'=0)$ state, the delayed photons were counted from 400 nsec or 500 nsec after beam cutoff until the end of the record length or approximately 5 μsec.

The beam energy is determined by a Kepco 100 volt D.C. power supply which floats on the output voltage of a digital to analog ramp generator. The ramp will scan from 0 volts to 10 volts in 1024 steps. The scan interval is fixed at 0 to 10 volts, but it may be offset with the D.C. supply.

The usual procedure followed is to set the voltage between the scattering cell and RPD to about one volt below the threshold of the state being investigated. This arrangement will allow energies of 9.0 volts above threshold which includes regions of interesting structure. If larger voltage sweeps of the beam energy are desired, the KEPCO supplies may be voltage programmed using the ramp generator as a programming voltage. By this method the accelerating voltage may be swept from 0 to 100 volts.

Energy Scale Calibration:

The energy scale is calibrated by comparison of structure on measured optical emission functions to those taken on high resolution experiments[16,17] and by comparison to differential scattering measurements.[18,19] Spectroscopic data[12] gives accurate positions of thresholds and thus, provides a low energy calibration point on all optical emission functions.

Transmitted electron spectra, especially those done at 0.100 meV resolution, provides accurate positions of thresholds, resonances and other structure in the decay channels studied.

Energy scales were calibrated using as a minimum the spectroscopic threshold and three structures in each excitation function that had been independently observed in

several other experiments. In the case of the $b^3\Sigma^+(v'=0)$ state, the threshold at 10.39 eV, a sharp peak at 10.7 eV and a broad peak at 11.2 and structure at 12.2 were used to determine the absolute calibration and linearity of the energy scale (±0.3 eV at low resolution).

This energy scale calibration is necessary, due to the difficulty in determining the potential difference between the cathode surface from which the electrons are emitted and the scattering cell. The potential between the metal base of the cathode and the scattering cell is measured by a digital panel meter (Digitek model 2780) and is determined within ±1%. However, the electrons are emitted from oxide layers that have been deposited on the cathode in the form of carbonates or hydroxides of the alkaline-earths barium, strontium and calcium.[35,83] These deposits are further reduced to oxides by a heating process, and it is the free metals that coat the oxide layers on the cathode that provide the high electron current density over that of the uncoated metal. There is a potential drop across the oxide layers that can amount to several volts[83] and which is dependent on past history of the cathode and its present condition. It is this cathode potential drop that makes direct measurement of the beam energy difficult and results in the use of energy calibration by comparing thresholds and structure positions. When the RPD is tuned to maximize the low

frequency signal detected by a phase sensitive amplifier (PAR) connected to the Faraday cup, the voltages are set so that the electrons cross the screen with almost zero enrgy (refer to RPD principle section). Thus, the potential difference between the RPD screen and the scattering cell is an accurate determination of the energy scale (± 100 meV with 100 meV peak to peak modulation).

Data Analysis and Tests of Computer Program RTLASL:

A computer program which is more fully described elsewhere,[67,79] was used to extract the lifetime components by fitting the data to Eq. (4-16) using a non-linear method of least squares. The program can fit up to four exponentials plus a constant background and was tested using synthesized data containing chosen exponentials plus varying amounts of Gaussian distributed noise.[84] It was found that the program could extract decay constants as long as the noise was less than one standard deviation. The effect of varying the numbers of parameters used in fitting synthesized data and the resulting reduced χ^2 is shown in Table 4-1. The parameters chosen for this test are shown in the first row of the table. It should be noted that the values determined by the analysis slowly converge to the chosen values as more exponentials are added. In this case, when few exponentials are present τ_K is too large. It can also

Table 4-1. Non-Linear Computer Fit on Synthesized Test Data.

τ_1 (ns)	τ_2 (ns)	τ_3 (μs)	A_1	A_2	A_3	C	Gaussian Noise Factor (Standard deviations)	Calib. (ns/ch)	No. of Exp. Used in Fit	Reduced χ^2	Initial Ch.	Final Ch.
51	350	1.50	54000	1600	700	100	1	5	3	-	20	980
56.99	-----	------	54406	-------	------	352	1	5	1	169	20	980
±0.27			±187			±9						
51.79	692	------	54240	1751	------	160	1	5	2	3.1	20	980
±0.04	±5		±20	±10		±2						
50.93	351	1.50	55970	1582	701	99	1	5	3	1.008	20	980
±0.04	±11	±0.07	±24	±26	±33	±5						
51.69	402	1.79	53855	1548	596	88	2	5	3	4.260	20	980
±0.08	±25	±0.26	±42	±61	±70	±12						
55.37	-----	------	54002	-------	------	1270	1	0.5	1	7.15	20	980
±0.09			±93			±7						
51.70	278	------	53780	2044	------	657	1	0.5	2	1.050	20	980
±0.10	±32		±110	±56		±71						
50.92	282	1.02	53970	1316	1053	112	1	0.5	3	1.040	20	980
±0.88	±1222	±291	±2050	±140380	±32900	$\pm 10^3$						
50.18	326	1.43	20306	1427	721	102	1	5	3	1.013	30	980
±0.11	±11	±0.62	±26	±24	±31	±4						
51.93	370	1.55	7583	1173	630	97	1	5	3	1.023	40	980
±0.23	±15	±0.91	±21	±28	±34	±5						
51.08	407	2.69	54029	1717	585	10^{-18}	1	5	3	0.890	20	500
±0.05	±17	±0.96	±28	±52	±55							
50.79	339	1.72	54123	1590	825	10^{-18}	1	5	3	0.961	20	250
±0.25	±97	±2.80	±174	±472	±421							

Uncertainties represent one standard deviation of the computer fit to the data.
First line selected decay parameters of synthesized data.
Other lines computer fits for various record lengths (time lengths), number of exponentials fit (see text).

be seen that doubling the Gaussian distributed noise greatly increases the error associated with each decay constant. The errors listed in Table 4-1 are one standard deviation. The lifetime components are obtained with less systematic error when a 5.0 μsec record length is used, as opposed to that obtained when a 0.5 μsec record length is used. Finally, moving the first channel of the analysis to longer times affects the short lived exponentials, and similarly, moving the last channel of the analysis to shorter times affects the long lived exponentials.

CHAPTER V

RESULTS AND DISCUSSION

The total optical excitation function shown in Fig. 5-1 was obtained using the total electron gun cycle. It should be noted that the prominent resonance peaks and general structure are in good agreement with the results given by Fukui et al.[16] and Bose.[17] These structures were used to calibrate the electron energy scale. A comparison of the structures in the optical emission functions of Fukui et al.[16] and Bose[17] shows good agreement with the locations on the energy scale of these same structures in the differential scattering measurements of Mazeau et al.[18] and Swanson et al.[19] and the electron transmission measurements on CO of Schulz.[15]

A delayed excitation function obtained using the time region marked C in Fig. 5-2 is shown in Fig. 5-3. Note that even though the excitation pulse has been off for eight prompt lifetimes, or 400 nsec, an excitation function with a threshold near that of the total function still persists. It is clear from this curve that measurement of the prompt lifetime using threshold excitation does not eliminate long lived cascades.

Fig. 5-1

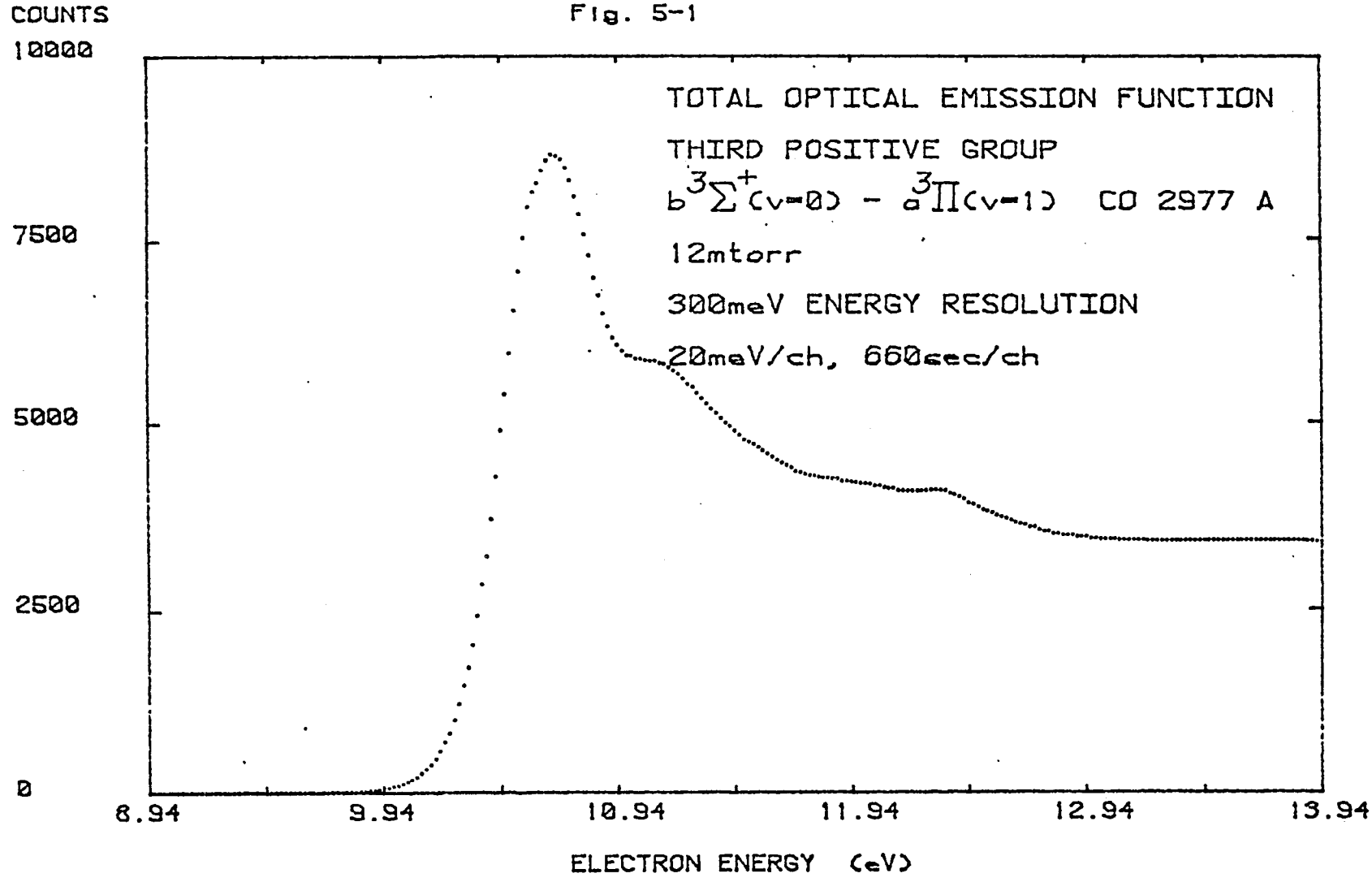
COUNTS
10000
7500
5000
2500
0
TOTAL OPTICAL EMISSION FUNCTION
THIRD POSITIVE GROUP
$b^3\Sigma^+(v=0) - a^3\Pi(v=1)$ CO 2977 A
12mtorr
300meV ENERGY RESOLUTION
20meV/ch, 660sec/ch
8.94
9.94
10.94
11.94
12.94
13.94
ELECTRON ENERGY (eV)

Fig. 5-2

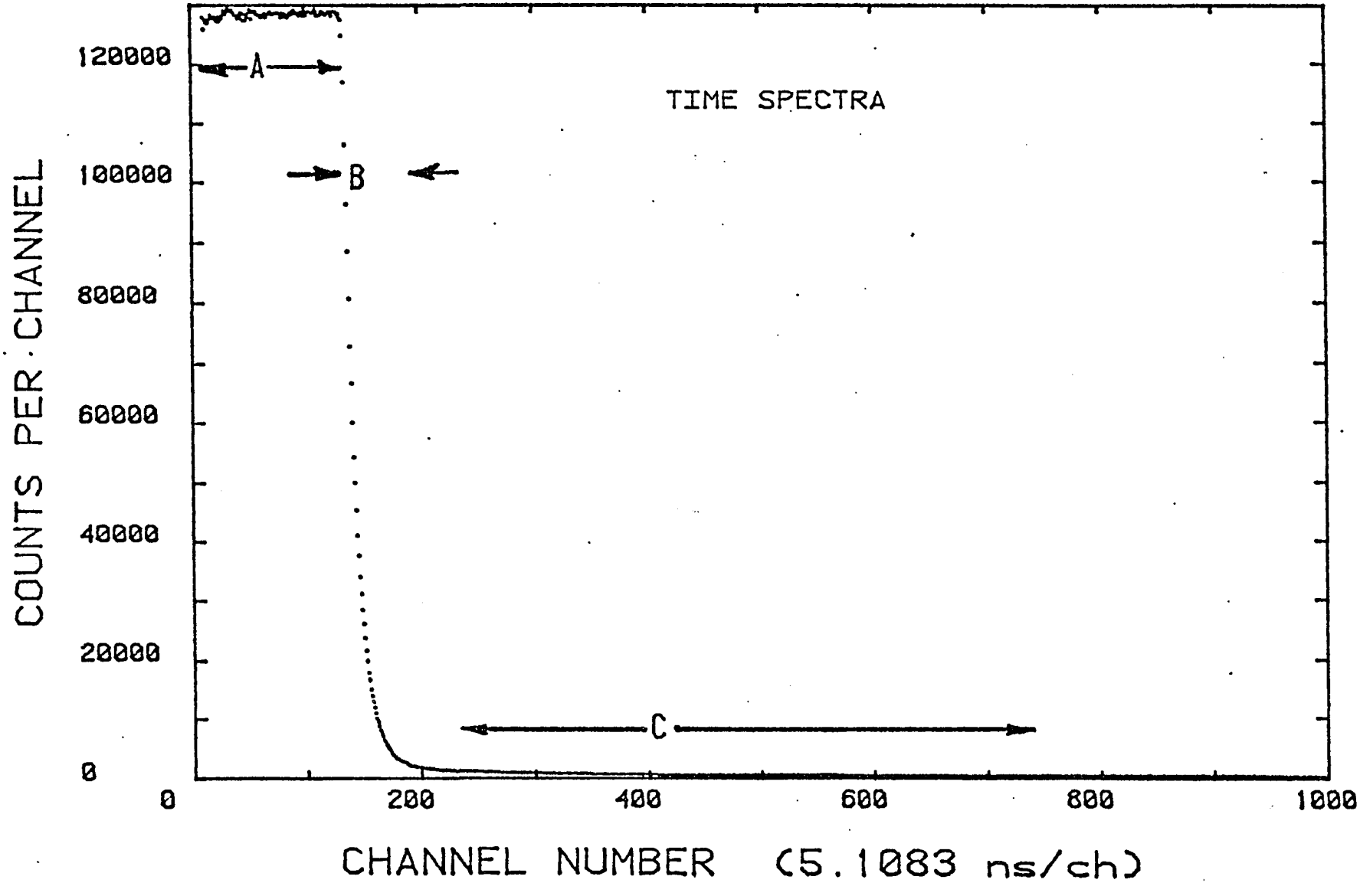
TIME SPECTRA
A
B
C
120000
100000
80000
60000
40000
20000
0
COUNTS PER CHANNEL
0
200
400
600
800
1000
CHANNEL NUMBER (5.1083 ns/ch)

Fig. 5-3: DELAYED 8γ EMISSION FUNCTION

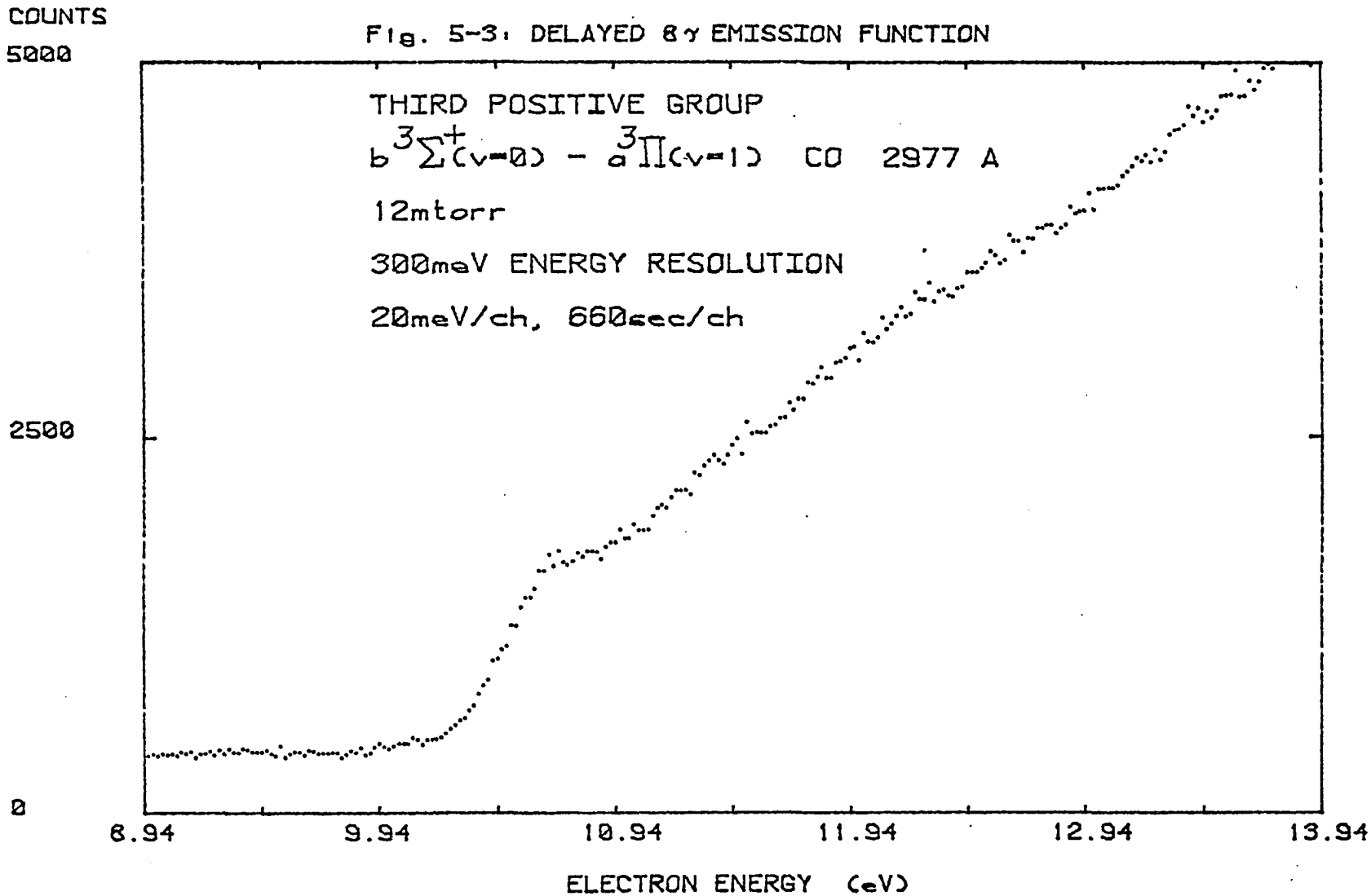

The delayed excitation function in Fig. 5-5 corresponds to photons that occur in the delay region approximately 10 prompt lifetimes (545 nsec) after the gun cutoff up to the start of the next excitation pulse. The two delayed curves (Fig. 5-3 and 5-5) show no substantial differences in structure and show that all but a very small fraction of the prompt emission has decayed away before either of these delayed emission functions were recorded. Fig. 5-6 shows a delayed emission function that runs from 1330 nsec to 5000 nsec after beam cutoff.

Fig. 5-4 is another total emission function that was collected simultaneously with the delayed curves shown.

The total and two delayed emission functions in Figs. 5-4, 5-5 and 5-6 were collected simultaneously so that comparisons of shape in the curves could be made without correction for electron optics.

A semilog decay curve for the b→a (0,0) transition in CO is shown in Fig. 5-7. The best fit to the data, using the method previously described, is shown as the solid line. The two dashed lines on the expanded scale represent the envelope of the extreme fits to the data as determined by the statistical error limits of the data at the 95% confidence level. Three lifetime components were extracted from data similar to that shown in Fig. 5-7. By taking data such as that shown at various pressures in the range from

Fig. 5-4

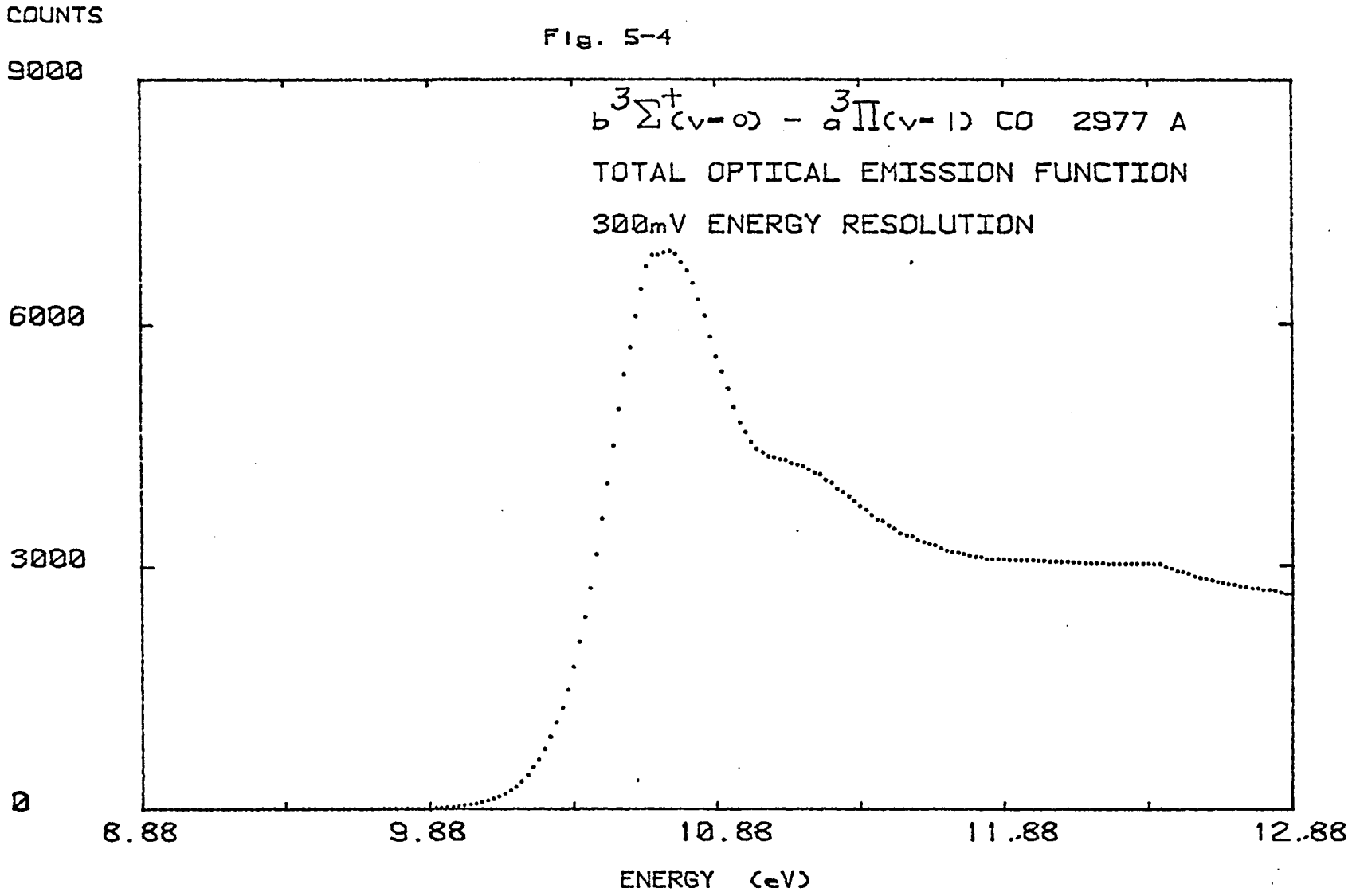
COUNTS
9000
6000
3000
0
$b\,^3\Sigma^+(v=0) - a\,^3\Pi(v=1)$ CO 2977 A
TOTAL OPTICAL EMISSION FUNCTION
300mV ENERGY RESOLUTION
8.88
9.88
10.88
11.88
12.88
ENERGY (eV)

Fig. 5-5

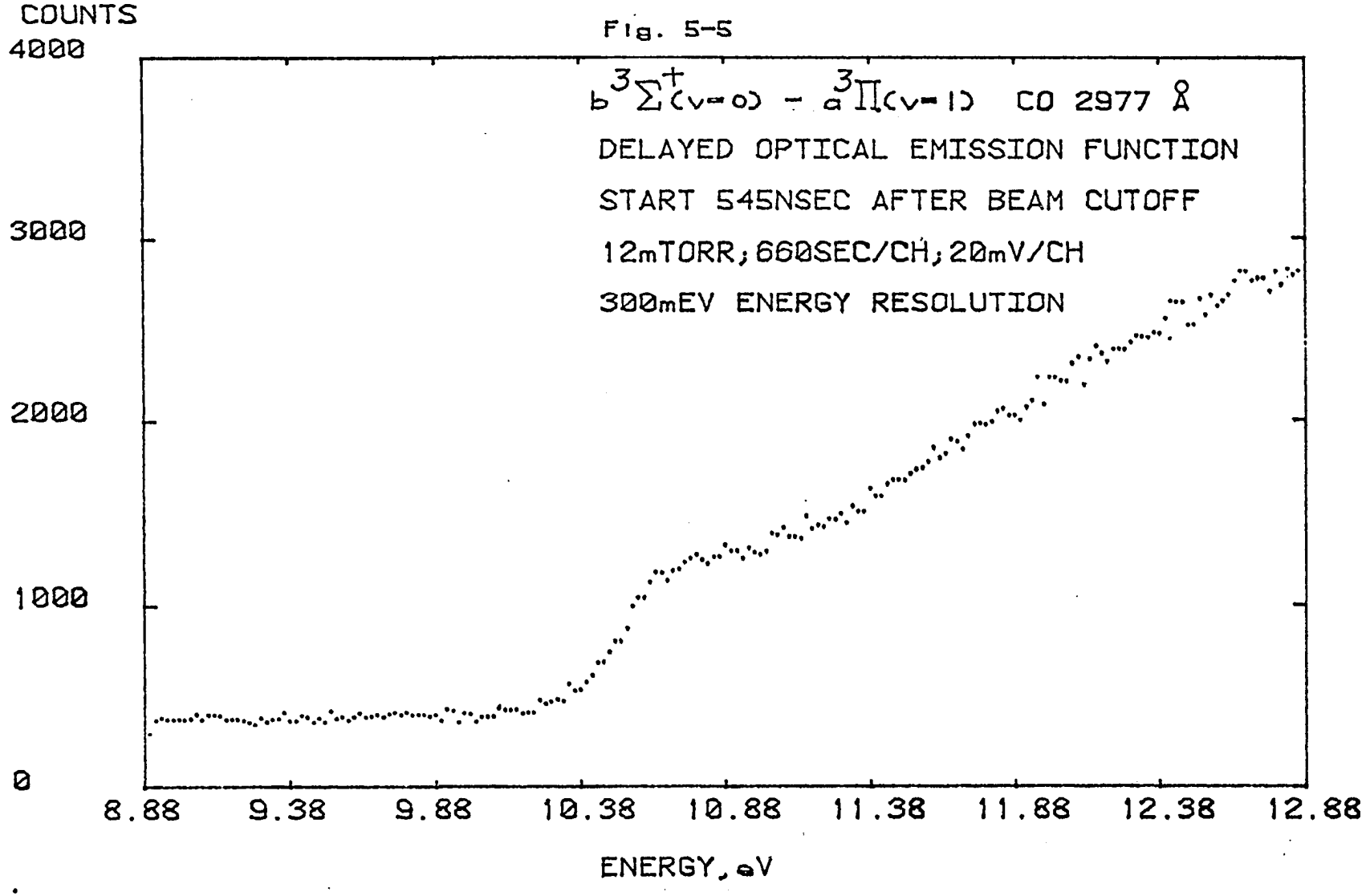
COUNTS
4000
3000
2000
1000
0
$b^3\Sigma^+_{(v=0)} - a^3\Pi_{(v=1)}$ CO 2977 Å
DELAYED OPTICAL EMISSION FUNCTION
START 545NSEC AFTER BEAM CUTOFF
12mTORR; 660SEC/CH; 20mV/CH
300mEV ENERGY RESOLUTION
8.88
9.38
9.88
10.38
10.88
11.38
11.88
12.38
12.88
ENERGY, eV

Fig. 5-6

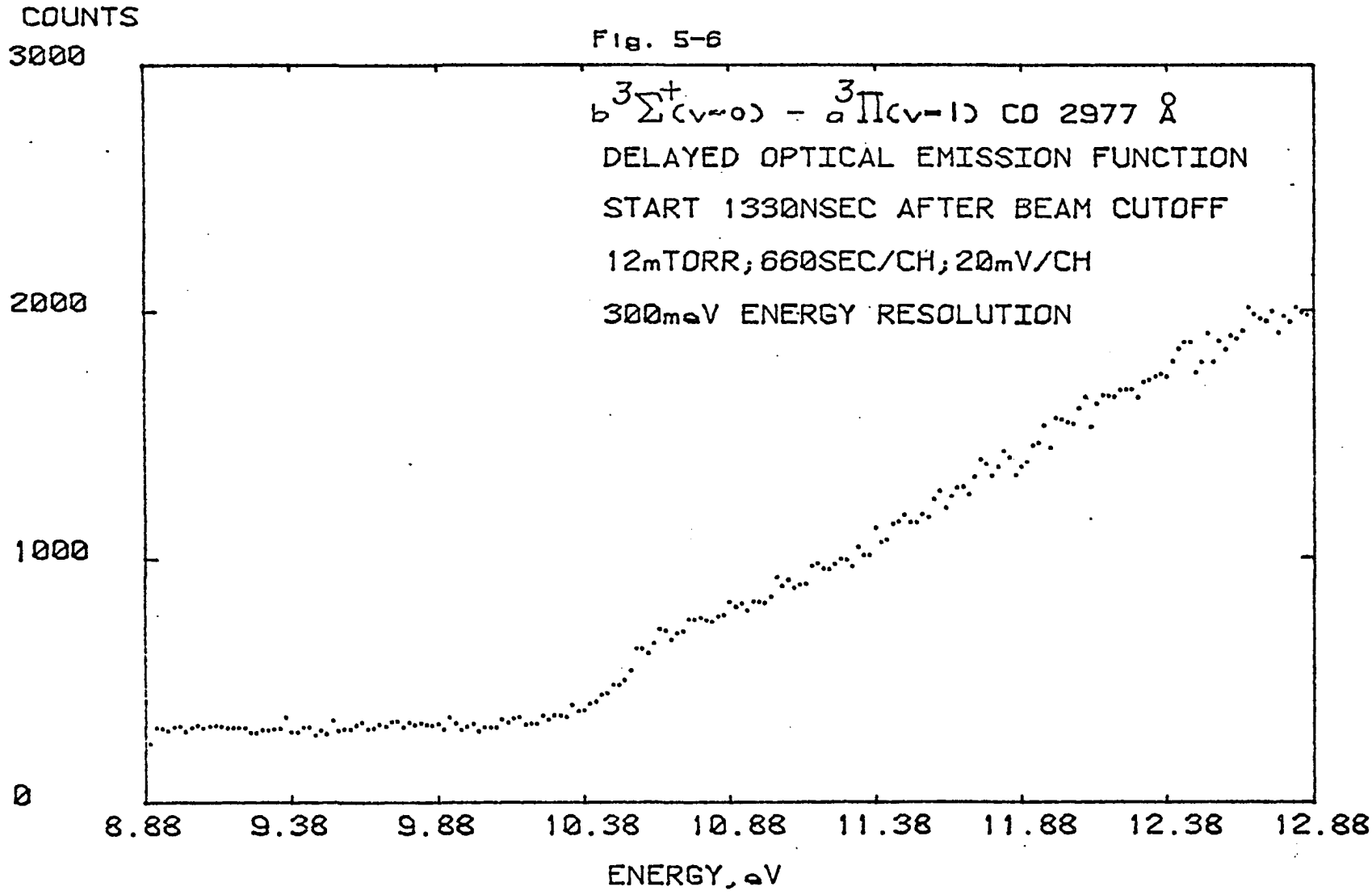
COUNTS
3000
2000
1000
0
$b^3\Sigma^+(v=0) - a^3\Pi(v=1)$ CO 2977 Å
DELAYED OPTICAL EMISSION FUNCTION
START 1330NSEC AFTER BEAM CUTOFF
12mTORR; 660SEC/CH; 20mV/CH
300meV ENERGY RESOLUTION
8.88
9.38
9.88
10.38
10.88
11.38
11.88
12.38
12.88
ENERGY, eV

Figure 5-7. Fluorescence Decay with Best Fit and Error Limits.

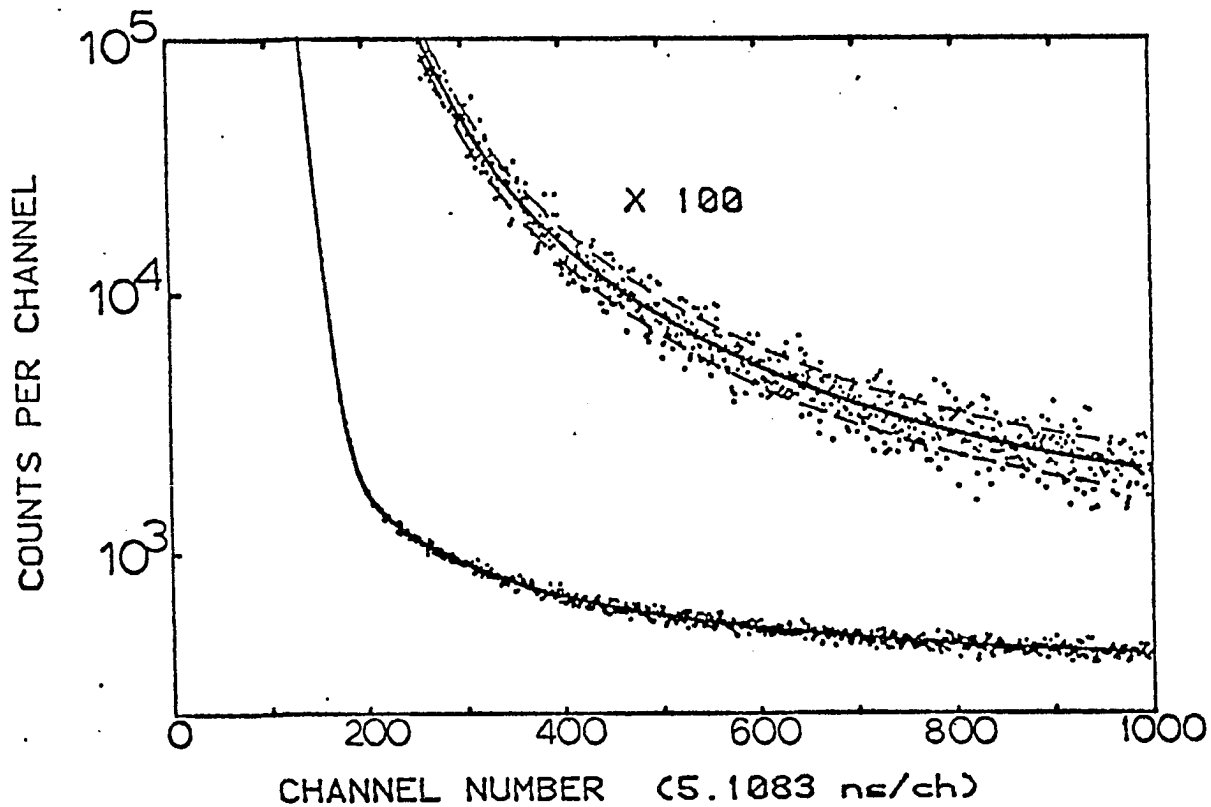

$(1\text{-}20)\times10^{-3}$ torr, we studied the pressure dependence of the various decay components.

The reciprocal prompt lifetime versus pressure is shown in Fig. 5-8. The zero pressure extrapolated lifetime for this decay is 51.86±0.24 ns at the 95% confidence level. The slope of the plot yields the collisional quenching cross section which is $(7.7\pm3.8)\times10^{-15}cm^2$.

The pressure dependence of the first cascade component feeding the b-a transition is shown in the reciprocal lifetime versus pressure curve in Fig. 5-9. The zero pressure extrapolated lifetime for this cascade component is 358±20 ns at the 95% confidence level and the slope of this plot yields a collisional quenching cross section which is $(7.1\pm3.5)\times10^{-15}cm^2$ at the 95% confidence level.

The second cascade component feeding the b-a transition was very weak and we measured its lifetime to be (1.5±0.9) μsec at the 95% confidence level. The poor statistics associated with this cascade did not allow its pressure dependence to be extracted.

We have summarized the present results in Table 5-1. We have also included the previous results of Carlson et al.,[9] Van Sprang et al.,[1] Smith et al.,[2] and Rogers and Anderson,[3] as well as our reanalysis of the data of Rogers and Anderson.[14] As has been discussed above, if either too short an excitation pulse or too short a record length

Table 5-1. Lifetimes and Collisional Quenching Cross Sections

$b^3\Sigma^+(v'=0)$ State of CO.

Investigator	Prompt Lifetime (ns) (τ_K)	First Cascade Lifetime (ns) (τ_I)	Second Cascade Lifetime (ns) (τ_J)	Prompt Quenching Cross Section (cm^2)	First Cascade Quenching Cross Section (cm^2)
This work	51.86±0.24	358 ± 20	1500 ± 900	$(7.7\pm3.8)\times10^{-16}$	$(7.1\pm3.5)\times10^{-16}$
Carlson et al(Ref. 9)	53.7±1.5	not mentioned	not mentioned	not mentioned	not mentioned
Van Sprang et al.(Ref. 1)	56 ± 1	not mentioned	not mentioned	not mentioned	not mentioned
Smith et al.(Ref. 2)	53.6±0.3	not mentioned	not mentioned	$<2\times10^{-16}$	not mentioned
Rogers and Anderson (Ref. 3)	57.6±1.24	not mentioned	not mentioned	pressure independent	not mentioned
Rogers and Anderson (present analysis, see Ref. 14)	54.6±5.8	340 ± 200	indeterminate	$(1.28\pm0.51)\times10^{-16}$	indeterminate

Figure 5-8. Prompt Reciprocal Lifetime A_K versus Pressure.

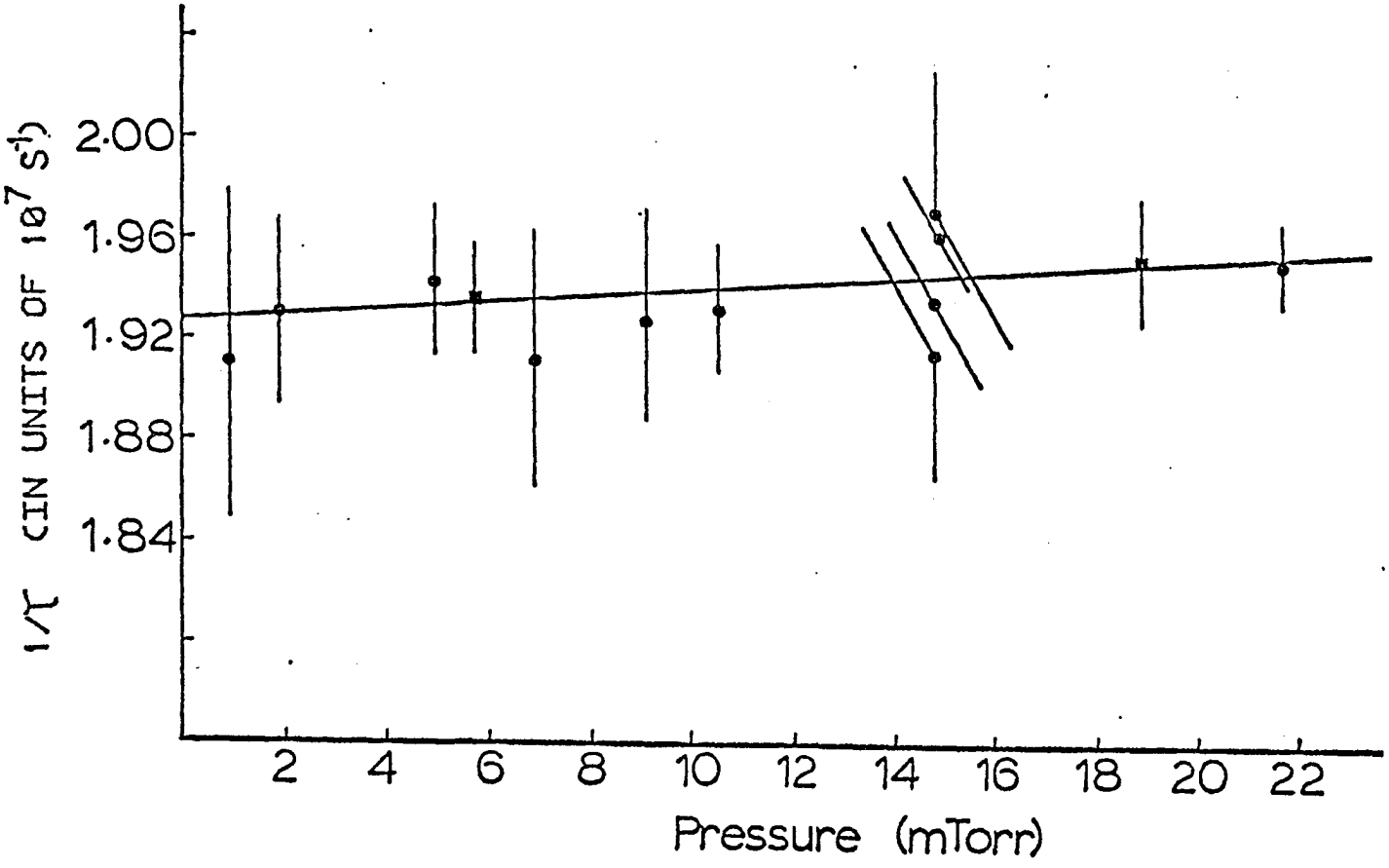

Figure 5-9. First Cascade Reciprocal Lifetime versus Pressure.

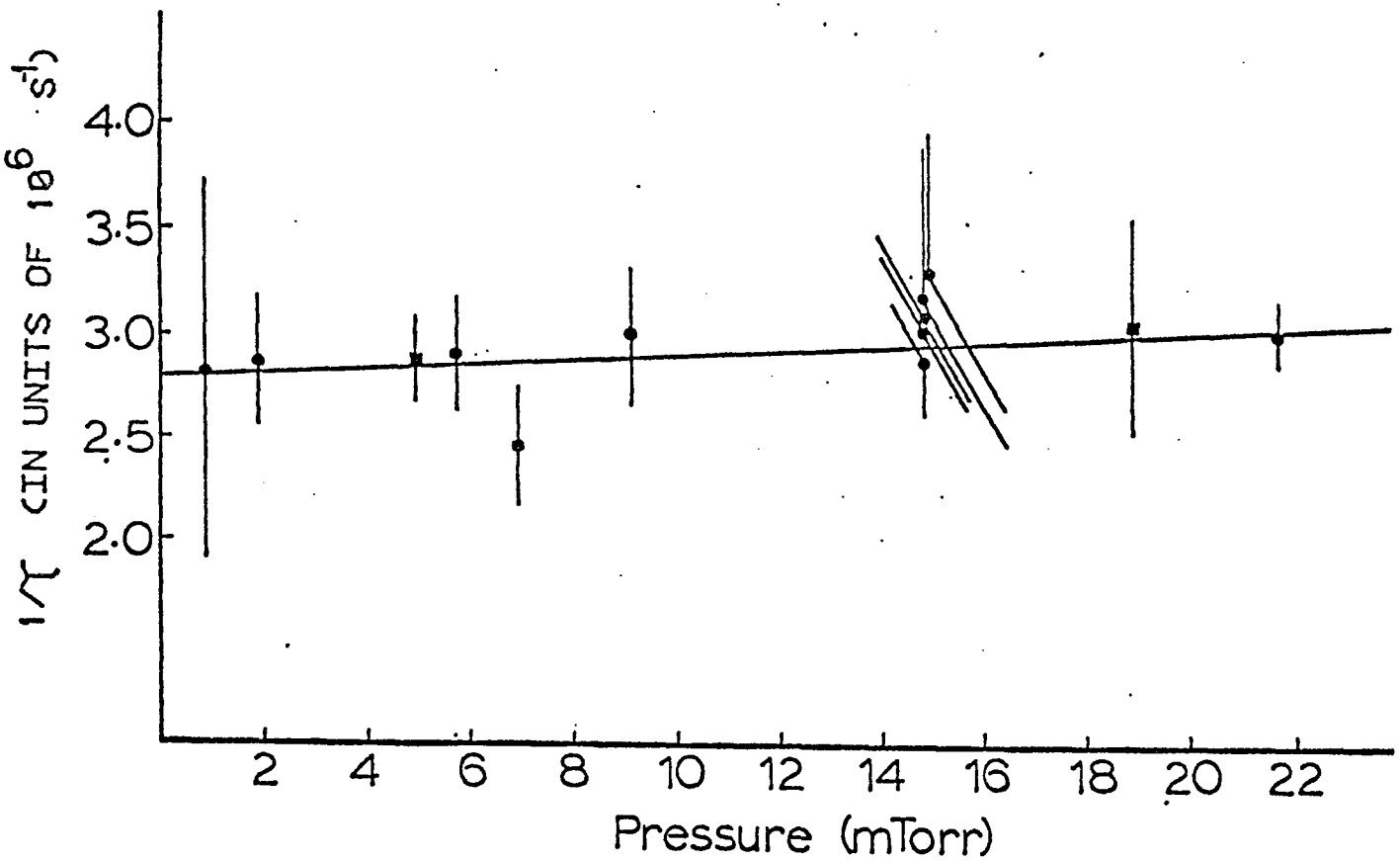

is used, too long a prompt lifetime will be extracted from the data. Computer fits to our data consistently gave a prompt decay lifetime of 56 ns when a data record of 0.5 μs or less was used. This lifetime was also obtained when computer fits were made to data sets collected on 0.5 μs and 5μs time scales when an 87 ns excitation pulse was used. In all cases a 350 nsec component was detected. It should be noted that our experiment with a 0.5 μs time scale and an 87 ns excitation pulse is similar to the arrangement used in two of the previous studies.[1,3] This kind of arrangement has been commonly used for measuring lifetimes in the 30-100 ns range, since a short excitation pulse and a short record length will allow a higher repetition rate and a shorter collection time. In addition to the systematic errors seen in the prompt decay lifetimes if cascades are present, fitting to short data record lengths makes finding long lived exponentials difficult, since usually not even one e-folding is present, and the use of short excitation pulses will not allow the long lived processes to saturate. In both cases, the long lived processes are not eliminated but are decreased to the point that they cannot be accurately determined although they may still effect the prompt lifetime of interest. In this work excitation pulses several times longer than the longest lifetime detected have been used so that the long lived components could be fitted with precision.

The difference between the prompt lifetime determined by Smith, Imhoff and Read,[2] and that determined in the present work is about 1 ns larger than that given by the combined error limits of the two experiments. Smith et al.[2] made a 3% slope correction to their data before analysis. The 3% slope could correspond to an exponential with a lifetime of about 450 ns. It is possible, therefore, that the cascade process was misinterpreted as the photon count rate error commonly encountered in coincidence work. Since in the present work the data rate is less than 0.1% of the pulse repetition rate, we should have an insignificant photon count rate error. In addition, we found that three exponentials were necessary to analyze our data. In our analysis of real data and synthesized data containing three exponentials, we found that when two exponentials were used for data anlysis, a prompt lifetime which was 1 ns too long was recovered. It is likely that the explanation of the discrepancy is that too few exponentials were used to fit the data of Smith et al.[2] It is also possible that the electron monochromator in the experiment of Smith et al.[2] did not exclude electrons that had scattered from the nearby perturbing vibrational levels of the $a'^3\Sigma^+$. In this case, feeding from the long lived a' levels could have been counted as coincidences, causing a systematic lengthening of the measured decay constant due to the long lived background.

Our computer analysis of the data of Rogers and Anderson[14] yields at best two exponential decay curves. Our attempts to fit three exponentials to the data of Rogers and Anderson[3] have not been successful. We attribute this failure to their short data record length (600 ns) and their poor statistics (typically 3000 counts in the initial channels). Our reanalysis of their data yields a pressure dependent lifetime of 54.6±5.8 ns with a quenching cross section of $(1.28\pm0.51)\times10^{-14}$ cm in agreement (within error bars) with the present results. We believe that their result is systematically high due to the short record length used (see Table 5-1). This explanation is also applicable to the difference between the prompt lifetime result of Van Sprang et al.[1] and that given by the present work. In addition, Van Sprang et al. used an electron energy of 13 eV which is only 1 eV below the ionization potential of CO. This introduces a number of problems which have been discussed above. Furthermore, our reanalysis of the data of Rogers and Anderson,[3] supports the conclusion based on our own data that multiple exponentials are present in this decay. The first cascade component found by us in our reanalysis of the data of Rogers and Anderson has a lifetime of (340±200) ns. However, the statistics for this cascade component are so poor that it is difficult to determine if any pressure dependence exists. The lifetime given in Table 5-1 for the

first cascade from our analysis of the data of Rogers and Anderson is the mean of all of their data. The error given in the table is the square root of the variance of the mean.

Long lived (1 ms) metastable thresholds have been observed in the region of 10-11 eV by Wells et al.[26] In order to insure that the cascades observed in the present work were not due to such metastable states, we used an electron gun repetition rate of 12 kHz square wave and a TAC record length of 40 μs. In this way, an extremely weak exponential was detected with a lifetime of (5±10) μs. Its amplitude was only 25% of the background, and no other long components were detected. We do not consider this conclusive evidence for attributing the cascades to such a long lived metastable.

It is likely that the origin of the first cascade into the $b^3\Sigma^+$ state is due to the v"=31-36 levels of the a' state, since the high vibrational levels of the a' state are known to strongly perturb the v'=0 and 1 level of b state.[9,12,59,63] This conclusion is supported by the fact that the quenching cross sections of both the prompt and first cascade components of the decay are equal. The origin of the long lived cascade is not clear at this time. It may be another perturbation occurring with the a' state which couples to the b state.

Fig. 5-5 shows the delayed optical emission functions when photons were collected from $545 \approx 10\tau_b$ (where τ_b is

the prompt lifetime) to 5000 nsec after cutoff of the electron gun. While Fig. 5-6 shows the delayed optical emission function when photons were collected from 1300 to 5000 nsec after cutoff of the electron beam. Although the difference between the two curves is not dramatic, Fig. 5-6 does show the shoulder at 10.7 eV as less dominant than the shoulder in Fig. 5-5. This indicates that the shoulder may be due to the medium lifetime cascade component.

A study of the time spectra at 10.7 eV and 11.2 eV showed that at 10.7 eV the ratio of the medium cascade amplitude/long lived cascade amplitude was approximately 4 and at 11.2 eV the ratio was 1.

This indicates that the two cascade components have different shaped cross sections or that there is a difference in the threshold energy of the cross sections. Probably, both possibilities are true in the present case.

Carlson et al.[9] have pointed out the relationship between perturbations of molecular vibrational levels by long lived states and the systematic errors introduced in lifetime measurements when these long lived feed processes are not considered in the data analysis. Gelbart and Freed[81] discuss the effect of perturbed molecular states on the intensities in the $B^2\Sigma^+ \rightarrow X^2\Sigma^+$ system of CN due to perturbation by the $A^2\Pi$ level. The collisional transfer of excitation between these perturbed levels occurs even at low

pressures (less than 1 Torr) due to the partial $A^2\Pi$ character of certain of the $B^2\Sigma^+$ rotational vibrational levels. Since the perturbed levels have very nearly the same energy, this is a resonant collisional transfer which is highly preferred, because very little energy exchange is involved. The mixed character of the perturbed levels also enhances the probability of a transfer of excitation, since the electronic configuration of one mixed level must only be distorted by a small amount during the collision in order to make the transition to the other level.

In order to estimate the excitation transfer coefficients, we calculate the ratio of the amplitude of the prompt and first cascade from Eq. 3-11.

prompt amplitude/medium cascade:

$$C_K/C_J = \frac{(\lambda_K-\lambda_J)}{\lambda_{JK}} \frac{N_K^0}{N_J^0} + \frac{C_J}{C_I} + 1 \qquad (5\text{-}1)$$

where level K is the $b^3\Sigma^+$ (v'=0) level; level J is the 400 nsec cascade component; level I is the 1.5 μsec cascade component.

This assumes that $\lambda_{IJ} = 0$. This is physically reasonable for an electron energy of 10.7 eV the medium cascade amplitude/long cascade amplitude; C_J/C_I is approximately 4/1.

Thus, the transfer directly from level I to level K is small compared to the transfer of level J to level K, and the transfer I to J to K must be even smaller, since it would involve one more branching ratio. Assuming $\lambda_K > \lambda_J$, $\lambda_K > \lambda_I$, Eq. (5-1) simplifies to

$$\frac{C_K}{C_J} = \frac{1}{\lambda_{IK}} \frac{nQ_K I_0}{\frac{1}{\lambda_J} nQ_J I_0} = \frac{\lambda_J}{\lambda_{JK}} \frac{Q_K}{Q_J} \tag{5-2}$$

$$\lambda_{JK}(p) = \lambda_J(p) \frac{Q_K}{Q_J} \frac{C_J(p)}{C_K(p)} \tag{5-3}$$

A linear least squares procedure was used to fit a straight line to

$$(\lambda_J(p) \frac{Q_K}{Q_J} \frac{C_J(p)}{C_K(p)}) \text{ versus pressure, p}$$

assuming $Q_K/Q_J = 1.0$.

The data used in the fit is shown in Table 5-2. It was found that at 10.7 eV electron energy λ_{JK} had the form:

$$\lambda_{JK}(p) = A_{JK} + K_{JK}p \quad . \tag{5-4}$$

Table 5-2. $\lambda_{JK}(p)$ versus p.

Pressure mTorr, p	$\frac{C_K}{C_J}$: $\frac{\text{prompt}}{\text{medium}}$ amplitude ratio	$\lambda_{JK}(p)$
1.88	35.9	77,172.5
4.95	31.1	90,159.3
6.61	24.1	117,097.5
9.08	27.5	103,599.0
14.8	25.1	115,988.8
14.8	21.4	136,043.0
14.8	33.7	86,389.3
20.76	31.9	93,300.4

$$A_{JK} + pK_{JK} = \frac{C_J}{C_K}\frac{Q_J}{Q_K}(A_J + pK_J)$$

Values used in fit:

$A_J = 2.75 \times 10^6 \text{ sec}^{-1}$

$K_J = 1.09 \times 10^{-4} \text{ sec}^{-1}/\text{mTorr}$

$\frac{Q_J}{Q_K} = 1$ Assume a' cross section = b cross section for lack of other better information.

Energy: 10.7 eV.

where

$A_{JK} = 92060 \pm 14483 \text{ sec}^{-1}$

$K_{JK} = 950 \pm 713 \text{ sec}^{-1}/\text{mTorr}.$

It should be stressed that this is only a rough estimate. More extensive data must be collected and a multiparameter fit made before reliable values for A_{JK} and K_{JK} will be available.

The indicated error is for the 68% confidence limits which was obtained from the error of the linear least squares fit to the data in Table 5-2.[80]

Carlson et al.[9] have studied the collisional resonant transfer of excitation as a function of the catalyst gas pressure due to the process shown below where M represents the catalyst gas.

$$(a') + (M) \xrightarrow{K_{JK}} (b) + (M)$$

Argon was found to be the most effective catalyst gas in the case of the $A^1\Pi$ state of CO. However, they found that when argon was used as the catalyst gas for the $b^3\Sigma^+$ state, they observed no pressure dependence in the collisional exchange process. An upper limit was placed on $K_{JK} < 3.2 \times 10^4 \text{ sec}^{-1}/\text{mTorr}$. The collisional energy transfer rate determined in the present work for self quenching

of CO cannot be compared to that found in Carlson et al.[9], since the two processes used different quencher gases.

The similarity in the upper limit in the two cases may indicate that both experiments are observing the same phenomenon with different quencher gases. It has been assumed that $Q_J/Q_K = 1$ where Q_K is the cross section of the $b^3\Sigma^+(v=0)$ level and Q_J is the cross section of the $a'^3\Sigma^+(v)$ level. The value of v is the level from which the major cascade originates. The largest source of error in the estimate of λ_{JK} is probably the value taken for Q_J.

Carlson et al.[9] using a fitting procedure obtained $Q_K/Q_J = 5$. Carlson et al.[9] also obtained the lifetime of the $b^3\Sigma^+(v=0)$ state at 53.7±1.5 nsec. Their result probably disagrees with the present work due to the short excitation pulses used in the electron gun and the subsequent problems in fitting the longer lived cascade components.

REFERENCES

1. H. A. Van Sprang, G. R. Mohlman, F. J. de Heer, Chem. Phys. 24, 429 (1977).
2. A. J. Smith, R. E. Imhof, and F. H. Read, J. Phys. B 6, 1333 (1973).
3. J. Rogers and R. Anderson, J. Quant. Radiat. Transfer 10, 515 (1970).
4. J. H. Moore Jr. and W. W. Robinson, J. Chem. Phys. 48, 4870 (1968).
5. E. H. Fink and K. H. Welge, Z. Naturforsch. 23a, 358 (1968).
6. T. Wentinck Jr., E. P. Marram, L. Isaacson and R. J. Spindler, ABLATIVE MATERIAL SPECTROSCOPY, AFWL TR 67-30.
7. R. G. Fowler and T. M. Holzberlein, J. Chem. Phys. 45, 1124 (1966).
8. R. P. Schwenker, J. Chem. Phys. 42, 1895 (1965).
9. T. A. Carlson, N. Duric, P. Erman and M. Larsson, Z. Physik A 287, 123 (1978).
10. P. Erman, Physica Scripta 11, 65 (1975).
11. P. Erman and J. Brzozowski, Physica Scripta 12, 177 (1975).

12. P. H. Krupenie, 1966 Natl. Stand. Ref. Data Ser. 5, Natl. Bur. Stand.

13. T. M. Holzberlein, Rev. Sci. Instrum. 35, 1041 (1964).

14. R. Anderson has kindly supplied us his raw data for reanalysis.

15. G. J. Schulz, Rev. Mod. Phys. 45, 423 (1973).

16. K. Fukui, T. Hirotsu, and K. Kuwata, Chem. Phys. Lett. 44, 13 (1976).

17. N. Bose, Chem. Phys. Lett. 61, 367 (1978).

18. J. Mazeau, F. Gresteau, G. Joyez, J. Reinhardt and R. I. Hall, J. Phys. B 5, 1890 (1972).

19. N. Swanson, R. J. Celotta, C. E. Cuyatt and J. W. Cooper, J. Chem. Phys. 62, 4880 (1975).

20. L. Sanche and G. J. Schulz, Phys. Rev. A 6, 69 (1972).

21 J. Comer and F. H. Read, J. Phys. B 4, 1678 (1971).

22. J. N. Bardsley and F. H. Read, Chem. Phys. Lett. 2, 333 (1968).

23. A. S. Newton and G. E. Thomas, Chem. Phys. Lett. 11, 171 (1971).

24. W. C. Wells and E. C. Zipf, J. Chem. Phys. 57, 3583 (1972).

25. W. L. Borst and E. C. Zipf, Phys. Rev. A 3, 979 (1971).

26. W. C. Wells, W. L. Borst, and E. C. Zipf, Phys. Rev. A 8, 2463 (1973).

27. J. N. H. Brunt, G. C. King, and F. H. Read, J. Phys. B 11, 173 (1978).

28. D. E. Golden, D. J. Burns, and V. C. Sutcliffe Jr., Phys. Rev. A 10, 2133 (1974).

29. Varian/NRC Instruction Manual VHS Vacuum Pumps (1975) Varian Corp., Lexington, Massachusetts.

30. S. Dushman, VACUUM TECHNIQUE (Wiley, New York, 1949).

31. Leybold-Heraens, VACUUM TECHNOLOGY, Leybold-Heraens Inc., Monroeville, Pennsylvania.

32. F. Rosebury, ELECTRON TUBE AND VACUUM TECHNOLOGY (Addison-Wesley, Reading, Massachusetts, 1965).

33. D. E. Golden and A. Zecca, Rev. Sci. Instrum. 42, 210 (1971).

34. J. R. Pierce, THEORY AND DESIGN OF ELECTRON BEAMS (D. Van Nostrand, New York, 1954).

35. K. R. Spangenberg, VACUUM TUBES, Chap. 4 (McGraw-Hill, New York, 1948).

36. R. E. Fox, W. M. Hickman, D. J. Grove and T. Kjeldass, Phys. Rev. 84, 859 (1951).

37. G. J. Schulz, Phys. Rev. 136, A650 (1964).

38. D. E. Golden and A. Zecca, Phys. Rev. A 1, 241 (1970).

39. E. Harting and F. H. Read, ELECTROSTATIC LENSES (Elsevier, Amsterdam, 1976).

40. D. E. Golden, N. G. Koepnick and L. Fornari, Rev. Sci. Instrum. 43, 1249 (1972).

41. R. V. Sutton, M.S. Thesis, Air Force Institute of Technology, Air University (1966).

42. American Radio Relay League, THE RADIO AMATEUR'S HANDBOOK (Newington, Connecticut, 1979).

43. ARRL Antenna Book, ARRL, (Newington, Connecticut).

44. FAIRCHILD TTL APPLICATIONS HANDBOOK, Fairchild Corporation (Mountain View, California, 1973).

45. I. A. D. Lewis and F. H. Wells, MILLIMICROSECOND TECHNIQUES (McGraw-Hill, New York, 1954).

46. Omega-T Systems Inc., Wide Band Noise Bridge TE7-02 (Richardson, Texas).

47. C. E. Kuyatt, METHODS OF EXPERIMENTAL PHYSICS, Vol. 7A (Academic Press, 1968).

48. V. C. Sutcliffe, Ph.D. Dissertation, University of Nebraska (1977).

49. G. A. Khayrallah and S. J. Smith, Phys. Rev. A 18, 559 (1978).

50. RCA Photomultiplier Tube Catalog PlT-700C (Lancaster, Pennsylvania, 1976).

51. RCA Pamphlet PlT-711, TIPS ON THE USE OF PM TUBES (Lancaster, Pennsylvania, 1972).

52. Metex Corporation, EMI/RFI Shielding Handbook (Edison, New Jersey, 1977).

53. Rawson-Lush Instrument Company (Acton, Massachusetts). See also T. C. Penn and F. G. West, Rev. Sci. Instrum. 35, 1361 (1964).

54. Avantek Amplifier #UTO-1521 (Avantek Corp., Santa Clara, California).

55. Vari-L Co., Inc. (Denver, Colorado).

56. W. Braker and A. L. Mossman, MATHESON GAS DATA BOOK (Matheson, East Rutherford, New Jersey).

57. Products for Research, Inc., CATALOG AND APPLICATIONS NOTE ON COOLING OF PM TUBES (Danvers, Massachusetts).

58. D. E. Golden and A. Zecca, Rev. Sci. Instrum. 42, 210 (1971).

59. R. K. Asundi, Indian J. Phys. 50, 241 (1976).

60. B. Rosen, SELECTED CONSTANTS SPECTROSCOPIC DATA RELATIVE TO DIATOMIC MOLECULES (Pergamon Press, 1970).

61. S. N. Suchard, SPECTROSCOPIC DATA--HETRONUCLEAR DIATOMIC MOLECULES (Plenum Publishing Co., 1975).

62. R. W. B. Pearse and A. G. Gaydon, THE IDENTIFICATION OF MOLECULAR SPECTRA (John Wiley & Sons, Inc., New York, 1976).

63. S. G. Tilford and J. D. Simmons, Physical and Chemical Ref. Data 4, 147 (1972), National Bureau of Standards.

64. C. A. Thayer and J. T. Yardley, J. Chem. Phys. 61, 2487 (1974).

65. D. J. Burns, D. E. Golden and D. W. Galliardt, J. Chem. Phys. 65, 2616 (1976).

66. G. E. Copeland, Ph.D. Dissertation, University of Oklahome (1970).

67. W. C. Paske, Ph.D. dissertation, University of Oklahoma (1974).

68. R. G. Fowler, PROGRESS IN ATOMIC SPECTROSCOPY, PART B (Plenum, New York, 1979), p. 1157.

69. Roger Gilbert, ELECTRO-OPTICAL SYSTEMS DESIGN (Oriel Corp., Stamford, Connecticut, 1975).

70. Ortec, TECHNIQUES FOR IMPROVED TIME SPECTROSCOPY, Ortec AN-41 (Oak Ridge, Tennessee). Also T. J. Paulus, Research and Development Manager, Ortec Corp., private communication.

71. E. H. Condon, HANDBOOK OF PHYSICS (McGraw-Hill, New York, 1958).

72. J. O. Hirschfelder, C. F. Curtiss and R. B. Bird, MOLECULAR THEORY OF GASES AND LIQUIDS (John Wiley, New York, 1954), p. 129.

73. D. E. Golden and H. W. Bandel, Phys. Rev. 138, A14 (1965).

74. A. H. Mahan and A. Gallagher, Rev. Sci. Instrum. 47, 81 (1976).

75. R. G. Fowler, private communication.

76. A. Corney, Adv. Elec. and Electron Phys. 29, 115 (1970).

77. R. E. Imhof and F. H. Read, Reports on Progress in Phys. 40, 1 (1977).

78. G. T. Egbert, Ph.D. Dissertation, University of Nebraska (1974).

79. R. T. Thompson, Ph.D. Dissertation, University of Oklahoma (1972).

80. P. R. Bevington, DATA REDUCTION AND ERROR ANALYSIS FOR THE PHYSICAL SCIENCES (McGraw-Hill, New York, 1969).

81. W. M. Gelbart and K. F. Freed, Chem. Phys. Letters 18, 470 (1973).

82. L. S. Curtiss and P. Erman, Physica Scripta 10, 65 (1978).

83. K. R. Spangenberg, FUNDAMENTALS OF ELECTRON DEVICES (McGraw-Hill, New York, 1957), p. 153.

84. G. E. P. Box and M. E. Muller, Annals of Math. Stat. 29, 610 (1958).